

Modern Parallel Coordinates

TUTORIAL

Eurographics 2006

Alfred Inselberg¹
School of Mathematical Sciences
Tel Aviv University
Tel Aviv, Israel
aaisreal@math.tau.ac.il

Vienna — September 2006

¹& Senior Fellow San Diego SuperComputing Center

Abstract

*The desire to augment our 3-dimensional perception and the need to understand multivariate problems spawned several multidimensional visualization methodologies. Understanding the underlying geometry of a multivariate problem provides insight into what is possible and what is not. After a short overview, **Parallel Coordinates** are introduced and developed rigorously showing, **using new didactic software**, how multidimensional lines, hyperplanes, flats, curves and smooth hypersurfaces can be visualized unambiguously. The development is interlaced with applications including Visual Data Mining (EDA) on real datasets (i.e. Feature extraction, GIS, Financial, Process Control, and others with hundreds of variables). There follow collision avoidance algorithms for air traffic control and detection of coplanarity and near-coplanarity with numerous applications. A geometric automatic classifier is applied to challenging clustering and classification problems. It provides the classification rule explicitly and visually. Nonlinear VISUAL models in terms of hypersurfaces are constructed from data and used interactively for Decision Support discovering Feasibilities, Interrelations, Sensitivities, enabling Constraint and Trade-Off Analysis. Our goal is to **concentrate the relational information within a dataset into clear patterns eliminating the polygonal lines altogether**. In view of recent results this prospect is becoming attainable as illustrated with a difficult problem central to many applications(Computer Vision, Geometric Modeling, Statistics).*

KEYWORDS: Multidimensional/Multivariate Visualization, Parallel Coordinates, Visual and Automatic (Classification) Data Mining, High Dimensional Datasets, Collision Avoidance, Process Control, Decision Support

Outline

Introduction – 1/3 hour

- **Visualization – Insight from Images** : incorporating our tremendous *pattern recognition ability* into the problem solving process.
- Examples of visualization successes.
- How can we *systematically* visualize multidimensional/multivariate problems?
- The course and its goals
- **Parallel Coordinates**
 1. Motivation and definition, point \leftrightarrow line duality .
 2. Mapping multivariate relations into distinct planar patterns, multidimensional graphs – demonstrated with didactic software.
 3. Examples with interactive demos: visual patterns reveal multivariate in multivariate satellite and financial data.

Visualizing N-Dimensional Linear and Near-Linear Relations

Multidimensional Lines – 1/3 hour

- Representation – generalization of the point \leftrightarrow line duality. Visualizing transformations on lines in N-dimensions.
- Visualizing and computing the minimum distance between pairs of lines in N-dimensions.
- Application to collision avoidance in air traffic control – (3 USA patents) – demo of real air traffic conflict scenarios and their resolution.
- Proximity – Visualizing "close" lines, line topologies, and detection of near-linear relations (USA Patent).

Planes, Hyperplanes & Flats – 1 hour

- Two Representations and detection of coplanarity.
- Industrial and commodity markets applications.
- Demo of Duality: Translation of planar points \leftrightarrow Rotation of a plane about a line – for N-dimensions.

- Representing flats of dimension 2 to $N - 1$ and reading their equations from the graphs.
- Proximity, approximate coplanarity, "close" flats, topology of hyperplanes and applications in Computer Vision and Geometric Modeling (USA patent).

Data Mining – 2/3 hour

- Visual Data Mining (Exploratory Data Analysis - EDA) (USA Patent) – navigating the discovery process from *visual cues* without prior hypothesis or biases. Examples :
 1. VLSI production data with 16 parameters, finding necessary conditions for high yield and quality, seeing how biases & "beliefs" defeat the goals.
 2. Visualizing the function of a neural network doing transaction approval for credit purchases and finding it seriously defective.
- Automatic Classification – a geometric classification algorithm (compared to 22 other well-known classifiers) finds the classification rule :
 1. explicitly – in terms of conditions on the parameters,
 2. displaying and visualizing the rule as a hypersurface,
 3. doing dimensionality selection – finding the minimal subset of parameters sufficing to state the rule (this is not an approximation),
 4. ordering the parameters to optimize separation between a class (selected subset of the data) and its complement,
 5. providing an estimate of rule's precision.
- Examples of classification
 1. Neural-pulse dataset with 32 parameters. Finding rule distinguishing two classes of neurons.
 2. Finding the rule distinguishing different vehicles types from afar by their noise signature.

Curves & Hypersurfaces – 2/3 hour

- Curves and their Images
- Duality : Cusp \leftrightarrow Inflection Point, Conics \leftrightarrow Conics, Convex sets and their relatives.

Hypersurfaces in N-Dimensions

- Representing smooth hypersurfaces, developable, ruled, quadrics, others and visually detecting their properties.
- Interior point construction and display algorithms – feasible states. Applications to process control and decision support.
- Demo constructing *visual* non-linear models (hypersurfaces) for Decision Support, discovering sensitivities, interrelationships, feasibility, criticalities, effect of constraints and doing trade-off analyses interactively.

Concentrating Relational Information into Patterns – 1/3 hour

- Eliminating the profusion of polygonal lines with recursion
- Visualizing families of close planes and hyperplanes – this is a difficult problem even in 3D. It is a central problem in Computer Vision, Geometric Modeling, Statistics and elsewhere.
- Separating clusters of coplanar points

End of Session

The tutorial and its goals

Learning the fundamentals of multidimensional visualization (extensively demonstrated with didactic software) and how to apply them to various multivariate/multidimensional problems in Visual & Automatic Data Mining, Artificial Neural Networks, Statistics, Computer Vision, Collision Avoidance and Non-linear Modeling concluding with some Research Topics.

Presenter

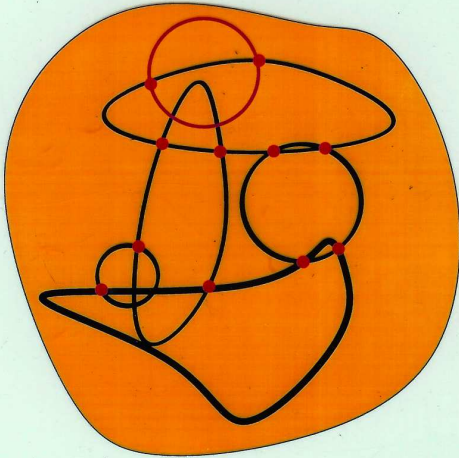
Alfred Inselberg received a Ph.D. in Applied Mathematics and Physics from the Univ. of Illinois (Champaign-Urbana) and held several academic positions in the USA (Univ. of Ill., UCLA, USC) and Israel. He was Senior Technical Corporate Staff Member (rank just below Fellow) at IBM doing research for 30 years. In 1996 he was elected Senior Fellow at the San Diego SuperComputing Center. He founded a company, Multidimensional Graphs Ltd, and teaches at the School of Mathematical Sciences Tel Aviv University. He invented and developed Parallel Coordinates, holds several patents, has numerous journal papers, professional and academic awards, and is completing the textbook on Parallel Coordinates.

Chapter 1

Introduction

VISUALIZATION

Insight through *Images*



Collection of application dependent *Mappings* :

Problem Domain \rightarrow *VisualRange*

Involves: *G* EOMETRY, *C* OGNITION, *A* RT, ?

Goal: *V*isual Model to help our *I*ntuition

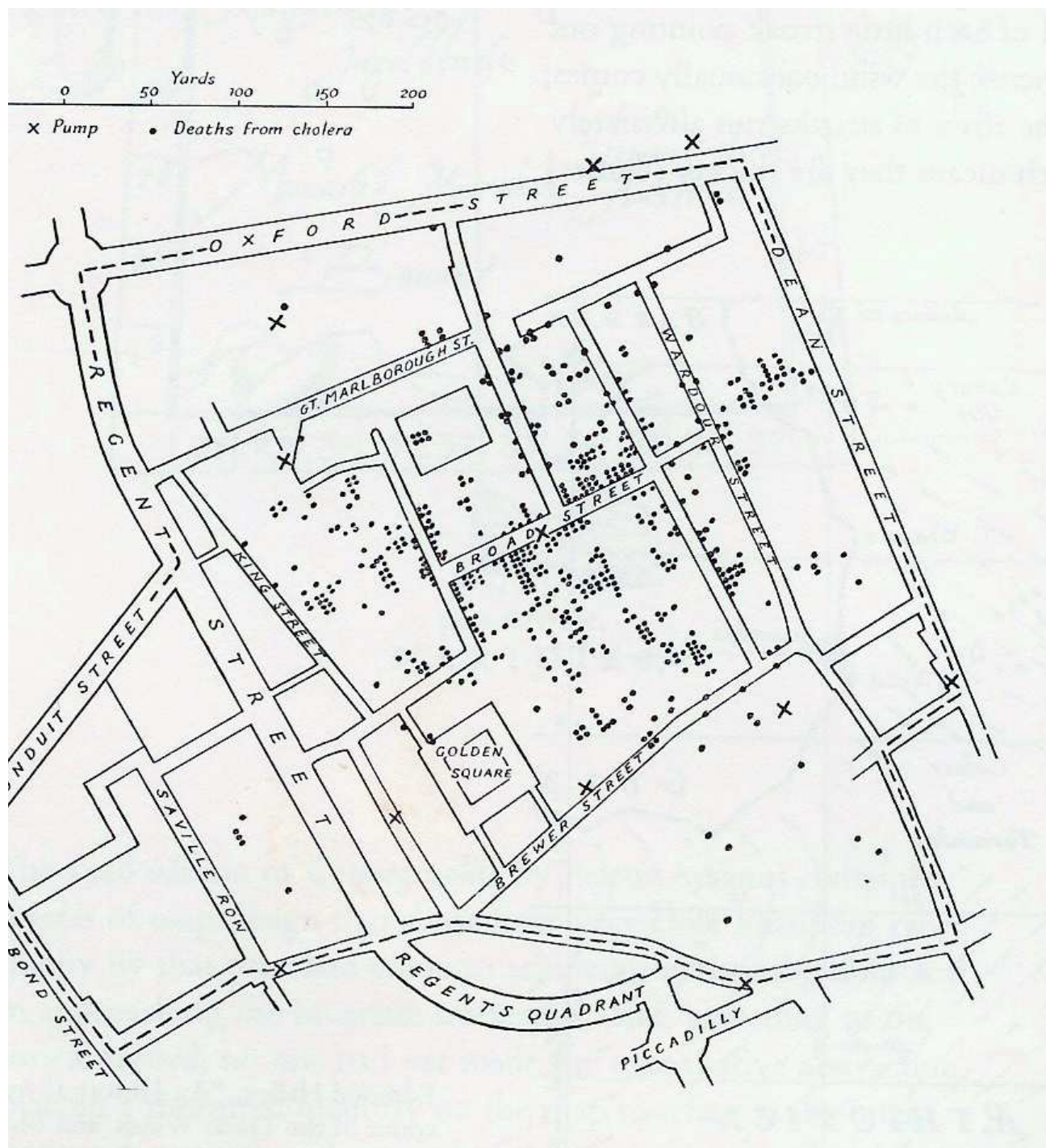


Figure 1.1: Cholera epidemic in London 1854. Dr. Snow placed dots at the addresses of the deceased and saw the concentration of deaths around the Broad street water pump. From E.W.Gilbert, Geog. J. 124] (1958) – By permission from E.R.Tufte “ The Visual Display of Quantitative Information”, Graphic Press 1983 p. 24

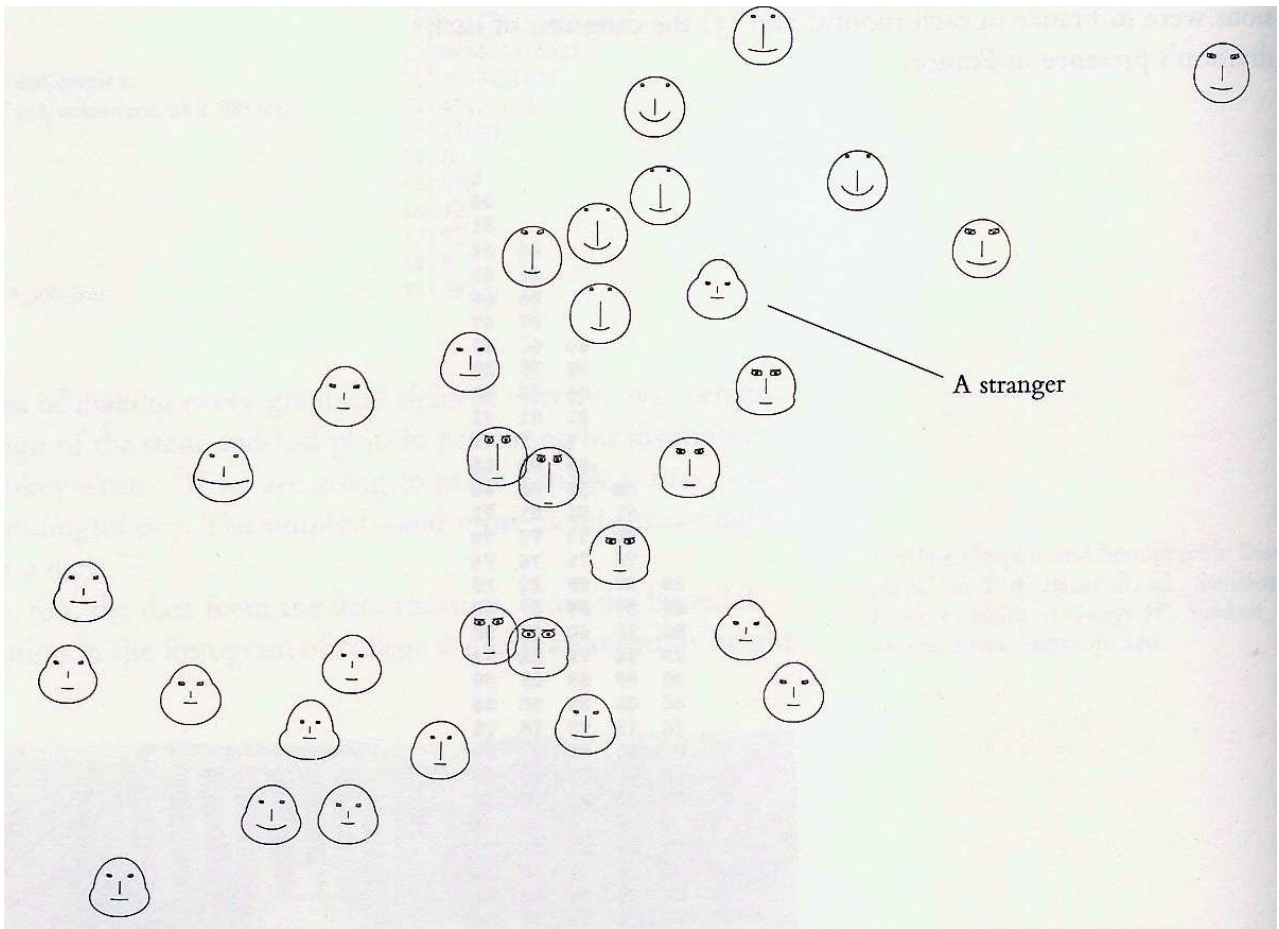


Figure 1.2: Multivariate data mapped to faces; each parameter corresponds and is measured on a facial feature. H. Chernoff, JASA 68 (1973)

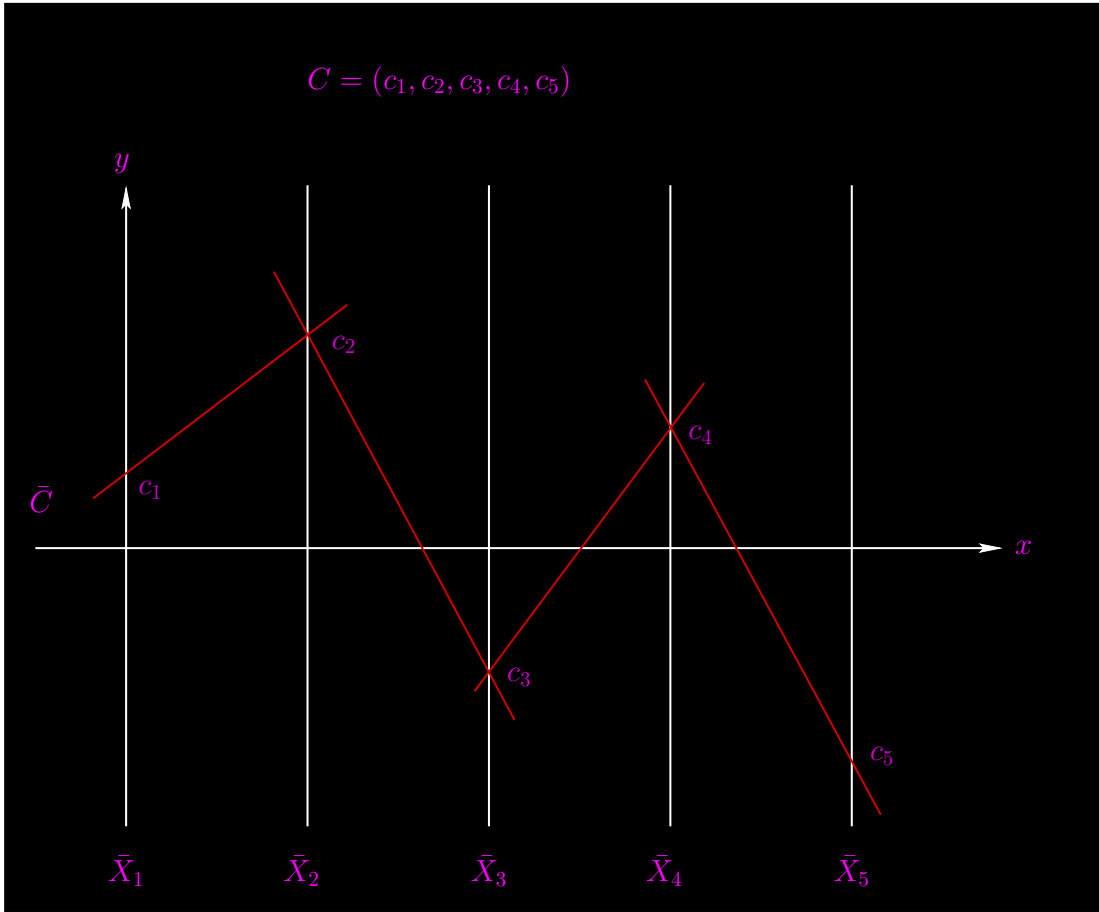


Figure 1.3: Parallel Coordinates – example for 5D.

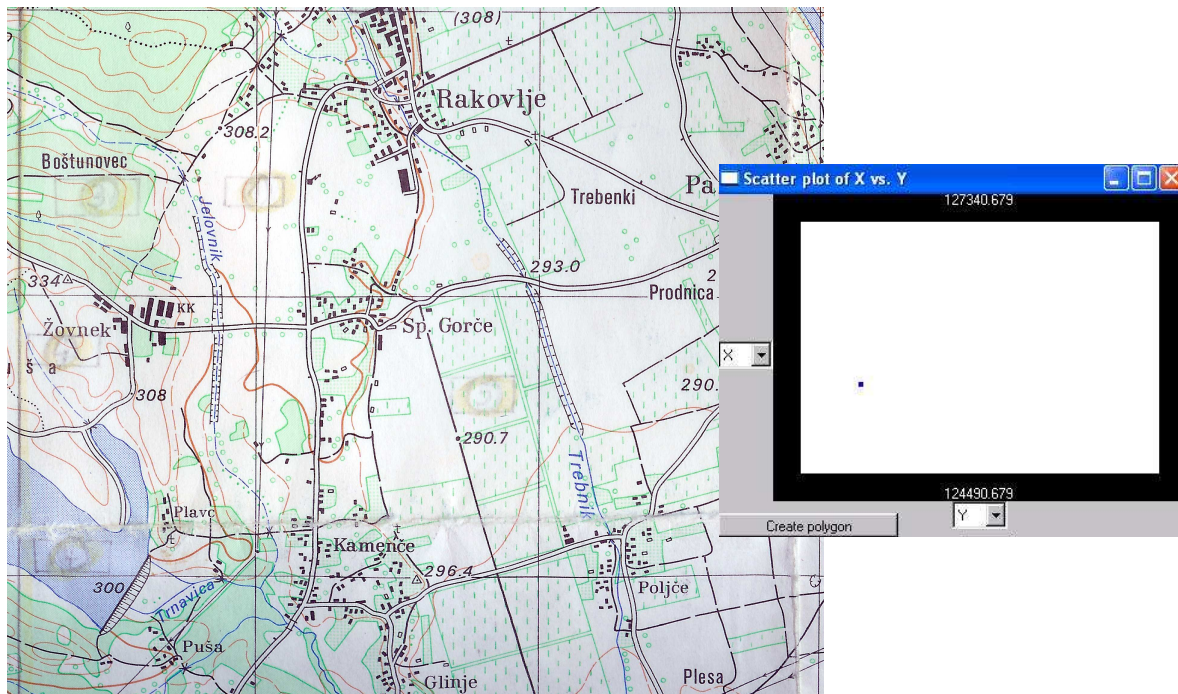


Figure 1.4: (Left) Region of Slovenia where 7 types of ground emissions were measured by the LandSat Thematic Mapper and shown in subsequent figures – Thanks to Dr. Ana Tretjak and Dr. Niko Schlamberger, Statistics Office of Slovenia. (Right) The display is the map’s rectangular region, the dot marks the position where the 7-tuple shown in the next figure was measured.

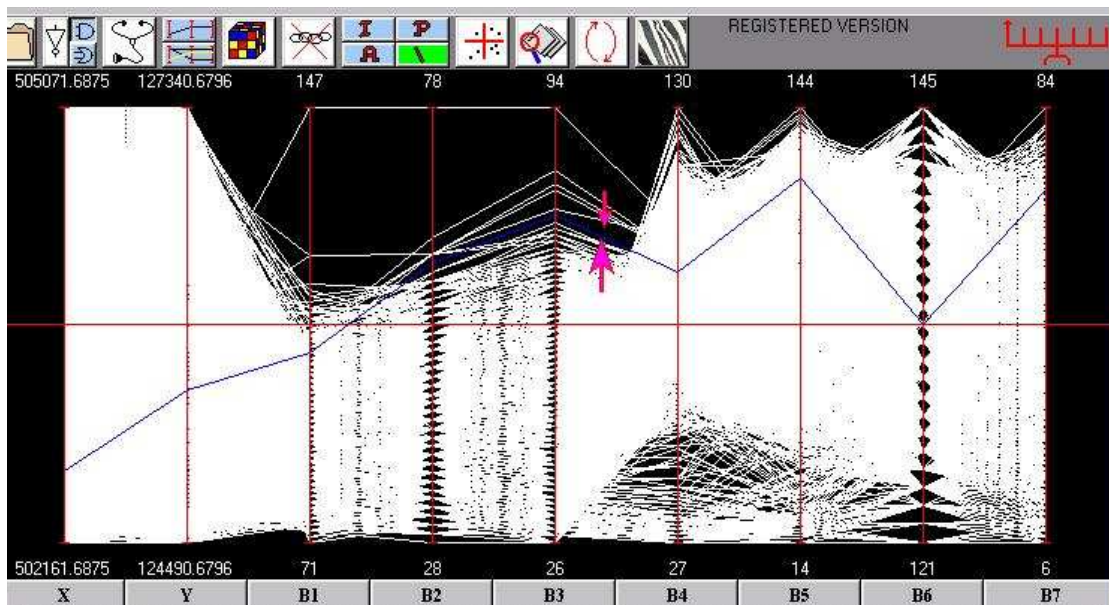


Figure 1.5: Query showing a single data item: the X, Y (position also shown on the right of Fig. 1.4) and values of the 7-tuple ($B_1, B_2, B_3, B_4, B_5, B_6, B_7$) at that point.

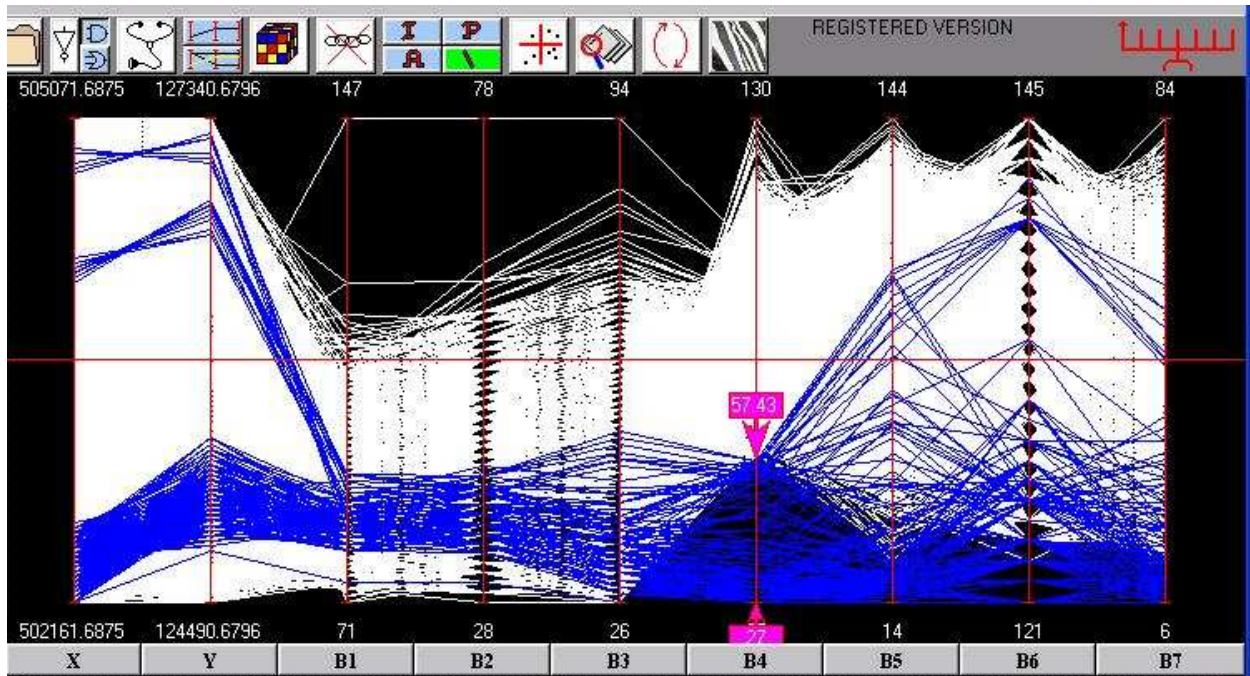


Figure 1.6: Finding water regions. The contrast due to density differences around the lower values of $B4$ is the *visual cue* prompting this query.

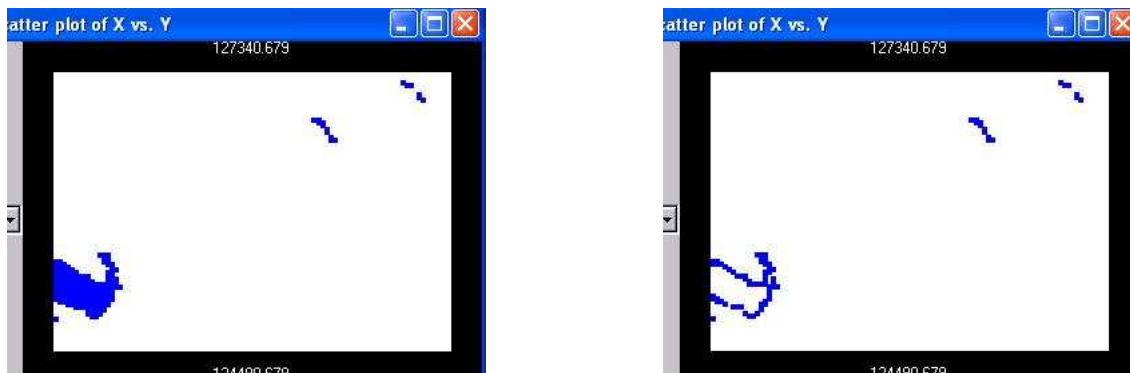


Figure 1.7: (Left) The lake and – result of query shown in Fig. 1.6 and (Right) just its boundary – result of query shown in Fig. ??.

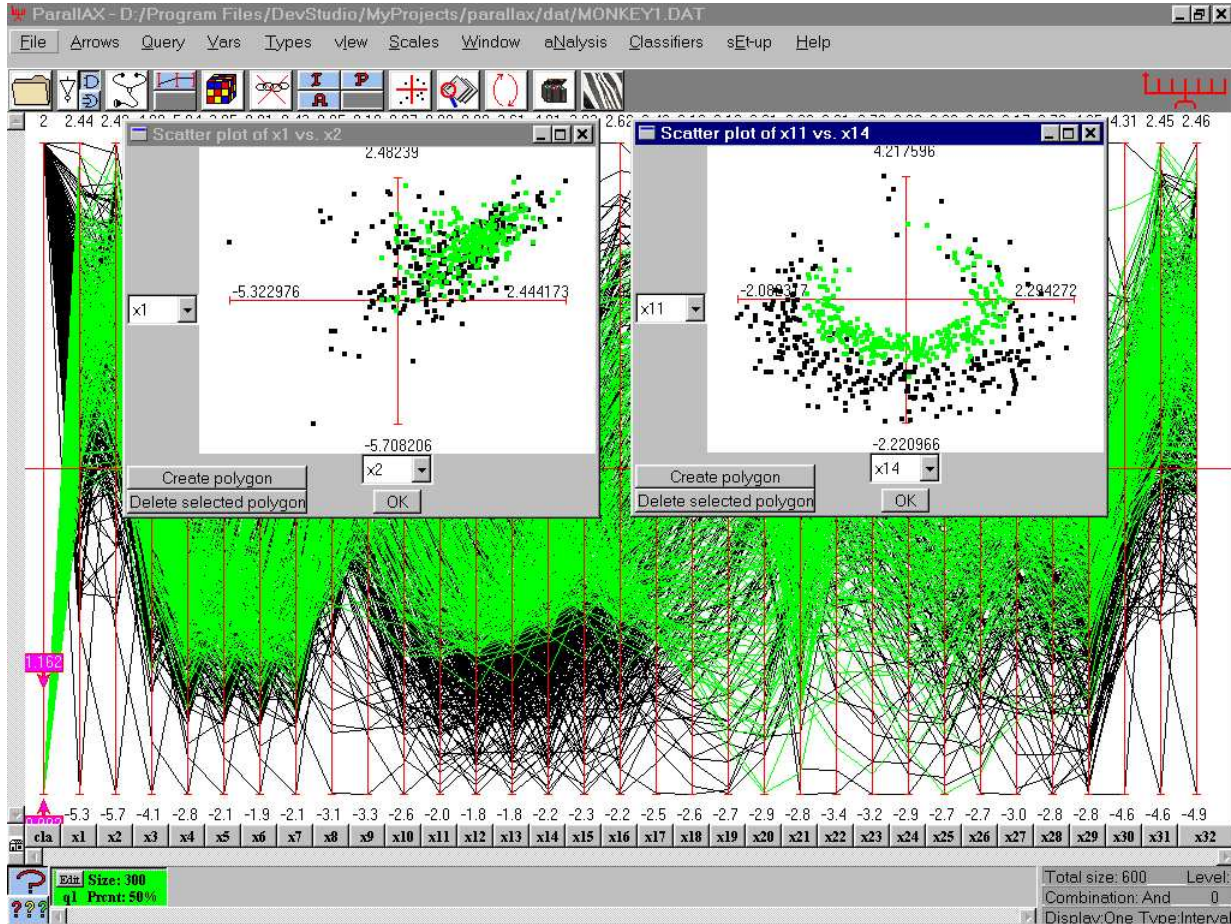


Figure 1.8: A dataset with 32 parameters and two categories is shown in the background. On the left plot are the first two parameters in the original order. The automatic classifier found the 9 parameters needed to state the rule with 4 % error and ordered according to their predictive value. The best two parameters are plotted on the right showing the separation achieved.

Chapter 2

The Plane \mathbb{R}^2 with $\|\|$ -coords

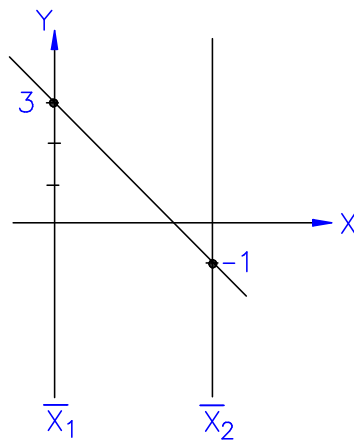


Figure 2.1: Points, above $(3, -1)$, on the plane are represented by lines.

With d the distance between the axes the correspondence is :

$$\text{line } \ell : x_2 = mx_1 + b \longleftrightarrow \text{point } \bar{\ell} : \left(\frac{d}{1-m}, \frac{b}{1-m} \right) \quad m \neq 1. \quad (2.1)$$

Lines with negative slope $m < 0$ (negative correlation) are mapped into points between the axes, $m > 1$ to the left of the \bar{X}_1 and $0 < m < 1$ to the right of the \bar{X}_2 axes. To include lines with $m = 1$ the Euclidean plane \mathbb{R}^2 is embedded in the Projective plane \mathbb{P}^2 . Then a line with slope $m = 1$ is mapped in the *direction* also called *ideal point* with slope b/d .

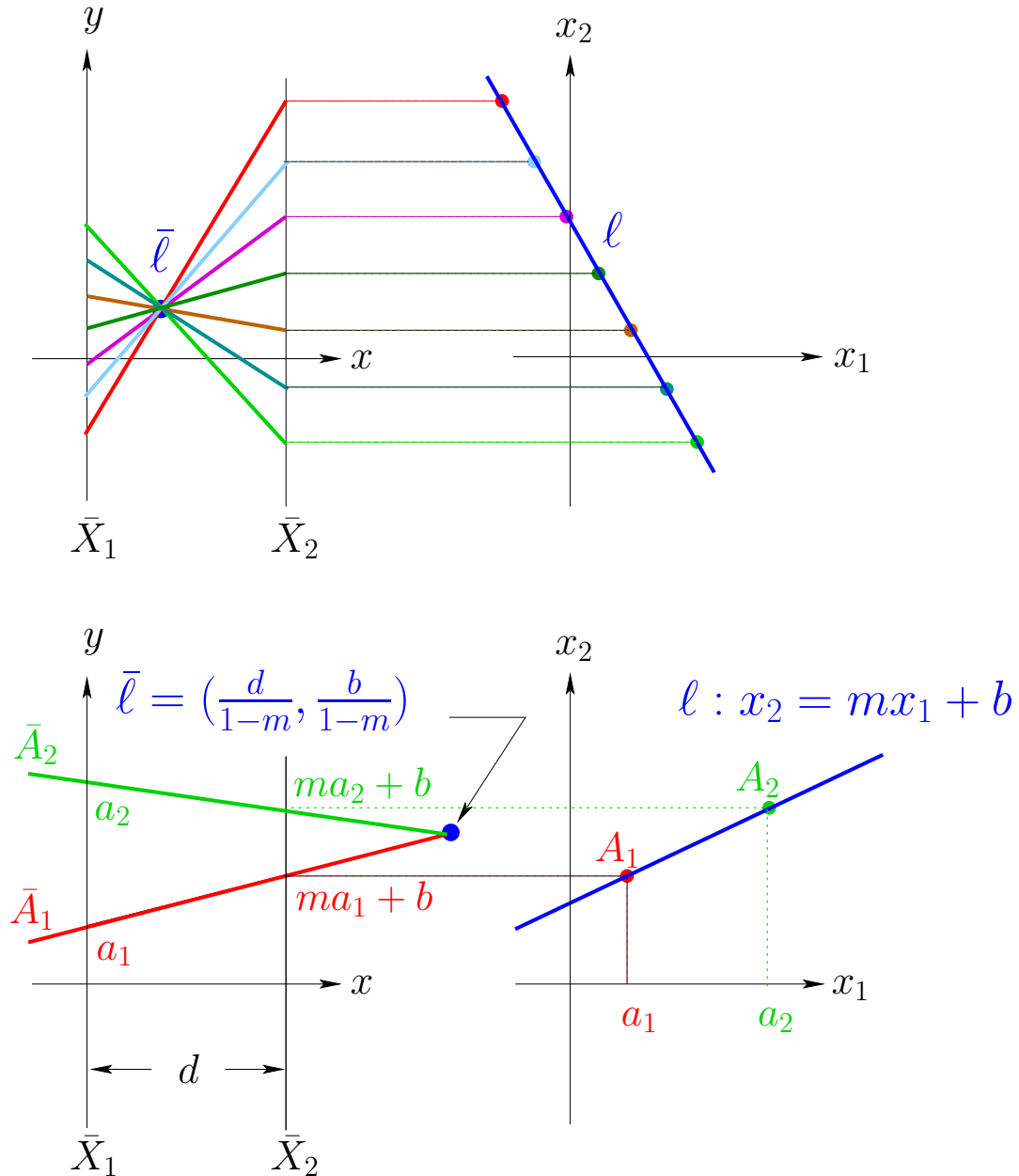


Figure 2.2: Conversely, lines are represented by points inducing a point \longleftrightarrow line duality.

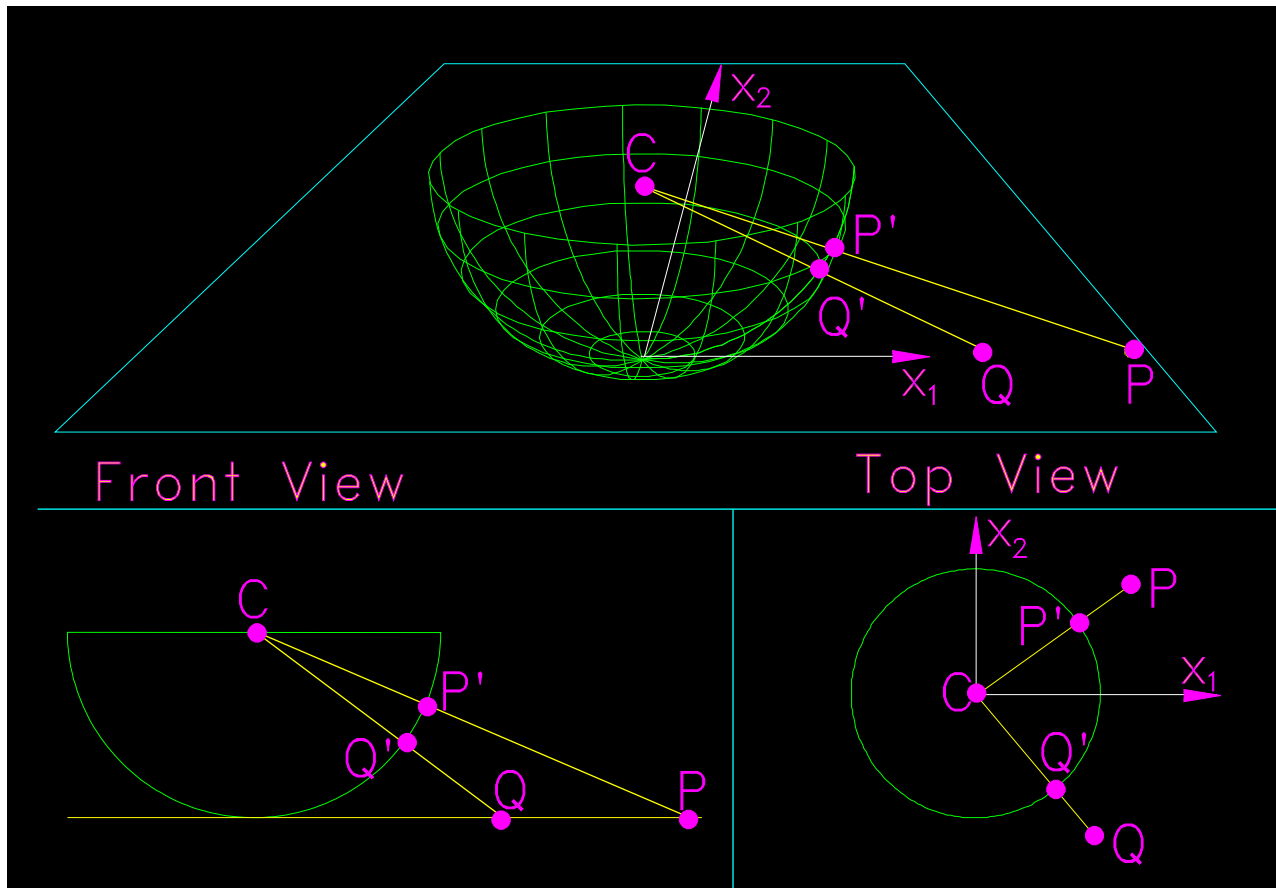


Figure 2.3: Model of the Projective Plane. Euclidean points are mapped into surface points of the hemisphere and *ideal points/directions* are mapped into the diameters of the “cap” with the same direction.

Homogeneous coordinates are very convenient and the conversion to/from Cartesian is easy i.e. *Cartesian* $(a, b) \rightarrow (a, b, 1) \rightarrow k(a, b, 1)$ for $k \neq 0$.

Sometimes it is preferable to describe the line ℓ by :

$$\ell : a_1x_1 + a_2x_2 + a_3 = 0 \quad (2.2)$$

and for $a_2 \neq 0$, $m = -\frac{a_1}{a_2}$ and $b = -\frac{a_3}{a_2}$, providing the correspondence :

$$\ell : [a_1, a_2, a_3] \longrightarrow \bar{\ell} : (da_2, -a_3, a_1 + a_2). \quad (2.3)$$

In turn this specifies a linear transformation between the triples ℓ and $\bar{\ell}$:

$$\bar{\ell} = A\ell, \ell = A^{-1}\bar{\ell},$$

where ℓ and $\bar{\ell}$ are considered as column vectors. The 3×3 matrix is :

$$A = \begin{bmatrix} 0 & d & 0 \\ 0 & 0 & -1 \\ 1 & 1 & 0 \end{bmatrix}, \quad A^{-1} = \begin{bmatrix} -1/d & 0 & 1 \\ 1/d & 0 & 0 \\ 0 & -1 & 0 \end{bmatrix}. \quad (2.4)$$

which can be easily computed by taking 3 simple triples, like for example, $[1,0,0]$, $[0,1,0]$ and $[0,0,1]$ for ℓ . For the other half of the duality, we look into the point $P \rightarrow \bar{P}$ line correspondence which is given by:

$$P : (p_1, p_2, p_3) \longrightarrow \bar{P} : [(p_1 - p_2), dp_3, -dp_1]. \quad (2.5)$$

Again taking P and \bar{P} as column vectors we have:

$$\bar{P} = B^{-1}P, \quad P = B\bar{P}$$

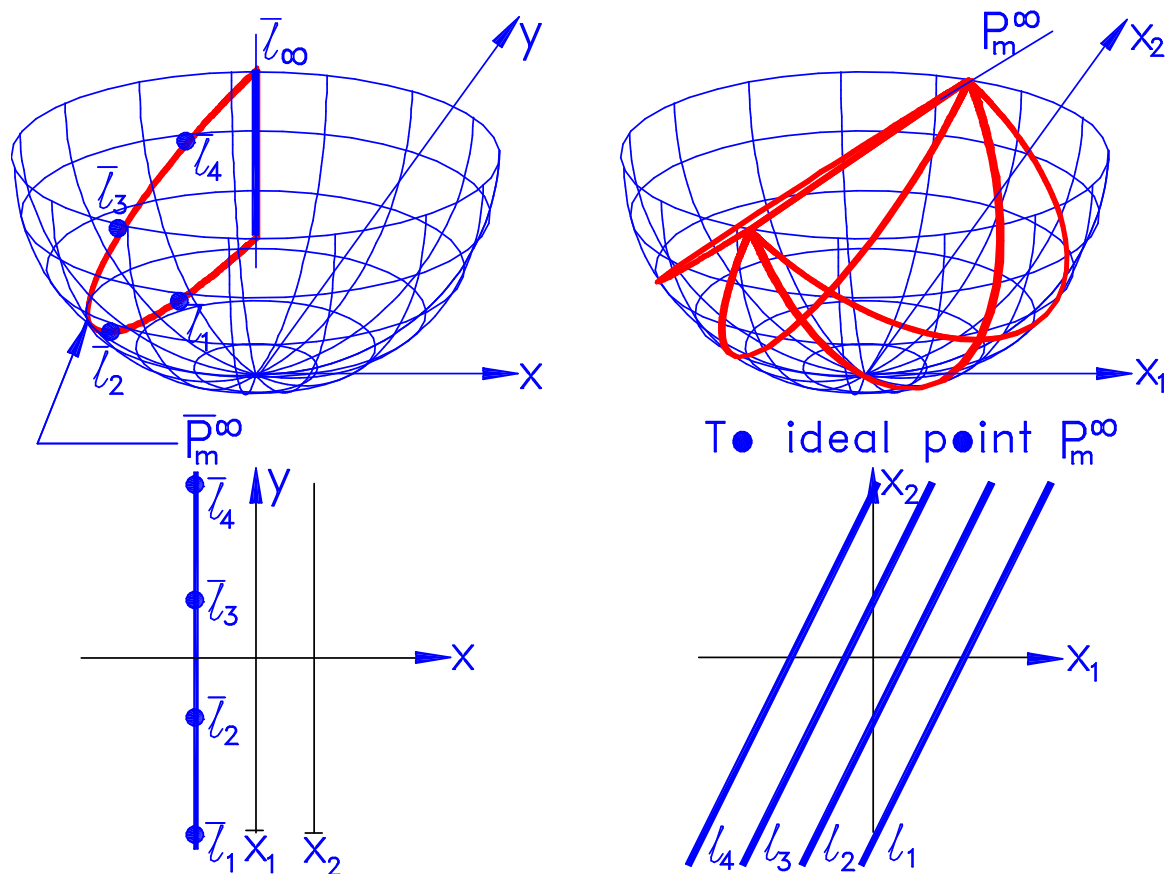


Figure 2.4: Under the duality parallel lines map into points on the same vertical line. On the projective plane model, the great semi-circles representing the lines share the same diameter since the lines have the same ideal point (direction). An ideal point in the direction with slope m is mapped into the vertical line \bar{P}_m^∞ .

with

$$B^{-1} = \begin{bmatrix} -1 & 1 & 0 \\ 0 & 0 & -d \\ d & 0 & 0 \end{bmatrix}, B = \begin{bmatrix} 0 & 0 & 1/d \\ 1 & 0 & 1/d \\ 0 & -1/d & 0 \end{bmatrix}. \quad (2.6)$$

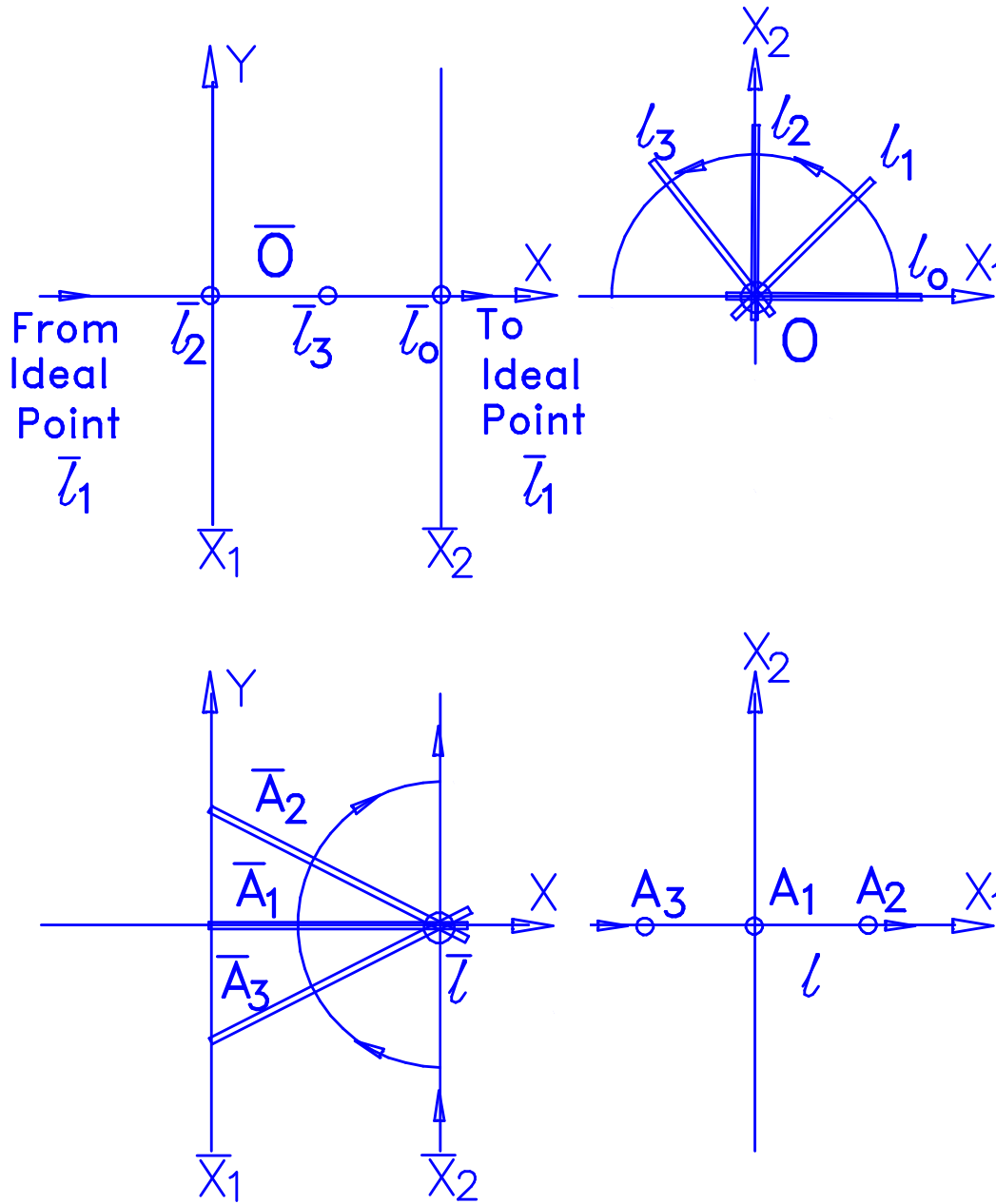


Figure 2.5: Duality : Rotation of a line about a point \leftrightarrow Translation of a point on a line.

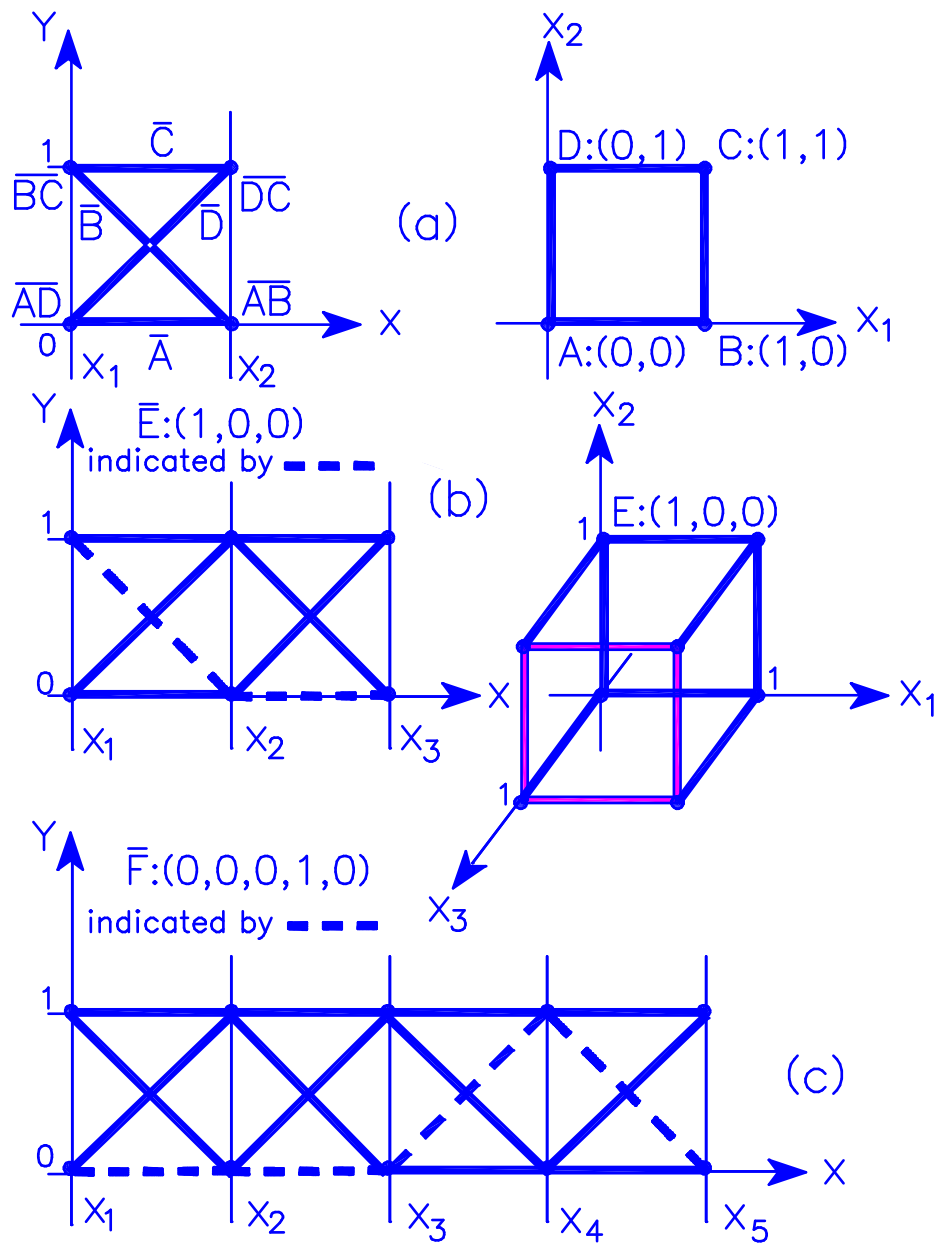


Figure 2.6: (a) Square, (b) 3-D cube (c) 5-D hypercube all with unit side. All vertices, edges, faces of all order can be seen – after learning the contents of sections Lines & Planes.

Chapter 3

Multidimensional Lines

Adjacent Variables Form

What is “a line in \mathbb{R}^N ” ?

In \mathbb{R}^3 a line is the intersection of two planes. So a line ℓ in \mathbb{R}^N is the intersection of $N - 1$ non-parallel hyperplanes. Equivalently, it is the set of points (specified by N-tuples) which satisfy a set of $N - 1$ linearly independent linear equations.

$$\ell : \begin{cases} \ell_{1,2} & : x_2 = m_2x_1 + b_2 \\ \ell_{2,3} & : x_3 = m_3x_2 + b_3 \\ & \dots \\ \ell_{i-1,i} & : x_i = m_ix_{i-1} + b_i \\ & \dots \\ \ell_{N-1,N} & : x_N = m_Nx_{N-1} + b_N \end{cases} , \quad (3.1)$$

Each equation contains a pair of *adjacently* labeled variables. In the $x_{i-1}x_i$ -plane the relation labeled $\ell_{i-1,i}$ is a line, and by our *point* \leftrightarrow *line* duality which we have already found (eq. (3) in Chapter 1) it can be represented by a point $\bar{\ell}_{i-1,i}$.

$$\bar{\ell}_{i-1,i} = \left(\frac{1}{(1 - m_i)} + (i - 2), \frac{b_i}{(1 - m_i)} \right)$$

or in homogeneous coordinates :

$$\bar{\ell}_{i-1,i} = ((i - 2)(1 - m_i) + 1, b_i, 1 - m_i). \quad (3.2)$$

There are $N - 1$ such points for $i = 2, \dots, N$ which represent the line ℓ .

Base Variable Form

Another common way of describing a line $\ell \subset \mathbb{R}^N$ is in terms of one, sometimes called the *base*, variable which after appropriate relabeling may be taken as x_1 . Then

$$\ell : \begin{cases} \ell_{1,2} & : x_2 = m_2^1 x_1 + b_2^1 \\ \ell_{1,3} & : x_3 = m_3^1 x_1 + b_3^1 \\ & \dots \\ \ell_{1,i} & : x_i = m_i^1 x_1 + b_i^1 \\ & \dots \\ \ell_{1,N} & : x_N = m_N^1 x_1 + b_N^1 \end{cases}, \quad (3.3)$$

and the $N - 1$ points representing it are :

$$\bar{\ell}_{1,i} = (i - 1, b_i^1, 1 - m_i^1), \quad (3.4)$$

Intersection and non-intersections of lines

It is convenient to illustrate the situation in 4-D using the base-variable representation of a line:

$$x_i = v_i T + p_{o,i} = 1, 2, 3. \quad (3.5)$$

and shown in Fig. 3.7. There the intersection of two lines described by eq. (3.5), each represented by 3 indexed points $\bar{\ell}_{T_i}$, is constructed. For T denoting time and $x_1 x_2 x_3$ the space coordinates of a particle moving with constant velocity $\vec{V} = (v_1 v_2 v_3)$ and initial position $P_o = (p_{o,1}, p_{o,2}, p_{o,3})$ eq. (3.5), and equivalently it's 3 point representation, provide the complete trajectory information of the particle. The two sets of triple points $\bar{\ell}_{T_i}$ and $\bar{\ell}'_{T_i}$ describe the trajectories of two moving particles. The construction in Fig. 3.7 shows that two such particles collide since they go through the same point in space **at the same time** (i.e. there is a time-space intersection). Perhaps some of the power of the $\|\|$ -coordinate representation can be appreciated from this simple example.

inselberg-eg06notes.pdf

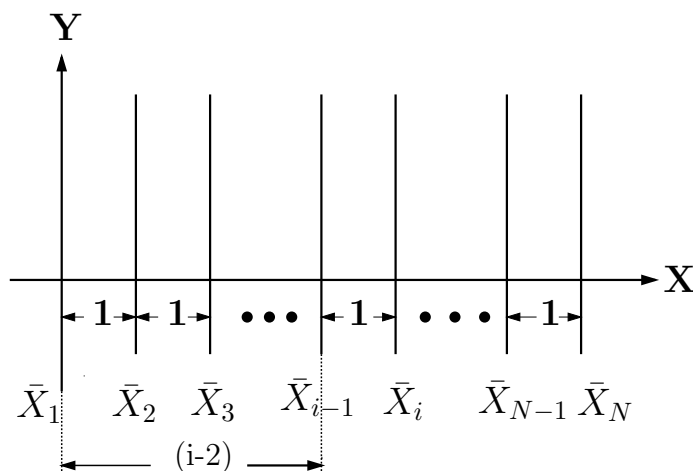


Figure 3.1: Spacing between adjacent axes is 1 unit.

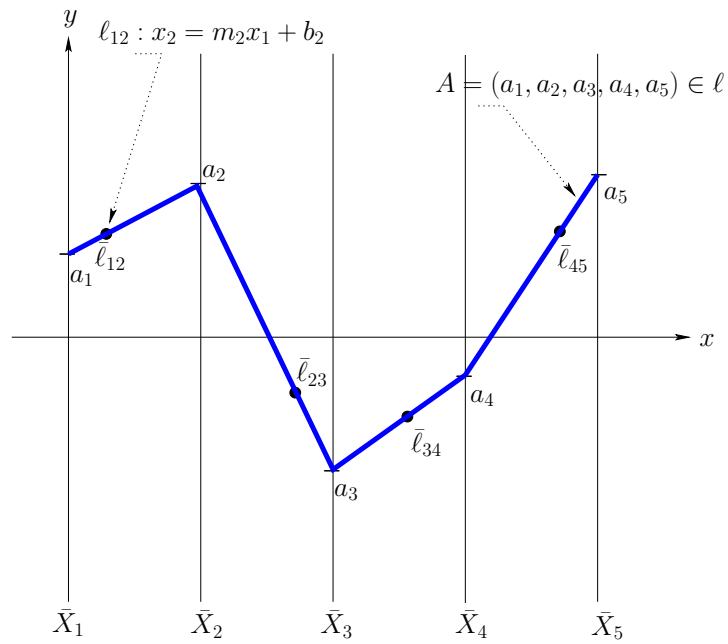


Figure 3.2: Point on line in 5-D.

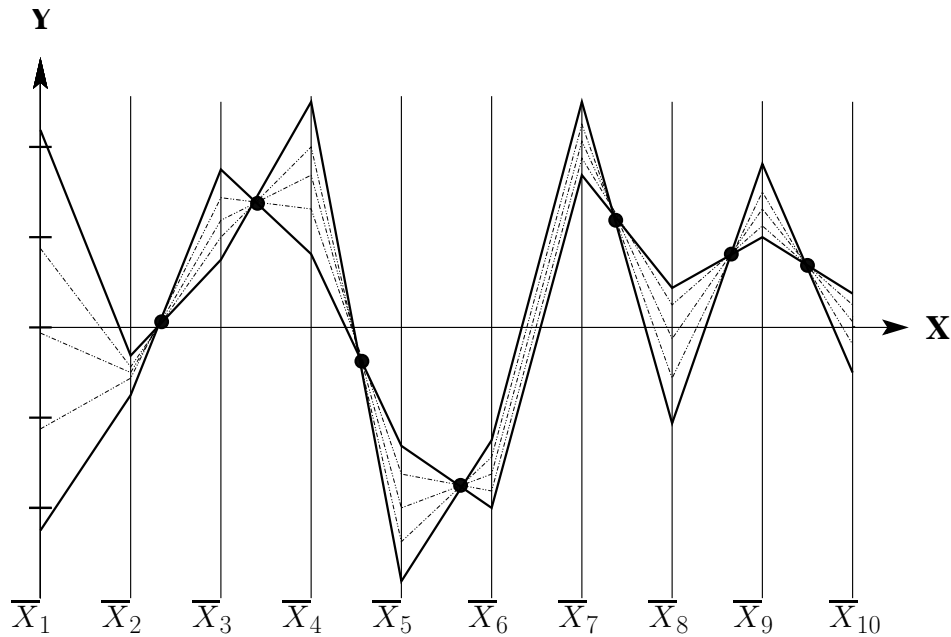


Figure 3.3: Line interval in 10-D – the thicker polygonal lines represent it's end-points. The adjacent variables representation, consisting of nine properly indexed points, is obtained by the sequential intersections of the polygonal lines' linear portions. Note that $\bar{l}_{1,2}$ is to the right of the X_2 -axis and $\bar{l}_{6,7}$ is an ideal point. The remaining points are in between the corresponding pairs of axes.

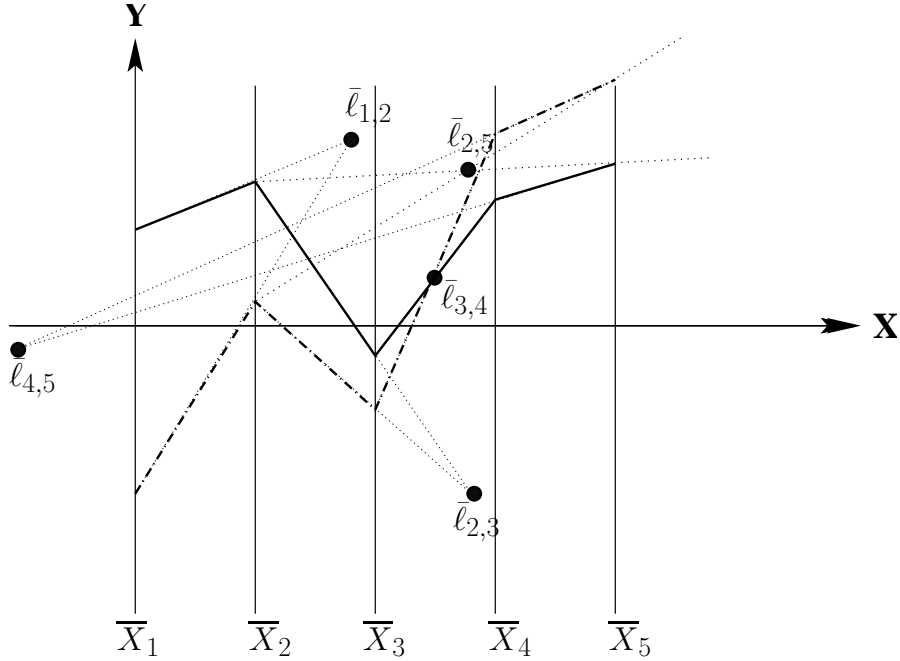


Figure 3.4: Algorithm for constructing a pairwise linear relation, in this case $\bar{\ell}_{25}$, given the $N - 1$ points, $\bar{\ell}_{i-1,i}$, representing the line.

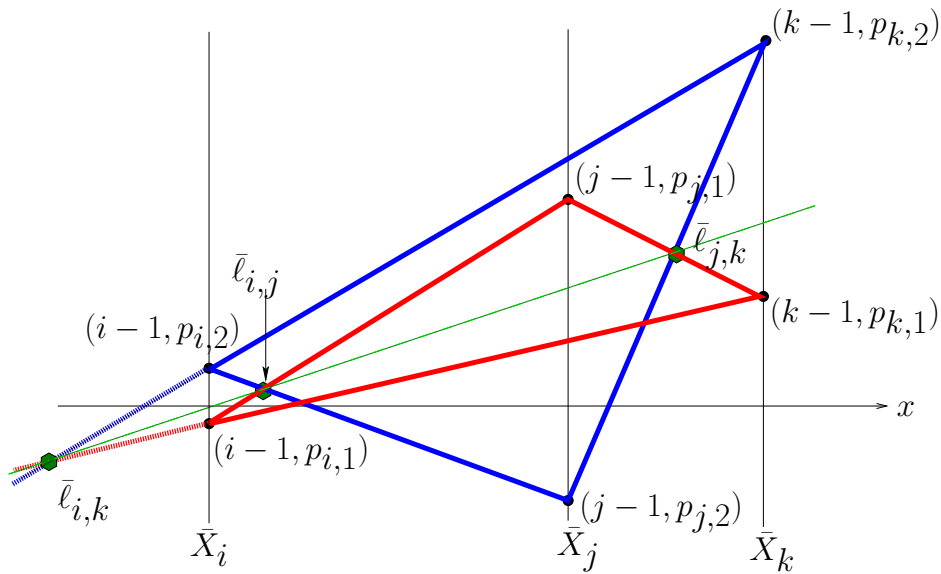


Figure 3.5: The Collinearity for the 3 points $\bar{\ell}_{i,j}, \bar{\ell}_{j,k}, \bar{\ell}_{i,k}$. The two triangles are in perspective with respect to the ideal point in vertical direction. The y-axis is offscale.

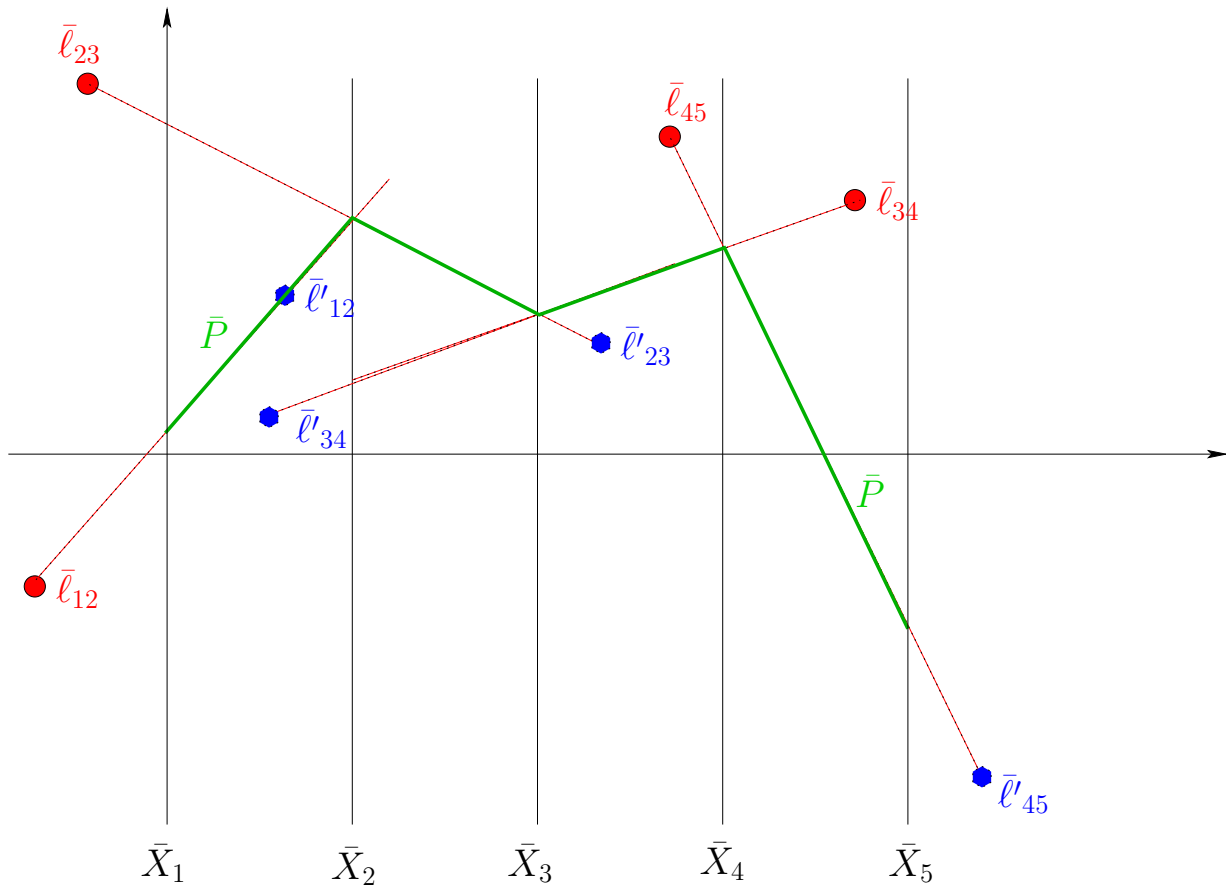


Figure 3.6: Two intersecting lines in 5-D.

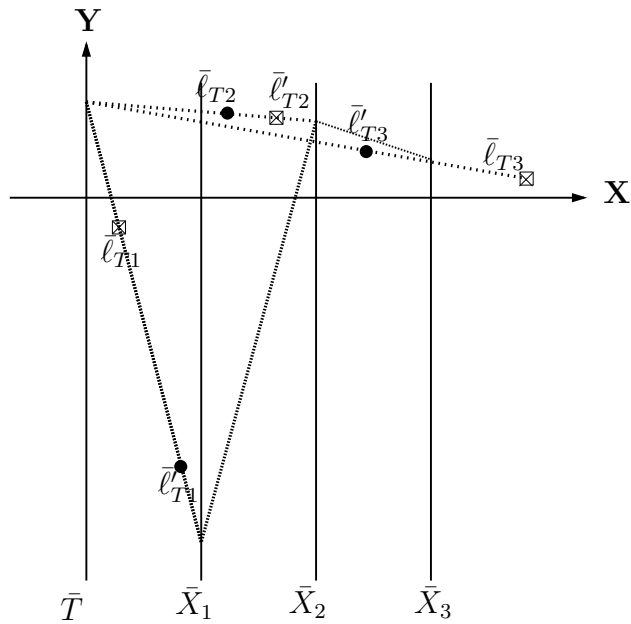


Figure 3.7: Intersection, for the base-variable line description, of two lines in 4-D. This provides the space **and** time coordinates of the place where two particles moving with constant velocity collide.

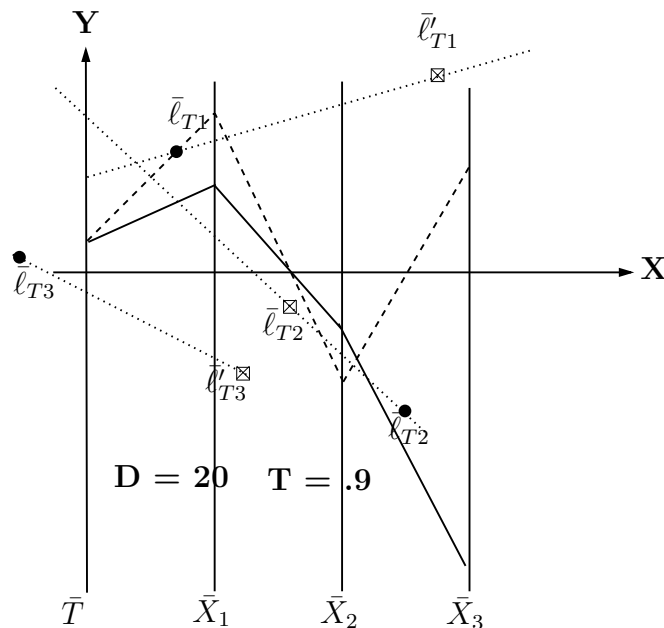


Figure 3.8: Non-intersection between two lines in 4-D. Here the minimum distance is 20 and occurs at time = .9. Note the maximum gap on the \bar{T} -axis formed by the lines joining the $\bar{\ell}$'s with the same subscript. The polygonal lines representing the points where the minimum distance occurs are shown and they have the *same* value of T.

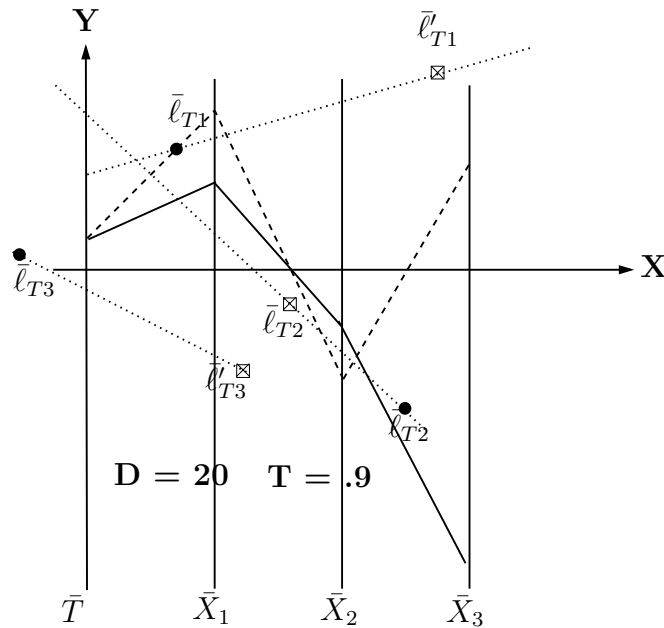


Figure 3.9: Non-intersection between two lines in 4-D. Here the minimum distance is 20 and occurs at time = .9. Note the maximum gap on the \bar{T} -axis formed by the lines joining the $\bar{\ell}$'s with the same subscript. The polygonal lines representing the points where the minimum distance occurs are shown and they have the *same* value of T.

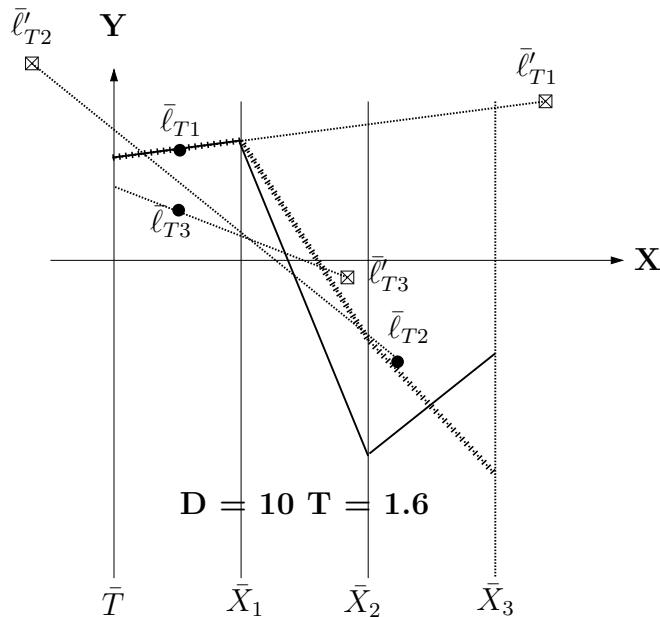


Figure 3.10: Non-intersection between two lines in 4-D. Here the minimum distance is 10 and occurs at time = 1.6. Note the the diminishing maximum gap on the \bar{T} -axis formed by the lines joining the $\bar{\ell}$'s with the same subscript and compare with Fig. 3.9. The polygonal lines representing the points where the minimum distance occurs are shown.

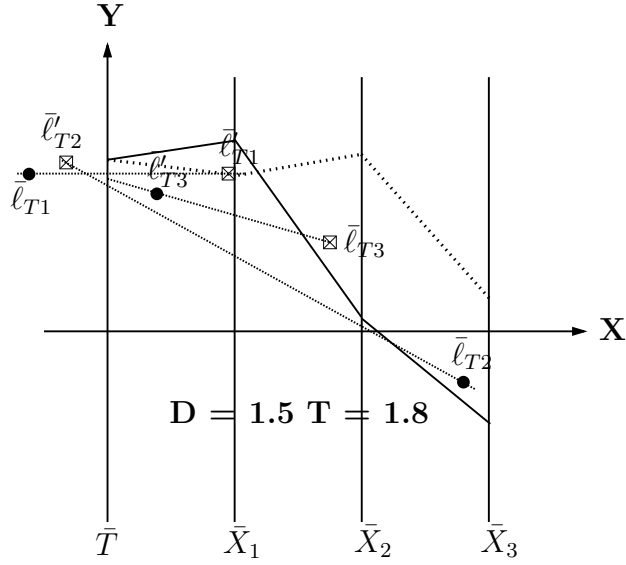


Figure 3.11: Near intersection between two lines in 4-D. Here the minimum distance is 1.5 and occurs at time = 1.8. Note the the diminished maximum gap on the \bar{T} -axis formed by the lines joining the $\bar{\ell}$'s with the same subscript. The polygonal lines representing the points where the minimum distance occurs are shown.

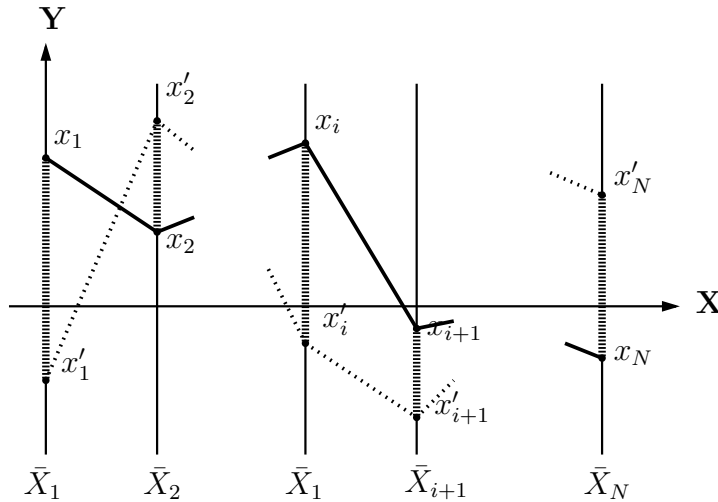


Figure 3.12: L_1 distance between the points $P = (x_1, \dots, x_i, \dots, x_N)$ and $P' = (x'_1, \dots, x'_i, \dots, x'_N)$.

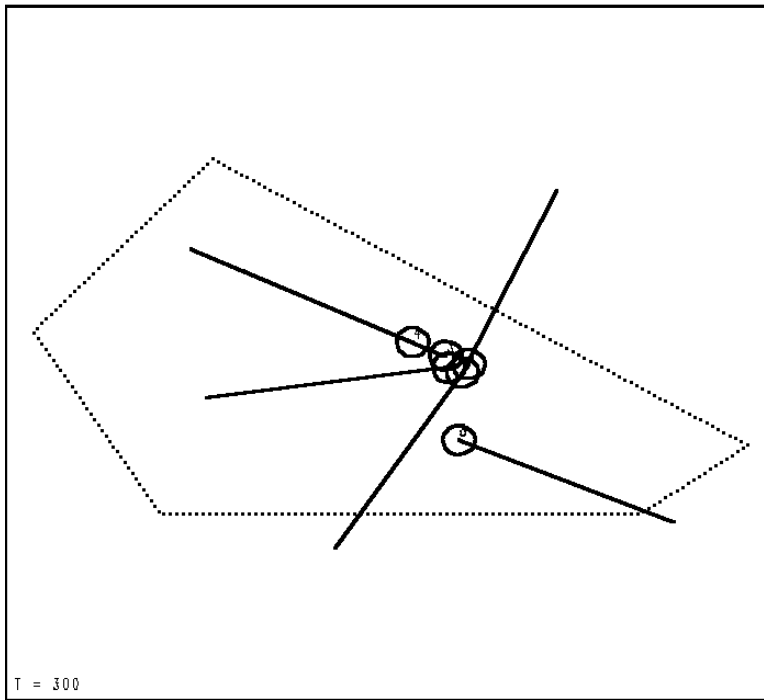


Figure 3.13: Conflicts, indicated by overlapping circles, within the next 5 minutes.

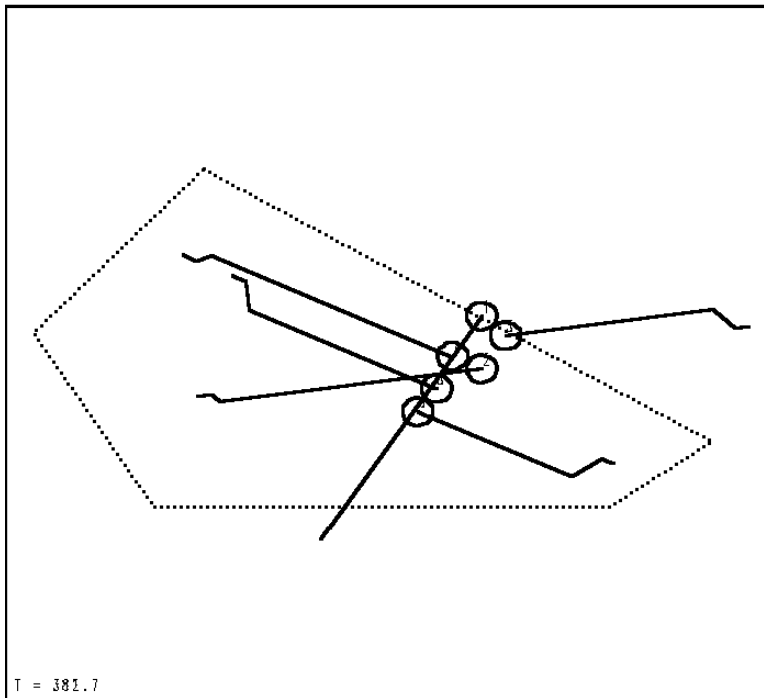


Figure 3.14: Conflict resolution with parallel-offset maneuvers. Three pairs of tangent circles.

Chapter 4

Planes, p-flats & Hyperplanes

Vertical Line Representation

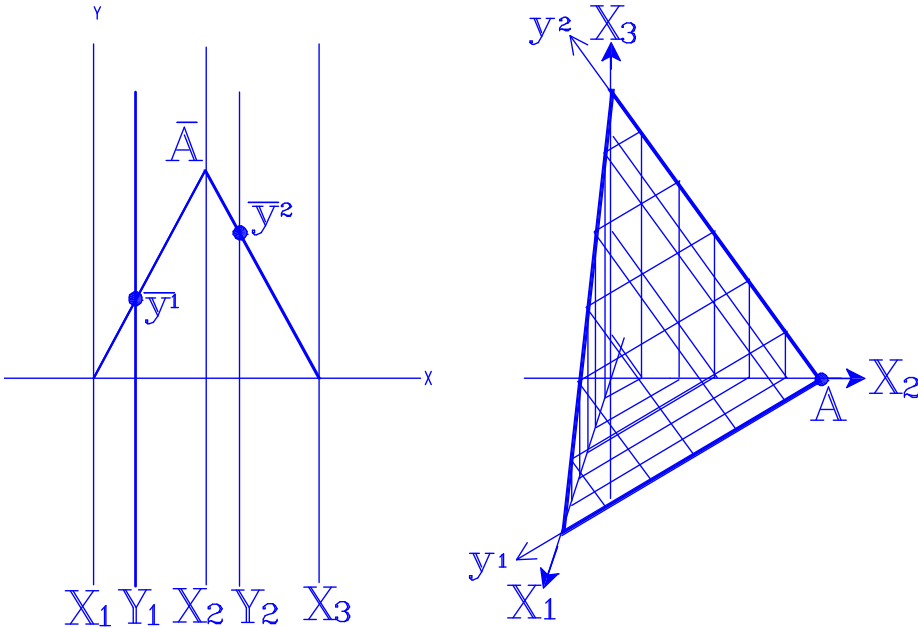


Figure 4.1: A plane π in \mathbb{R}^3 can be represented by two vertical lines and a polygonal line representing one of its points.

$$\ell : \begin{cases} \ell_{12} & : x_2 = m_2x_1 + b_2 \\ \ell_{23} & : x_3 = m_3x_2 + b_3 \end{cases} . \tag{4.1}$$

each value of k determines a (the rotated) plane and, in turn, the translated position $\bar{\eta}_{12}$:

$$\bar{\eta}_{12} = \left(\frac{m_3^2 - 2m_3 - k^2}{m_3^2 - m_3 + k^2(m_2 - 1)} , - \frac{b_2k^2 + m_3b_3}{m_3^2 - m_3 + k^2(m_2 - 1)} \right) \tag{4.2}$$

The above generalize to \mathbb{R}^N where a hyperplane being represented by $N - 1$ vertical lines.

Representation by Indexed Points

The family of “Super-Planes” \mathcal{E}

We consider the set of points $P \in \mathbb{R}^N$ whose representation in $\|\text{-coords}$ collapses to a straight line. They form a 2-D subspace (2-flat) That is, $\bar{P} : y = mx + b$ and for each choice of (m, b) the corresponding point is :

$$P = (md_1 + b, md_2 + b, \dots, md_N + b) = m(d_1, d_2, \dots, d_N) + b(1, \dots, 1) . \quad (4.3)$$

Therefore, the super-planes (abbr.*sp*) are on the line u containing the points $(0, 0, \dots, 0), (1, 1, \dots, 1)$. They can be described in terms of the axes spacing and for \mathbb{R}^3 the *sp* are given by:

$$\pi^s : (d_3 - d_2)x_1 + (d_1 - d_3)x_2 + (d_2 - d_1)x_3 = 0 \quad (4.4)$$

For the standard axes spacing used so far, $d_1 = 0, d_2 = 2, d_3 = 2$ the corresponding, called the first, *sp* is :

$$\pi_1^s : x_1 - 2x_2 + x_3 = 0 \quad (4.5)$$

For a plane

$$\pi : c_1x_1 + c_2x_2 + c_3x_3 = c_o , \quad (4.6)$$

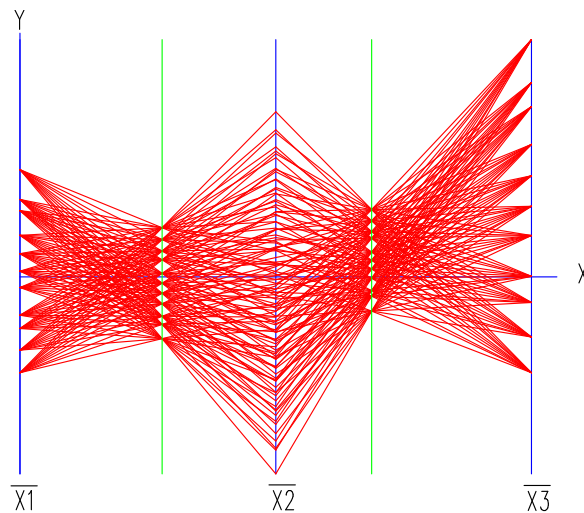


Figure 4.2: A set of coplanar points on a regular grid in \mathbb{R}^3 with the two vertical lines pattern.

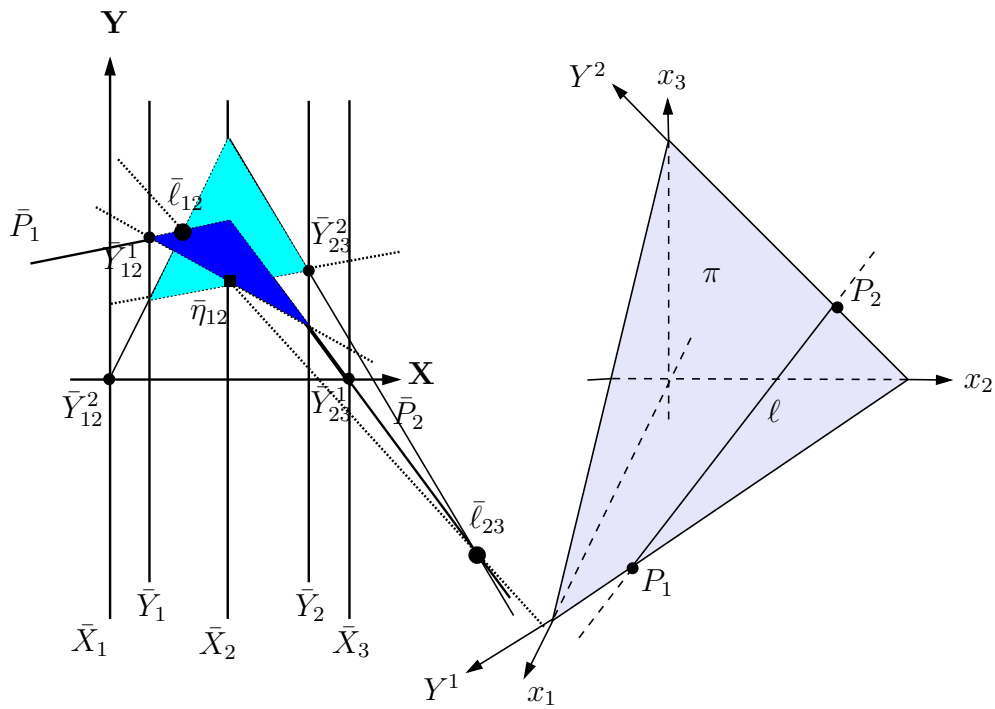


Figure 4.3: A line ℓ on a plane π is represented by one point $\bar{\eta}_{12}$ in terms of the coordinates (i.e. line in 2-D \rightarrow) point in \bar{Y}_1 and \bar{Y}_2 which is collinear with the two point $\bar{\ell}_{12}$ and $\bar{\ell}_{23}$. This is a consequence of Desargues projective geometry theorem.

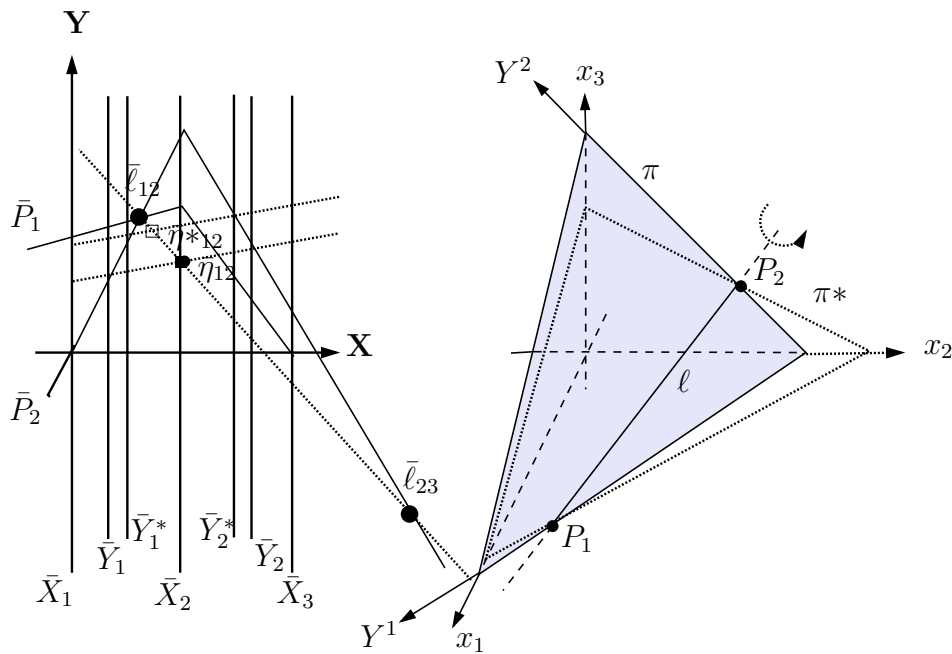


Figure 4.4: Rotation of a plane about a line \leftrightarrow Translation of a point along a line.

$$\ell_\pi = \pi \cap \pi_1^s : \begin{cases} \ell_{\pi_{12}} : x_2 = -\frac{c_1 - c_3}{c_2 + 2c_3}x_1 + \frac{c_o}{c_2 + 2c_3} \\ \ell_{\pi_{23}} : x_3 = -\frac{2c_1 + c_2}{c_3 - c_1}x_2 + \frac{c_o}{c_3 - c_1} \end{cases}, \quad (4.7)$$

These two points representing ℓ_π coincides since it is a line in a sp , and in homogeneous coordinates

$$\bar{\pi}_{123} = \bar{\ell}_{\pi_{12}} = \bar{\ell}_{\pi_{23}} = (c_2 + 2c_3, c_o, c_1 + c_2 + c_3). \quad (4.8)$$

This is the first indexed point for π . To understand its significance follow the next two figures. Next the axis \bar{X}_1 is translated to the position \bar{X}'_1 one unit to the right of the \bar{X}_3 providing the new axes spacing $d_1 = 4, d_2 = 1, d_3 = 2$. The corresponding sp is

$$\pi_{1'}^s : x_1 + x_2 - 2x_3 = 0. \quad (4.9)$$

The x_1 values of the coplanar points shown in Fig. 4.6 are transferred to the \bar{X}'_1 – see Fig. 4.10– and the construction in Fig. 4.7 is repeated providing the second point

$$\bar{\pi}_{231'} = \bar{\ell}'_{\pi_{1'2}} = \bar{\ell}'_{\pi_{23}} = (3c_1 + c_2 + 2c_3, c_o, c_1 + c_2 + c_3). \quad (4.10)$$

shown Fig. 4.11. These two points represent the plane π since from their coordinates

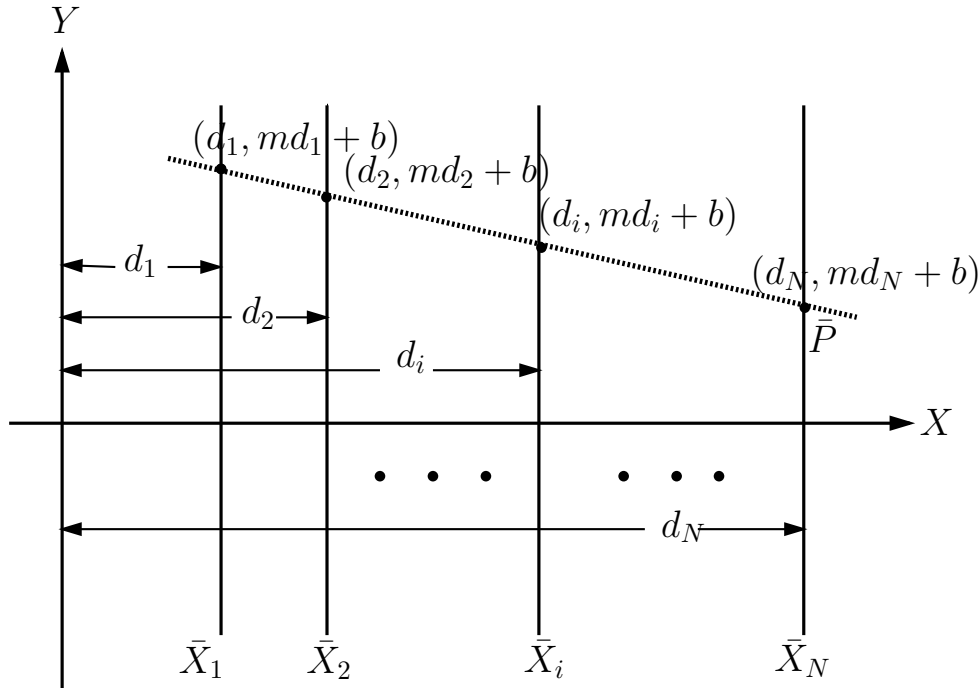


Figure 4.5: Points in \mathbb{R}^N represented by lines.

the coefficients of eq. (4.6). Geometrically, we have determined the plane π by the two lines $\ell_\pi, \ell'_\pi \subset \pi$ shown in Fig. 4.12. A plane in \mathbb{R}^3 can be specified in terms of any two intersecting lines it contains. The reason for choosing the lines in the sp is that in \parallel -coords such lines are represented by **one** rather than two points and there are further advantages. Note that

$$\bar{\pi}_{231'} - \bar{\pi}_{123} = (3c_1, 0, 0) . \quad (4.11)$$

The four Indexed Points

The \bar{X}_2 and \bar{X}_3 axes are each translated to positions \bar{X}'_2 and \bar{X}'_3 3 units to the right providing the third

$$\pi_{1'2'}^s : -2x_1 + x_2 + x_3 = 0 , \quad (4.12)$$

and similarly the fourth sp $\pi_{1'2'3'}^s$. Two new points are constructed and shown in Fig. 4.13 As for the previous 2 points

$$\begin{cases} \bar{\pi}_{31'2'} - \bar{\pi}_{231'} = (3c_2, 0, 0) \\ \bar{\pi}_{31'2'} - \bar{\pi}_{1'2'3'} = (3c_3, 0, 0) . \end{cases} \quad (4.13)$$

It is easily checked that the translations correspond to 120° rotations of the sp π_1^s about the line u on the points $(0, 0, 0), (1, 1, 1)$ with $\pi_{1'2'3'}$ coinciding with π_1^s . To simplify notation the index permutation is unimportant so that $\pi_{231'} = \pi_{1'23}$.

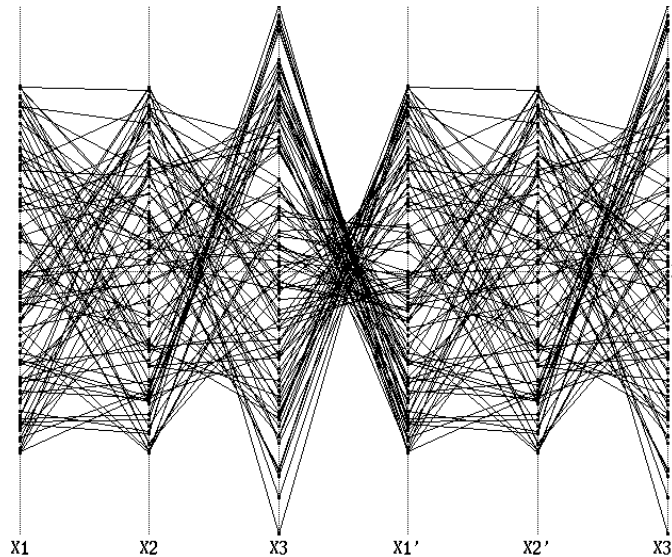


Figure 4.6: On the first 3 axes a set of polygonal lines representing a randomly sampled set of points on a plane $\pi \subset \mathbb{R}^3$.

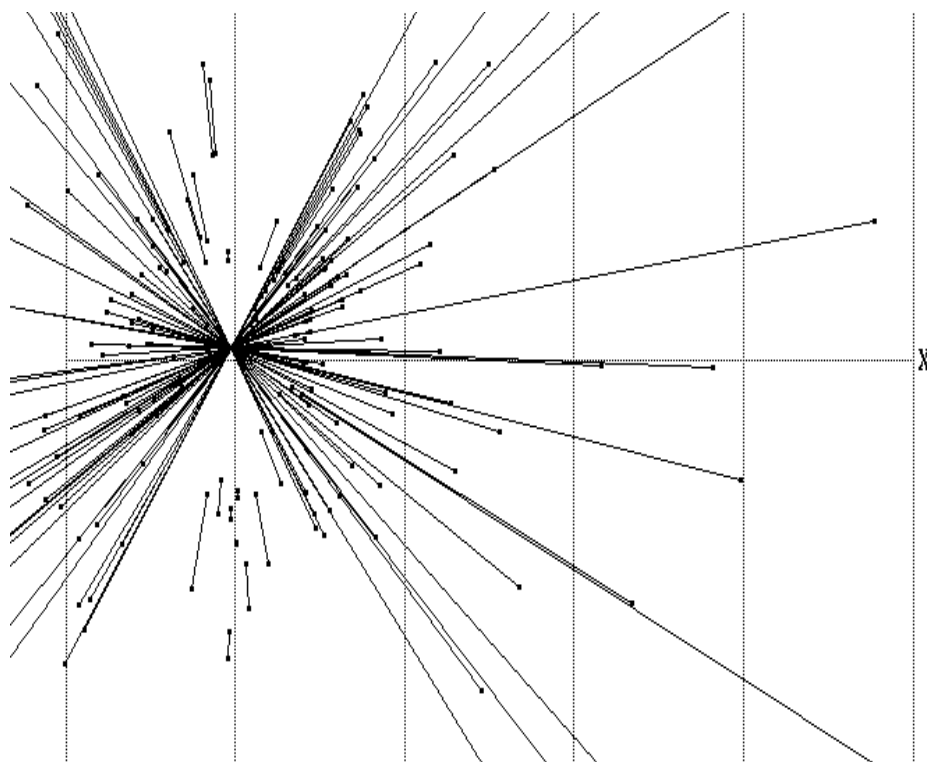


Figure 4.7: Coplanarity! In \parallel -coords joining the pairs of points representing lines on a plane forms a pencil of lines on a point. The point shown is $\bar{\pi}_{123}$ in eq. (4.8). Review also the 3-point-collinearity for multidimensional lines (previous chapter).

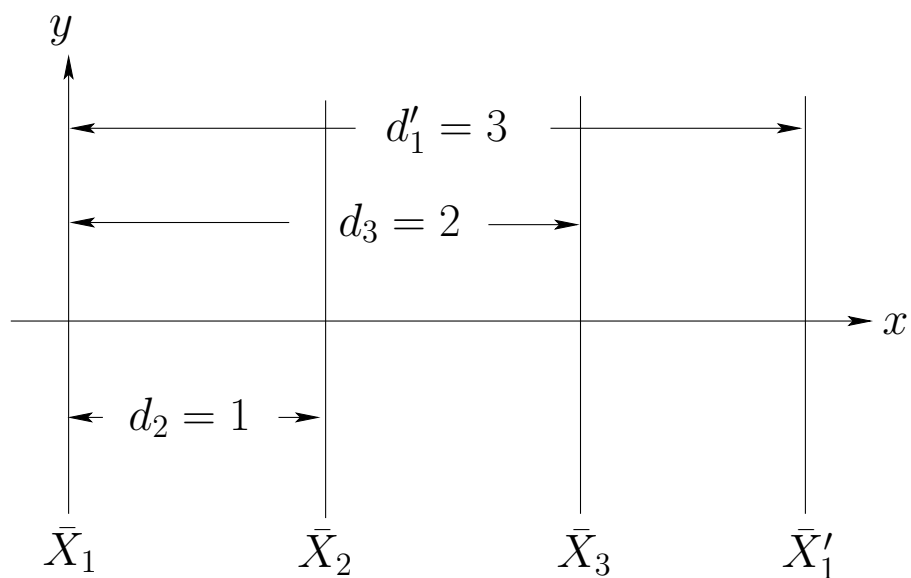


Figure 4.8: The axes spacing for the second super-plane π_1^s .

Rotation of a Plane about a Line and the Dual Translation

Hyperplanes and p-flats in \mathbb{R}^N

Theorem A p-flat in \mathbb{R}^N given by eq. (??) is represented by the $(N - p)p$ points :

$$\bar{\pi}_{i\dots N1'\dots(i-1)'} = \left(\sum_{k=1}^{p+1} d_{ik}c_{ik}, c_o, \sum_{k=1}^{p+1} c_{ik} \right), \quad (4.14)$$

where $i = 1, \dots, N - p$, d_{ik} are the distances specified by the standard axes spacing $S_{1'\dots i'}$ after the translation of the \bar{X}_i to the \bar{X}'_i axes and $i' = 1', \dots, p'$.

Collinearity Property

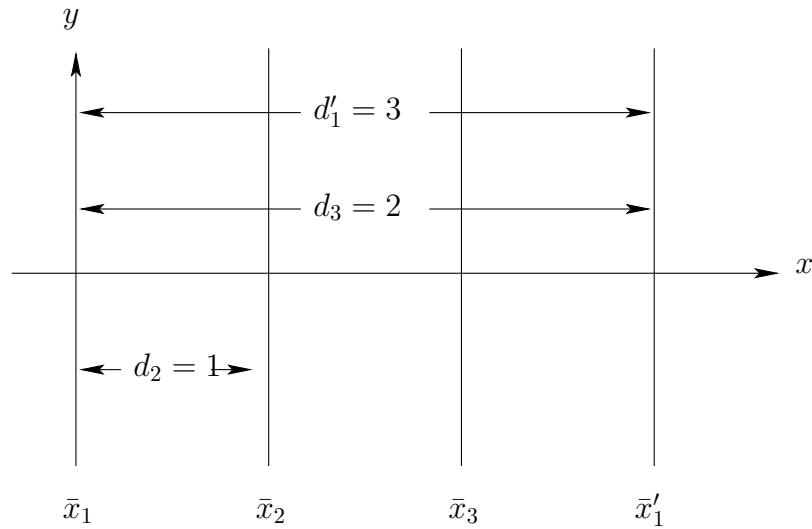


Figure 4.9: The axes spacing for the second super-plane $\pi_{1'}^s$.

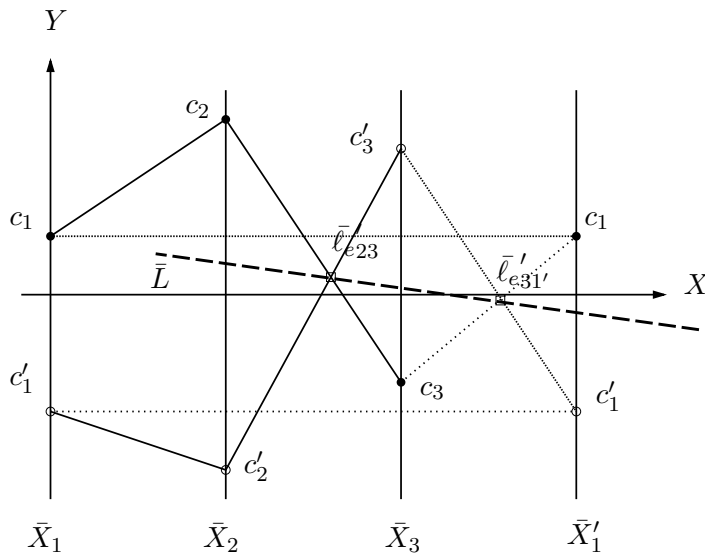


Figure 4.10: Transferring the values from the \bar{X}_1 to the \bar{X}'_1 -axis.

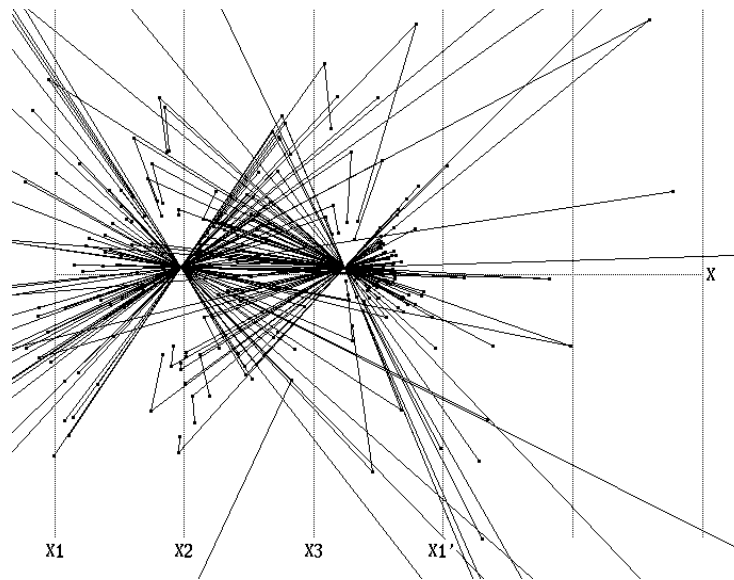


Figure 4.11: The plane π represented by two points

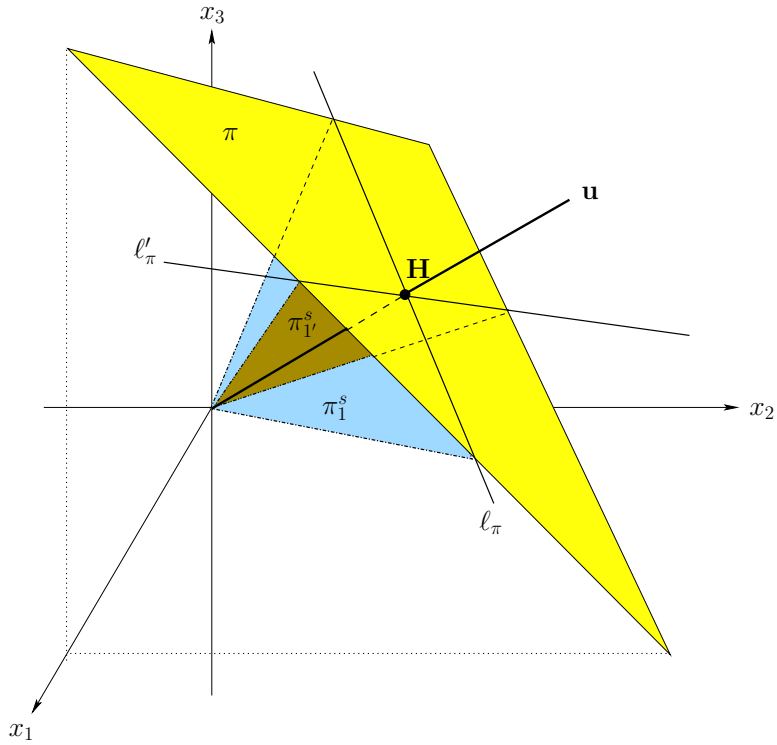


Figure 4.12: The intersections of a plane π with the two super-planes π_1^s and $\pi_1'^s$ are two lines ℓ_π , ℓ'_π which specify the plane and provide its representation. This is the equivalent of the previous figure but in cartesian coordinates.

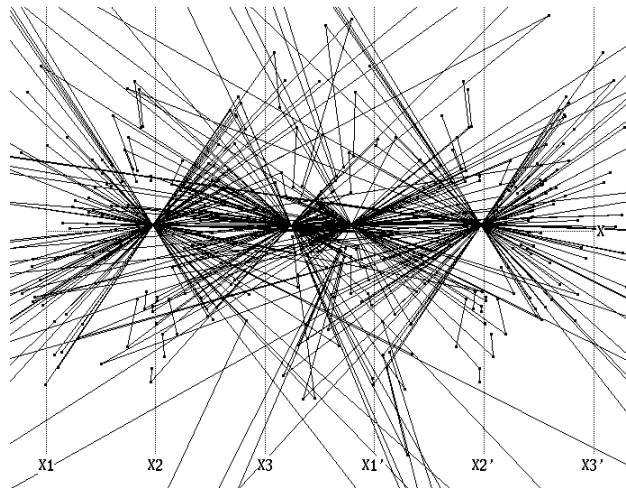


Figure 4.13: The plane π intersected with four super-planes. Each point represents one of the intersection lines.

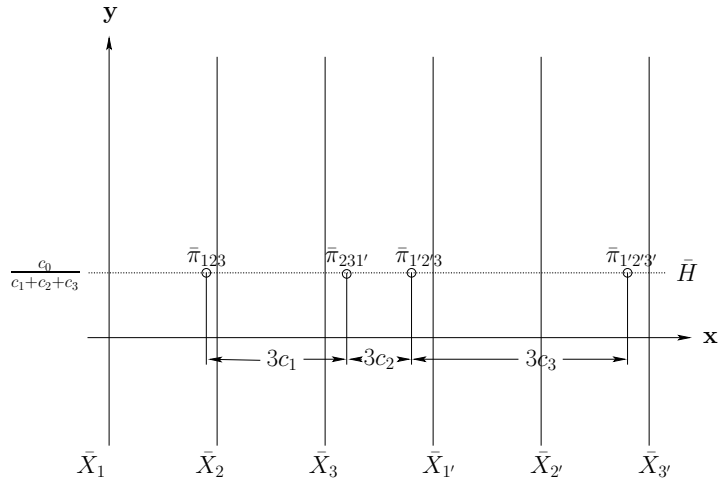


Figure 4.14: The distances between adjacent points are proportional to the coefficients of $\pi : c_1x_1 + c_2x_2 + c_3x_3 = c_0$. The proportionality constant is the dimensionality of the space. The plane's equation can be read from the picture!

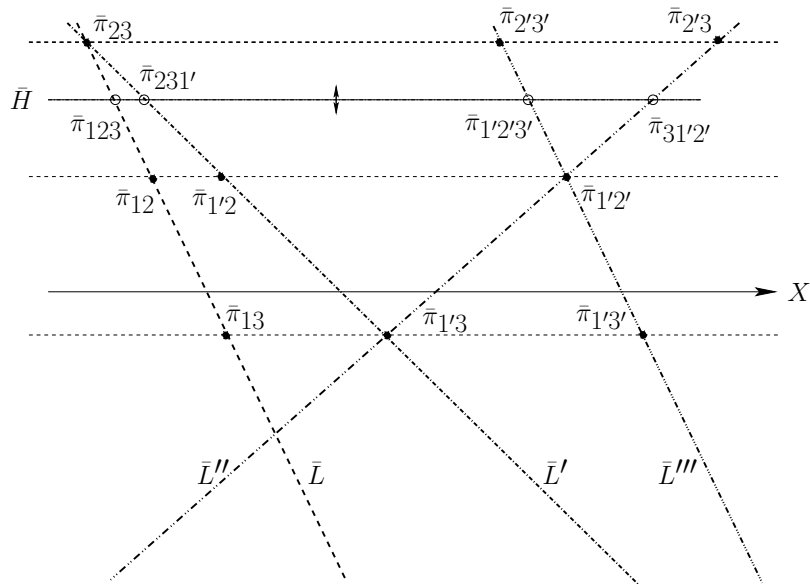


Figure 4.15: Rotation of a 2-flat (plane) about a 1-flat(line) in \mathbb{R}^3 corresponds to a translation of the points with 3 indices on the horizontal line \bar{H} along the lines \bar{L} , \bar{L}' , \bar{L}'' , \bar{L}''' joining the points with 2 indices.

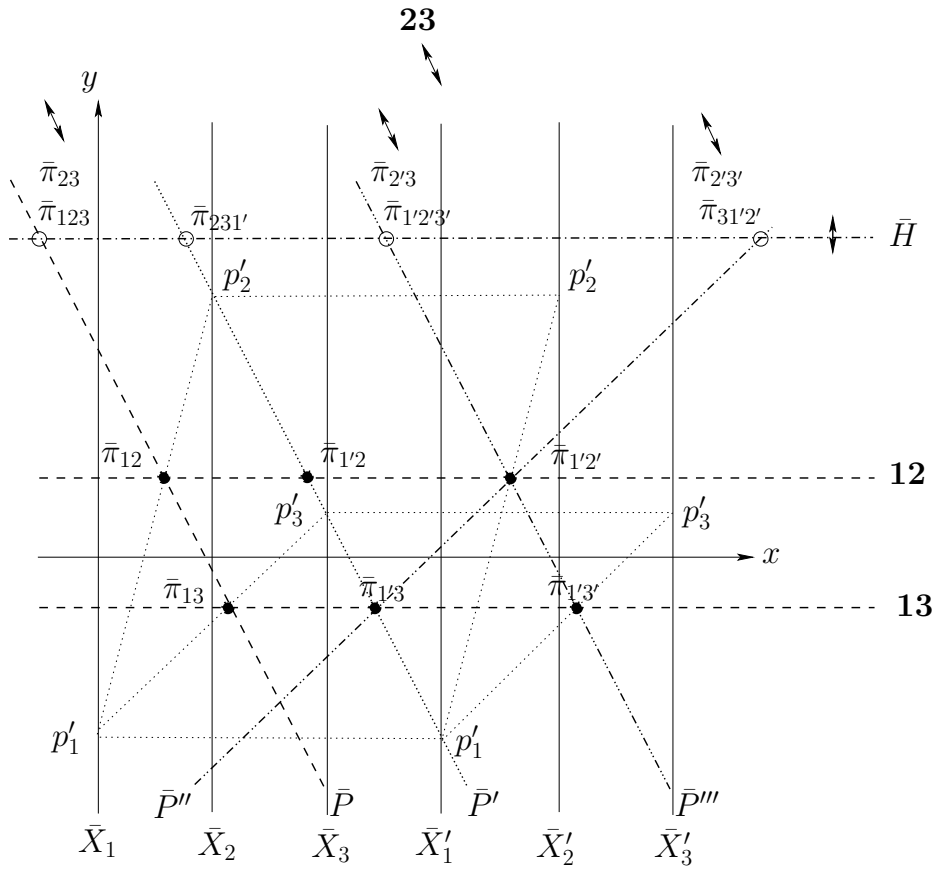


Figure 4.16: Rotation of a plane π^2 about a line π^1 such that c_1 remains constant.

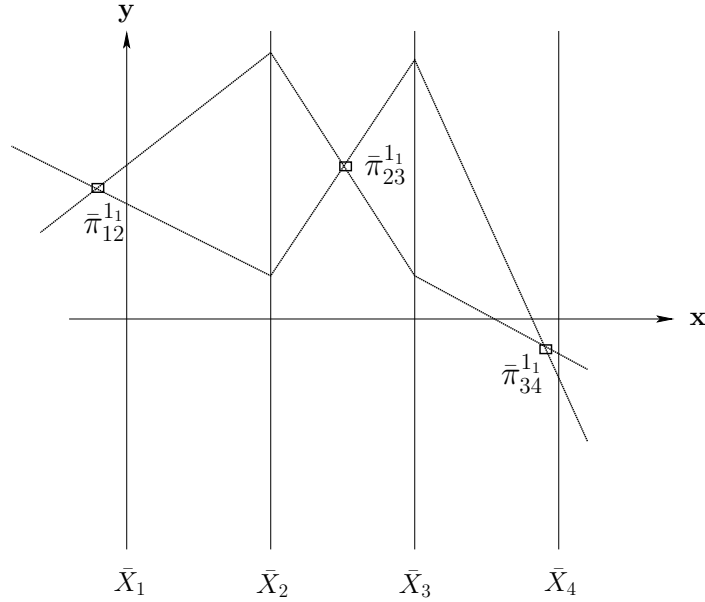


Figure 4.17: Recursive Construction in \mathbb{R}^4 – 1st step. A pair of points (polygonal lines) determines a line (1-flat) π^{1_1} represented by the 3 constructed points $\bar{\pi}_{i,i-1}^{1_1}$, $i = 1, 2, 3, 4$.

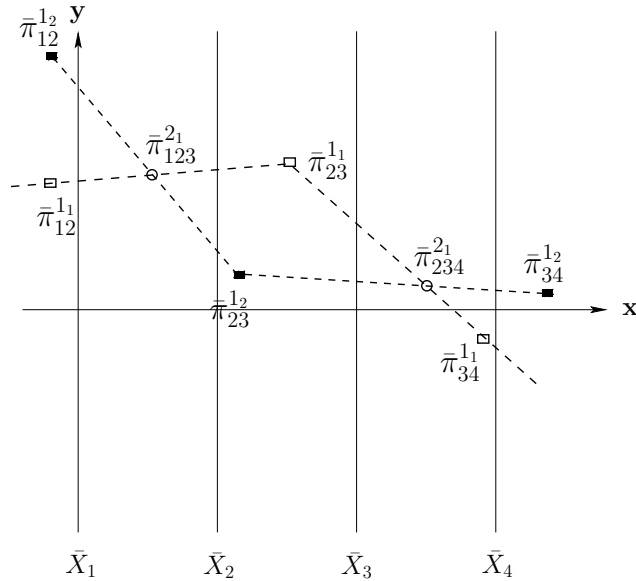


Figure 4.18: Recursive Construction in \mathbb{R}^4 – 2nd step. The 1-flat π^{1_1} and another π^{1_2} , represented by the 3 black points, determine a 2-flat (plane) π^{2_1} represented by the two points $\bar{\pi}_{123}^{2_1}$, $\bar{\pi}_{234}^{2_1}$. These points are the intersections of the two polygonal lines joining the points obtained from the previous step representing 1-flats.

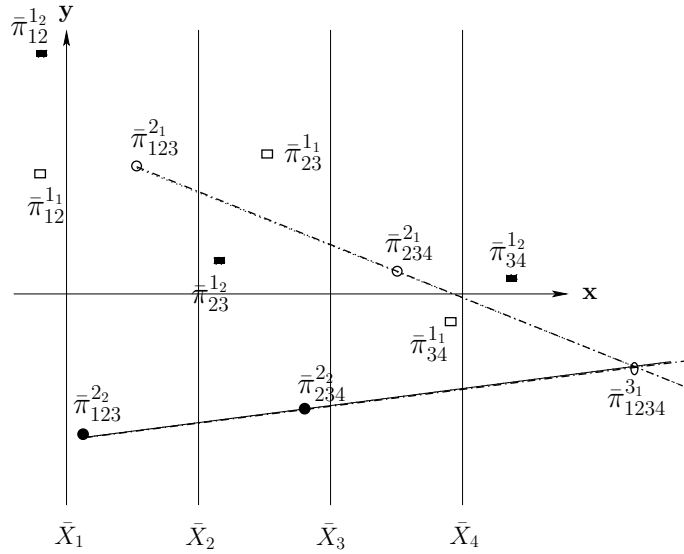


Figure 4.19: Recursive Construction in \mathbb{R}^4 – 3rd step. Two 2-flats, π^{2^1} constructed above and another π^{2^2} represented by the 2 black points, determine a 3-flat π^{3^1} . Pairs of points representing the same 2-flat are joined and their intersection is the point $\bar{\pi}_{1234}^{3^1}$. This is one of the 3 points representing the 3-flat. The “debris” from the previous constructions, points with fewer than 4 indices, can be discarded.

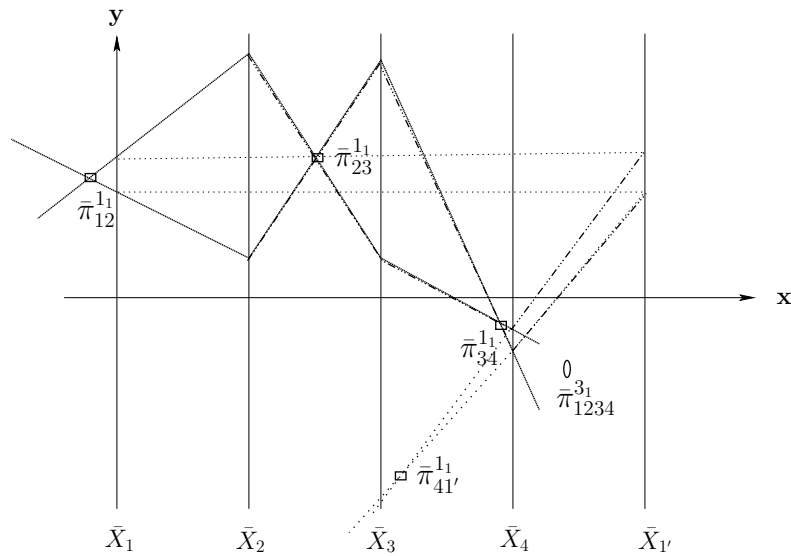


Figure 4.20: Recursive Construction in 4-D – 4th step. A new axis $\bar{X}_{1'}$ is placed one unit to the right of \bar{X}_3 and the x_1 values are transferred to it from the \bar{X}_1 axis. Points are now represented by new polygonal lines between the \bar{X}_2 and $\bar{X}_{1'}$ axes and one of the points $\bar{\pi}_{41'}^{1^1}$, representing the 1-flat π^{1^1} on the new triple of $\|\text{-coords}$ axes, is constructed as in 1st step.

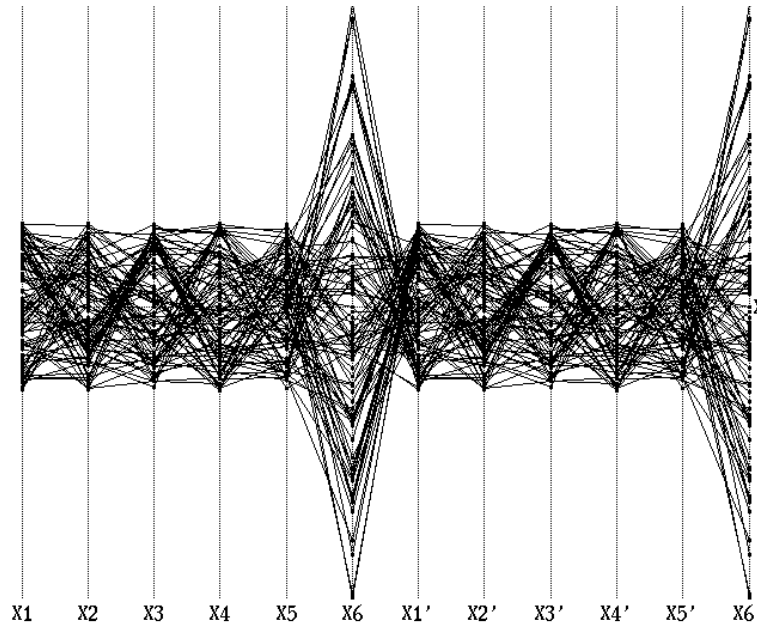


Figure 4.21: Polygonal lines on the $\bar{X}_1 \dots \bar{X}_6$ axes representing randomly selected points on a 5-flat $\pi^5 \subset \mathbb{R}^6$.

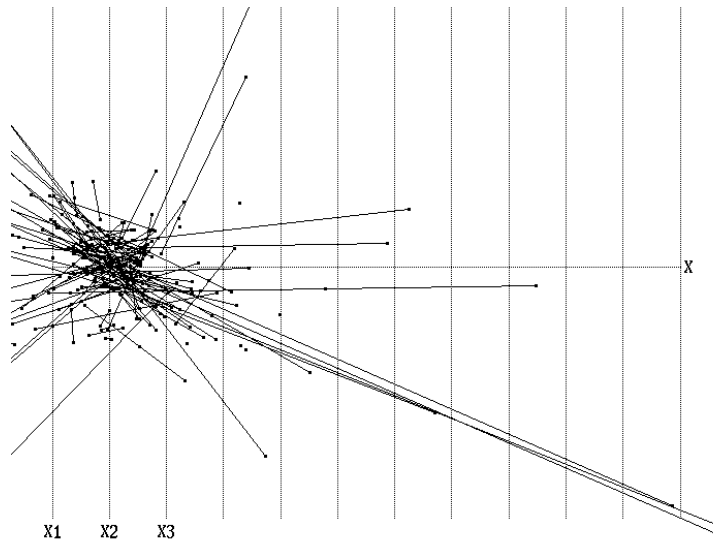


Figure 4.22: The $\bar{\pi}_{12}^{1_i}, \bar{\pi}_{23}^{1_i}$ portions of the 1-flats $\subset \pi^5$ constructed from the polygonal lines shown in Fig. 4.21, no evident pattern.

Remarkably, the collinearity construction property can be extended to higher dimensions enabling the recursive (on the dimensionality) construction of the representation of p-flats for $2 \leq p \leq N - 1$. To achieve this some intermediate steps are needed. In the ensuing, we denote by $\pi_{1' \dots i'}$ the “super-plane” constructed by translating the axes $\bar{X}_1, \dots, \bar{X}_i$ to the new positions $\bar{X}_{1'}, \dots, \bar{X}_{i'}$. Here $d_i = N + i - 1$ and for easy reference the partially translated standard axes spacing is denoted by $S_{1' \dots i'}$.

The underpinning of the construction algorithm for the point representation of a 2-flat $\pi^2 \subset \mathbb{R}^3$, as we saw, is the collinearity property. Namely for *any* $\pi^1 \subset \pi^2$ the points $\bar{\pi}_{12}^1, \bar{\pi}_{13}^1, \bar{\pi}_{23}^1$ are collinear with $\bar{\pi}_{123}$. The generalization for p-flats is also true. Without entering into the technical details yet for $\pi^{(p-2)}_1, \pi^{(p-2)}_2 \subset \pi^{(p-1)} \subset R^N$, let \bar{L}_1 and \bar{L}_2 be the lines determined by the corresponding two points

$$\bar{L}_1 : \bar{\pi}_{123 \dots (p-1)}^{(p-2)}_1, \bar{\pi}_{23 \dots (p-1)p}^{(p-2)}_1, \bar{L}_2 : \bar{\pi}_{123 \dots (p-1)}^{(p-2)}_2, \bar{\pi}_{23 \dots (p-1)p}^{(p-2)}_2 .$$

Then

$$\bar{\pi}_{123 \dots p}^{(p-1)} = \bar{L}_1 \cap \bar{L}_2 .$$

This is the basic recursive construction implied in the *Representation Mapping* stated formally below. Though the notation looks cumbersome the idea is not and to clarify it we illustrate it for $N = 4, p = 3$ in Figs. 4.17 through 4.20. Starting with the polygonal lines on a 3-flat π^{31} , first the points $\bar{\pi}_{12}^1, \bar{\pi}_{23}^1, \bar{\pi}_{34}^1$, representing 1-flats (lines) on π^3 , are constructed and joined to form polygonal lines having 3 vertices (the points) joined by **two** lines. From the intersection of these new polygonal lines the points $\bar{\pi}_{123}^2, \bar{\pi}_{234}^2$, representing 2-flats on π^{31} , are constructed. At any stage a point representing $\bar{\pi}^r$, where the superscript is the flat’s dimension, is obtained by *any pair* of lines joining points representing a flat $\bar{\pi}^{r-1}$ where $\pi^{r-1} \subset \pi^r$.

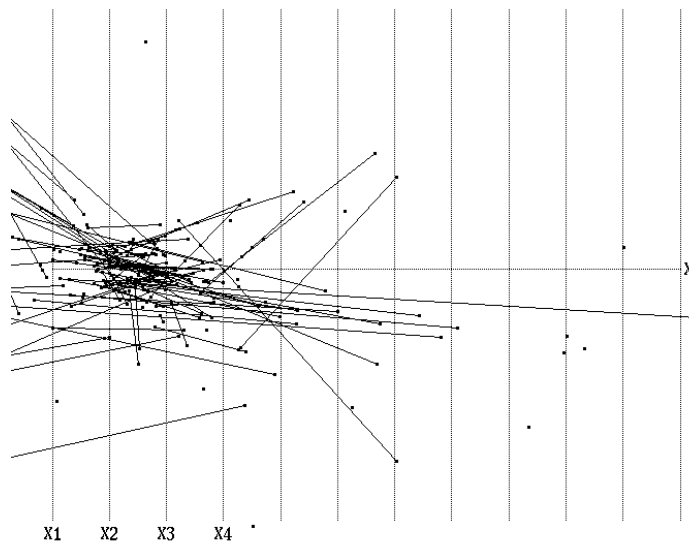


Figure 4.23: The $\bar{\pi}_{123}^2, \bar{\pi}_{234}^2$ portions of the 2-flats $\subset \pi^5$ constructed from the polygonal lines joining $\bar{\pi}_{12}^1, \bar{\pi}_{23}^1, \bar{\pi}_{34}^1$.

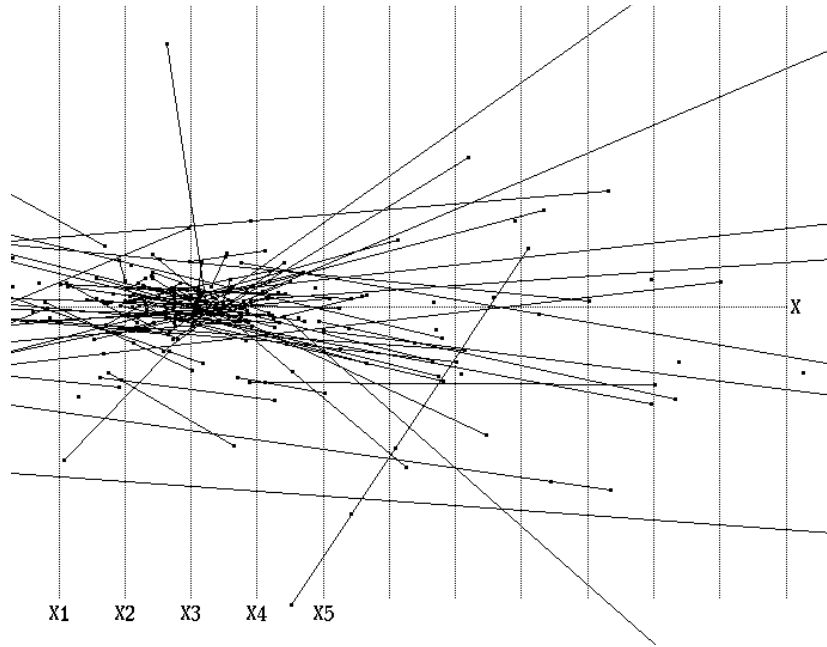


Figure 4.24: The $\bar{\pi}_{1234}^{3_i}$, $\bar{\pi}_{2345}^{3_i}$, of the 3-flats $\subset \pi^5$ constructed from the polygonal lines joining $\bar{\pi}_{123}^{2_i}$, $\bar{\pi}_{234}^{2_i}$, $\bar{\pi}_{345}^{2_i}$. Nothing yet ... but wait!

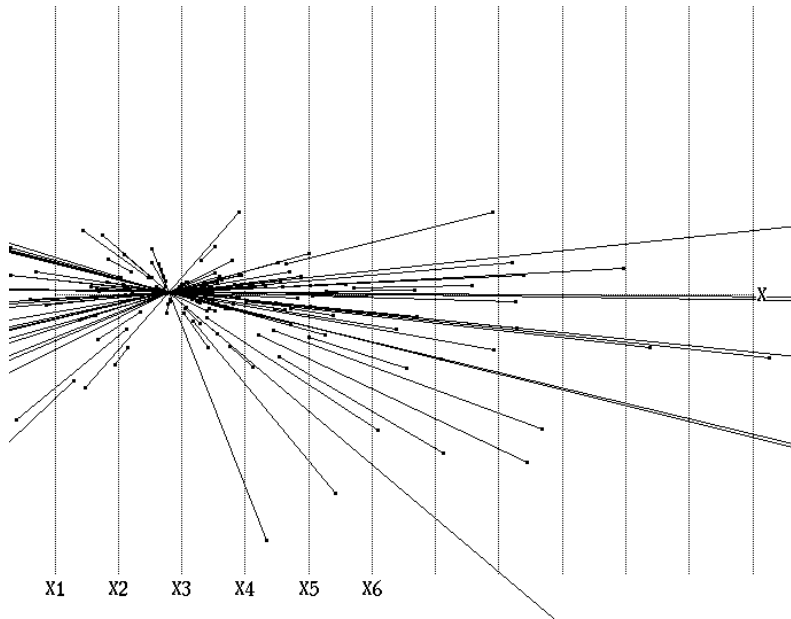


Figure 4.25: This is it! The $\bar{\pi}_{12345}^{4_i}$, $\bar{\pi}_{23456}^{4_i}$ of the 4-flats $\subset \pi^5$ constructed from the polygonal lines joining $\bar{\pi}_{1234}^{3_i}$, $\bar{\pi}_{2345}^{3_i}$, $\bar{\pi}_{3456}^{3_i}$. This shows that the original points whose representation is in Fig. 4.21 are on a 5-flat in \mathbb{R}^6 . The remaining points of the representation are obtained in the same way.

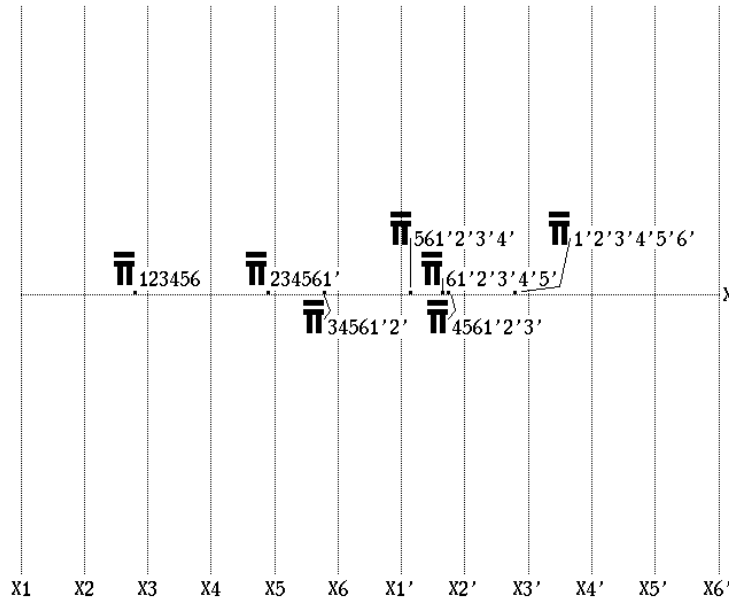


Figure 4.26: The full representation of π^5 . The coefficients of its equation are still the distances between sequentially indexed points as in Fig. 4.14 for \mathbb{R}^3 .

Detecting Near Coplanarity

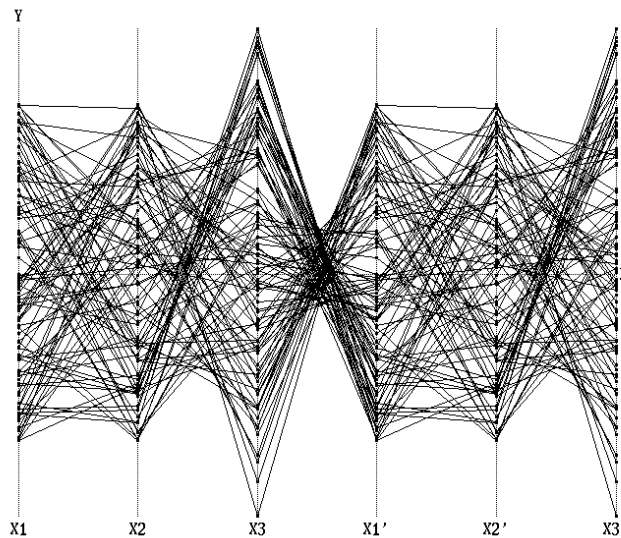


Figure 4.27: Polygonal lines representing a randomly selected set of “nearly” coplanar points (i.e. on a “slab”)

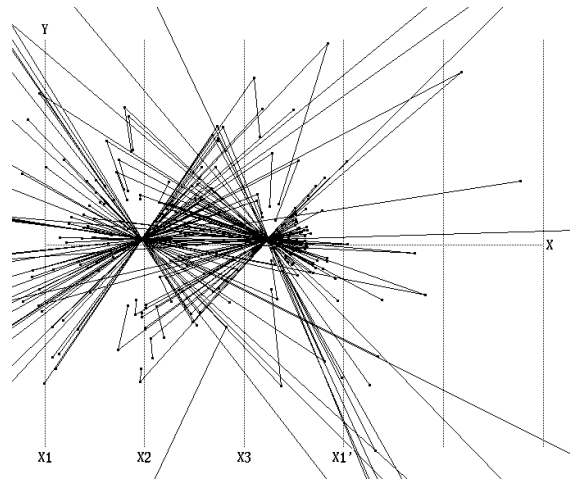


Figure 4.28: Representation of lines formed from the points shown in Fig. 4.27. The pattern for “near-coplanarity” is very similar to that obtained from coplanarity

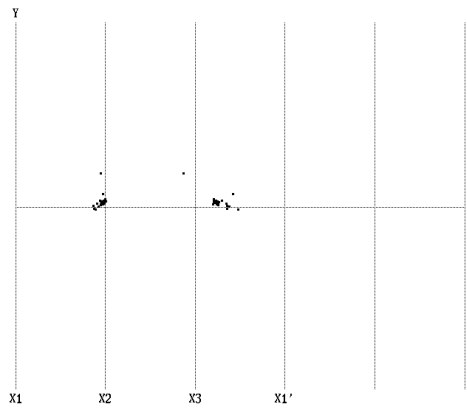


Figure 4.29: Close clusters from the intersection of the lines shown in Fig. 4.28

Bibliography

- [1] A.F. Beardon. *The Geometry of Discrete Groups*. Springer-Verlag, New York, 1983.
- [2] A. Chatterjee. *Visualizing Multidimensional Polytopes and Topologies for Tolerances*. Ph.D. Thesis, Dept. Comp. Sci., Univ. of S. Calif., 1995.
- [3] D. Cox, J. Little, and D. O’Shea. *Ideals, Varieties, and Algorithms*. 2nd edition, Springer-Verlag, New York, 1997.
- [4] B. Dimsdale. *Conic Transformations – IBM LASC Tech. Rep. G320-2713*. IBM LA Scientific Center, 1981.
- [5] B. Dimsdale. *Conic Transformations and Projectivities – IBM LASC Tech. Rep. G320-2753*. IBM LA Scientific Center, 1984.
- [6] L. Ernstom. A plucker formula for the singular projective varieties. *Commut. Algebra.*, 5-9:2897–2901, 1997.
- [7] J. Harris. *Algebraic Geometry*. Springer-Verlag, New York, 1992.
- [8] W. Hodge and D. Pedoe. *Methods of Algebraic Geometry, Vol. II*. Cambridge Univ. Press, Cambridge, 1952.
- [9] C.K. Hung and A. Inselberg. *Parallel Coordinate Representation of Smooth Hypersurfaces*. Univ. of S. Calif. Tech. Report # USC - CS - 92 -531, Los Angeles, 1992.
- [10] A. Inselberg. The plane with parallel coordinates. *Visual Computer*, 1:69–97, 1985.
- [11] A. Inselberg and B. Dimsdale. Multidimensional lines ii: Proximity and applications. *SIAM J. of Applied Math.*, 54-2:578–596, 1994.
- [12] A. Inselberg and C.K. Hung. *A New Representation of Hypersurfaces in Terms of their Tangent Hyperplanes*. In *Tutorial on Multidimensional Visualization – ACM SIGGRAPH*, 1995.
- [13] A. Inselberg, M. Reif, and T. Chomut. Convexity algorithms in parallel coordinates. *J. ACM*, 34:765–801, 1987.
- [14] M. M. Lipschutz. *Differential Geometry*. Shaum’s Outlines on Math., McGraw-Hill, New York, 1969.

- [15] T. Matskewich, A. Inselberg, and M. Bercovier. *Approximated Planes in Parallel Coordinates*. Proc. of Geometric Model. Conf., St. Malo, Vanderbilt Univ. Press, 257-266, 2000.
- [16] R. J. Walker. *Algebraic Curves*. Springer-Verlag, New York, 1978.
- [17] V. O. Ya. Some integral calculus based on euler characteristic, lect. notes. *Amer. Math. Monthly*, 1346:127–138, 1988.

Chapter 5

Curves

5.1 Point-Curves and Line-Curves

Recall the fundamental duality in the plane point-to-line correspondence :

$$P : (p_1, p_2, p_3) \longrightarrow \bar{P} : [(p_1 - p_2), dp_3, -dp_1] , \tag{5.1}$$

where the distance between the x_1 and x_2 axes is d , and as usual, the triples within [...] and within (...) denote line and point homogeneous coordinates respectively. For regular (i.e. in the Euclidean plane) points

$$P : (p_1, p_2, 1) \longrightarrow \bar{P} : [(p_1 - p_2), d, -dp_1].$$

The second half of the duality is the line-to-point correspondence :

$$\ell : [a_1, a_2, a_3] \longrightarrow \bar{\ell} : (da_2, -a_3, a_1 + a_2), \tag{5.2}$$

where the $a_i, i = 1, 2$ are the coefficients of the x_i in the equation of ℓ and a_3 is the constant. When $a_2 \neq 0$, the slope of ℓ is $m = -\frac{a_1}{a_2}$ and the intercept $b = -\frac{a_3}{a_2}$ so :

$$\ell : [m, -1, b] \longrightarrow \bar{\ell} : (d, b, 1 - m). \tag{5.3}$$

A way to obtain (5.2) from (5.1) is to find the *envelope* of all the lines \bar{P} which are the images of the points $P \in \ell$. Applied to each point of a smooth point-curve c results in the line-curve \bar{c} shown in Fig. 5.1.

$$point - curve \leftrightarrow line - curve .$$

Point-Curves from Point-Curves

Early in the development (1980) of ||-coords the direct construction of the a curve's image as a **point curve** was accomplished as outlined below. Among benefits this when applied judiciously avoids **over-plotting** by the plethora of the lines which are the tangents at the *non-convex* portions of the image curve.

Consider a general planar curve c given by :

$$c : F(x_1, x_2) = 0, \tag{5.4}$$

Substituting in eq. (5.3) yields the point-coordinates

$$x = \frac{\partial F / \partial x_2}{(\partial F / \partial x_1 + \partial F / \partial x_2)}, \quad y = \frac{(x_1 \partial F / \partial x_1 + x_2 \partial F / \partial x_2)}{(\partial F / \partial x_1 + \partial F / \partial x_2)}. \tag{5.5}$$

There is an important special case when the original point-curve is given explicitly by $x_2 = g(x_1)$. Then eq. (5.5) reduces to :

$$x = \frac{1}{1 - g'(x_1)}, \quad y = \frac{x_2 + x_1 g'(x_1)}{1 - g'(x_1)} \tag{5.6}$$

Conic Transforms

The treatment is particularly pleasing for the conic sections which are described by the quadratic function

$$\begin{aligned} F(x_1, x_2) &= A_1 x_1^2 + 2A_4 x_1 x_2 + A_2 x_2^2 + 2A_5 x_1 + 2A_6 x_2 + A_3 = \\ &= (x_1, x_2, 1) \begin{pmatrix} A_1 & A_4 & A_5 \\ A_4 & A_2 & A_6 \\ A_5 & A_6 & A_3 \end{pmatrix} \begin{pmatrix} x_1 \\ x_2 \\ 1 \end{pmatrix}, \end{aligned} \tag{5.7}$$

where the type of conic is determined by the sign of the *discriminant* $\Delta = (A_4^2 - A_1 A_2)$. The coefficient matrix is denoted by A and its determinant, which plays an important role in the development, is

$$\det A = A_3(A_1 A_2 - A_4^2) - A_1 A_6^2 - A_2 A_5^2 + 2A_4 A_5 A_6. \tag{5.8}$$

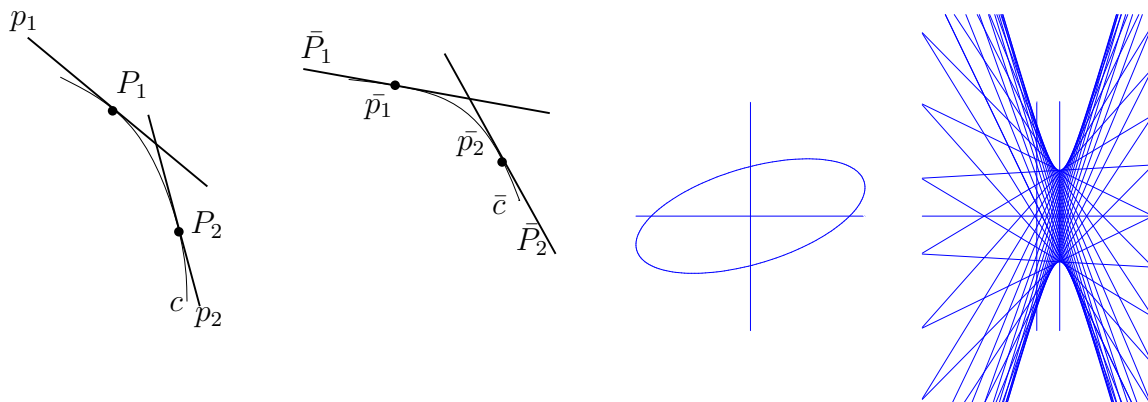


Figure 5.1: **Point-curve** and their **line-curve** images.

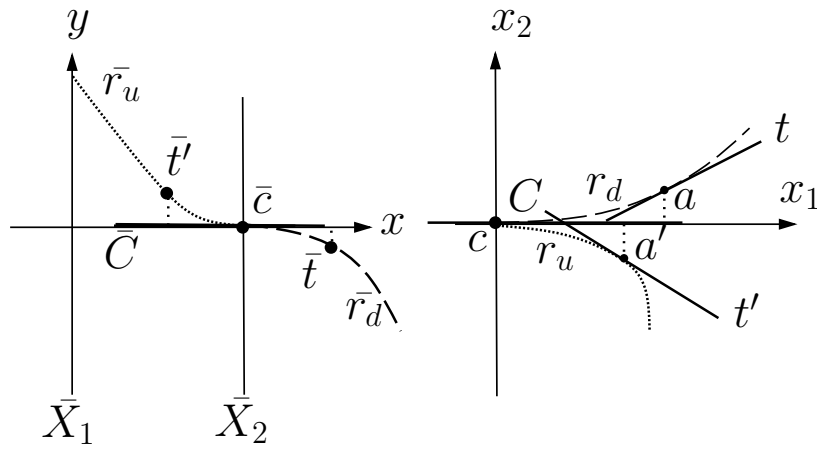


Figure 5.2: Cusp \leftrightarrow Inflection point duality is independent of the curves' orientation.

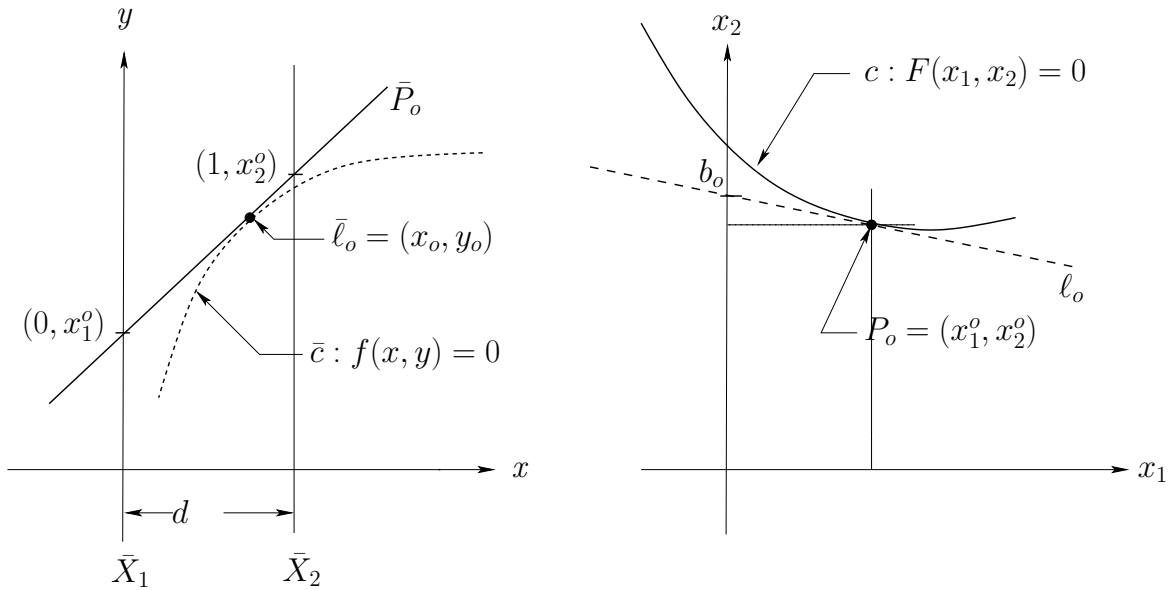


Figure 5.3: Obtaining the *point-curve* \bar{c} directly from the *point-curve* c .

For conics, using the identity that for a polynomial F of degree n $F(\mathbf{x}) = 0 \Rightarrow \nabla F \cdot \mathbf{x} = \nabla F \cdot \mathbf{x} - nF$ with the second expression being linear, eq. (5.5) and becomes

$$\begin{aligned}
 x &= \frac{A_4x_1 + A_2x_2 + A_6}{[(A_1 + A_4)x_1 + (A_2 + A_4)x_2 + (A_5 + A_6)]} \\
 y &= -\frac{A_5x_1 + A_6x_2 + A_3}{[(A_1 + A_4)x_1 + (A_2 + A_4)x_2 + (A_5 + A_6)]}.
 \end{aligned}
 \tag{5.9}$$

These are *Mobius*¹ transformations which form a group (see any good book in modern

¹Also called *linear rational* transformations.

Algebra) [1]). This observation enables substantial simplifications of the earlier treatment of conics and their transforms (see [4] and [5]). The *inverse*, expressing x_1 and x_2 in terms of x and y , is a Möbius transformation of the form

$$x_1 = \frac{a_{11}x + a_{12}y + a_{13}}{a_{31}x + a_{32}y + a_{33}}, \quad x_2 = \frac{a_{21}x + a_{22}y + a_{23}}{a_{31}x + a_{32}y + a_{33}}, \quad (5.10)$$

The result obtained is

$$f(x, y) = (x \ y \ 1)\mathbf{a} \begin{pmatrix} x \\ y \\ 1 \end{pmatrix} = 0. \quad (5.11)$$

The conclusion then is that

$$\text{conics in the } xy\text{-plane} \mapsto \text{conics in the } x_1x_2\text{-plane}$$

The specific result obtained is

$$f(x, y) = (x \ y \ 1)\mathbf{a} \begin{pmatrix} x \\ y \\ 1 \end{pmatrix} = 0. \quad (5.12)$$

with \mathbf{a} is a 3×3 matrix whose elements are given in terms of the coefficients in eq. 5.7 enabling the classification of the conic transforms into six cases.

Classification of the Conic Transforms

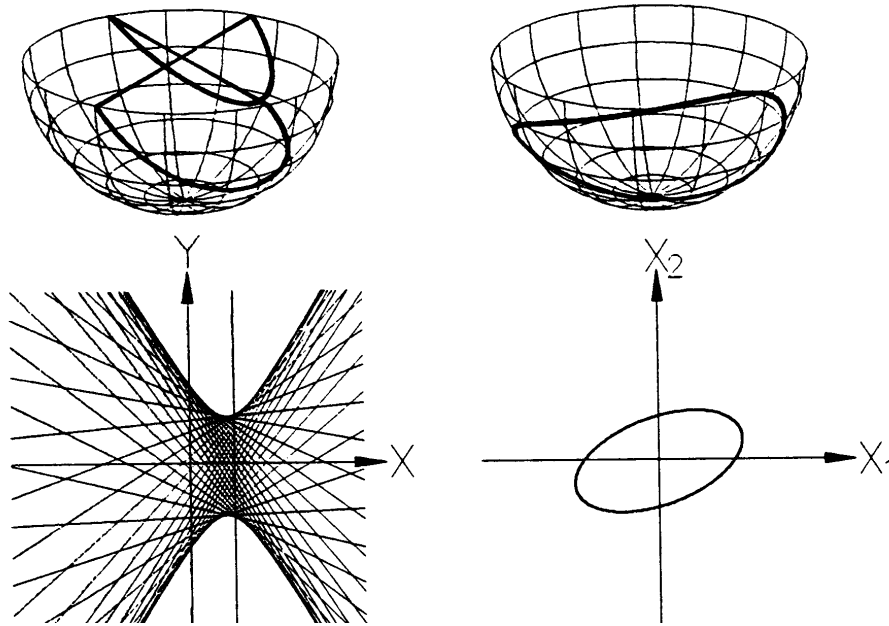


Figure 5.4: Ellipses always map into hyperbolas. Each asymptote is the image of a point where the tangent has slope 1.

Transforms of Algebraic Curves

Conic transforms are studied for two reasons. For one, it is the ease of use of Mobius transformations which is completely general for *Quadratics*, the surfaces prescribed by quadratic

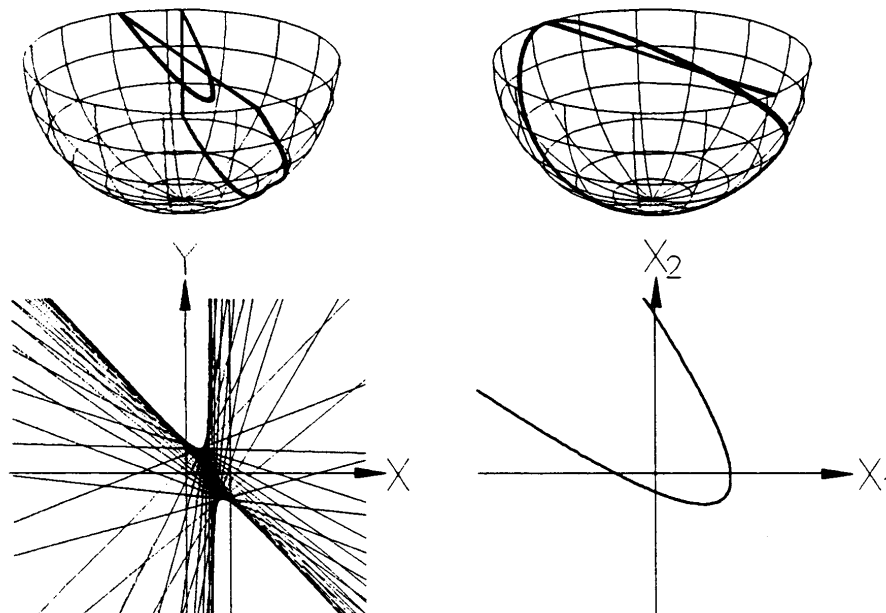


Figure 5.5: A parabola whose ideal point does not have direction with slope 1 **always** transforms to a hyperbola with a vertical asymptote. The other asymptote is the image of the point where the parabola has tangent with slope 1.

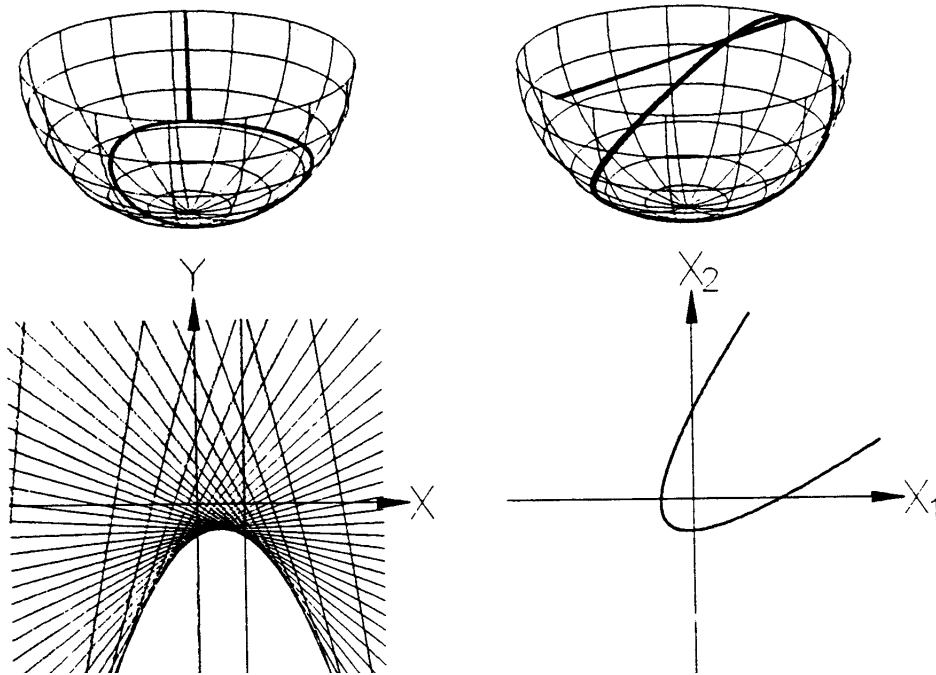


Figure 5.6: A parabola whose ideal point has direction with slope 1 transforms to a parabola - self-dual.

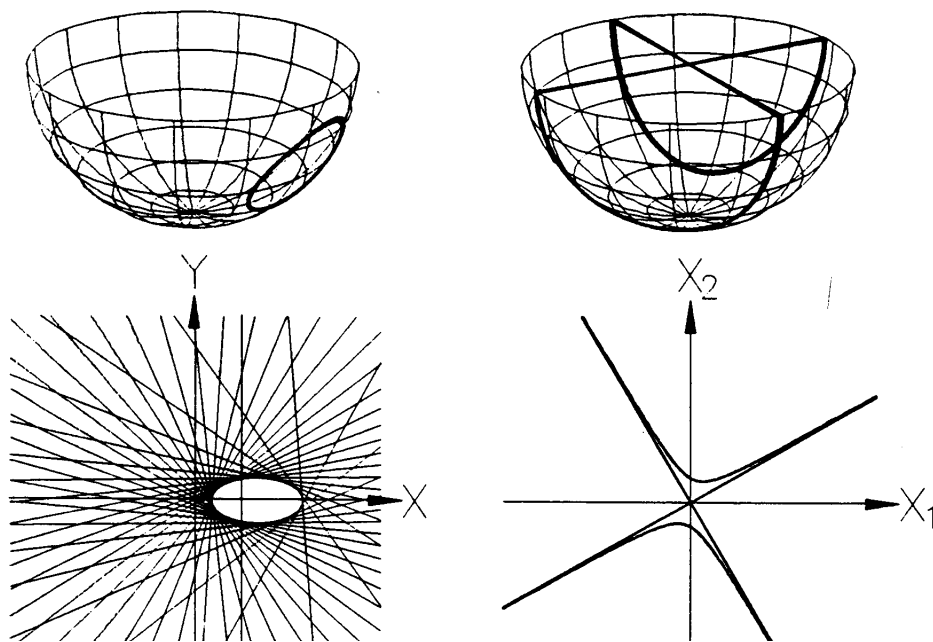


Figure 5.7: Hyperbola to ellipse – dual of case shown in Fig. 5.4

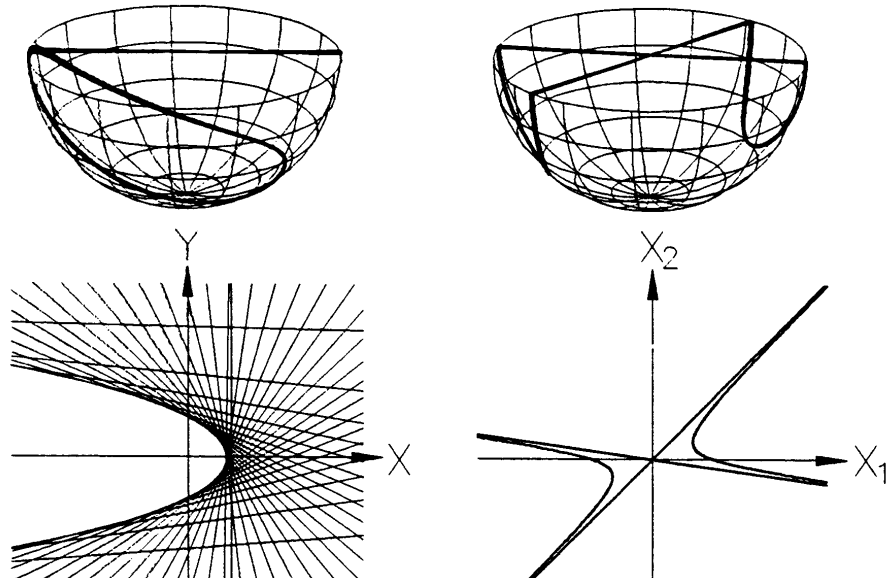


Figure 5.8: Hyperbola to parabola. This occurs when one of the asymptotes has slope 1 – dual of case shown in Fig. 5.5

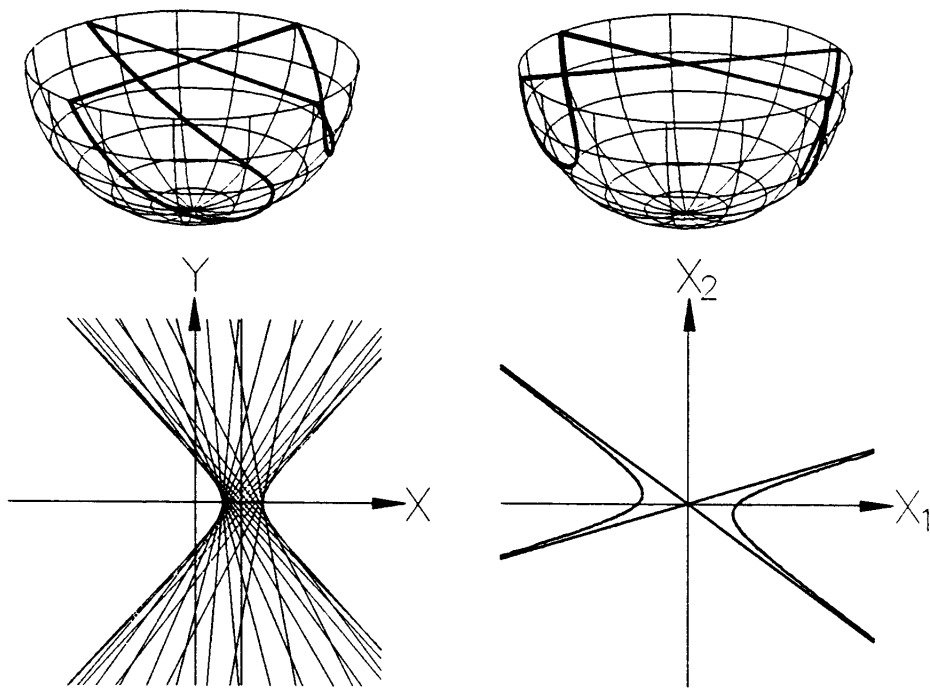


Figure 5.9: Hyperbola to hyperbola – self-dual case.

equations, in *any dimension*. For another they are a model for the far more general curves, regions and their ramifications in the next section. A few words are in order on the transforms of algebraic curves in general. In Algebraic Geometry the topic of *duals of algebraic curves* has been studied extensively and solved explicitly over a century ago by Julius Plücker with the conclusions applying also in our case which is a specific kind of duality. The results have been codified and are known as the Plücker formulae apply to algebraic curves with restricted kinds of singular points. Specifically, the Plücker class formula says that for a curve c of degree n , $n \geq 2$ with s cusps and d (double)crossing-points the image \bar{c} is also an algebraic curve of degree $n^* = n(n - 1) - 2d - 3s$ (see [3], [7], [16] and [8] for the more general algebraic methods).

Unless the curve is given explicitly, and its transform is easily obtained via eq. (5.6), there is no sensible reason to work with the image of algebraic curves in $\|\text{-}$ coords. The price in finding the polynomial equation of raised degree and then computing the curve is too steep with no benefit. The same curve can be computed numerically and directly from eq. 5.5. Alternatively one can work with approximations as is done routinely in Geometric Modeling and other applications. The image of portions algebraic curve and more general curves can be understood *qualitatively* well with the help of the following considerations.

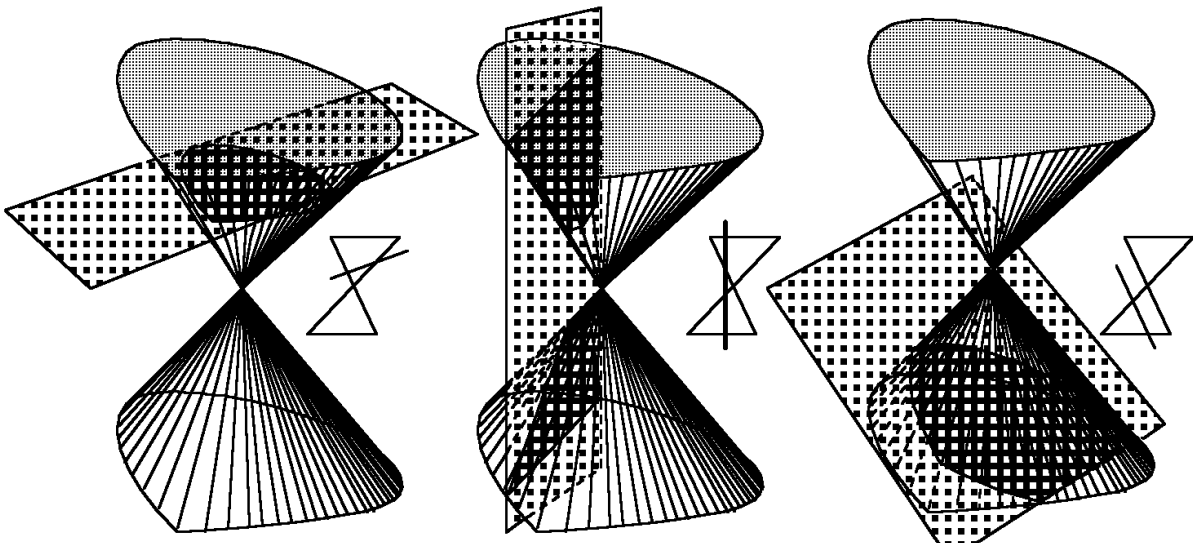


Figure 5.10: Gconics - three types of sections: (left) bounded convex set bc , (right) unbounded convex set uc and (middle) hyperbola-like gh regions.

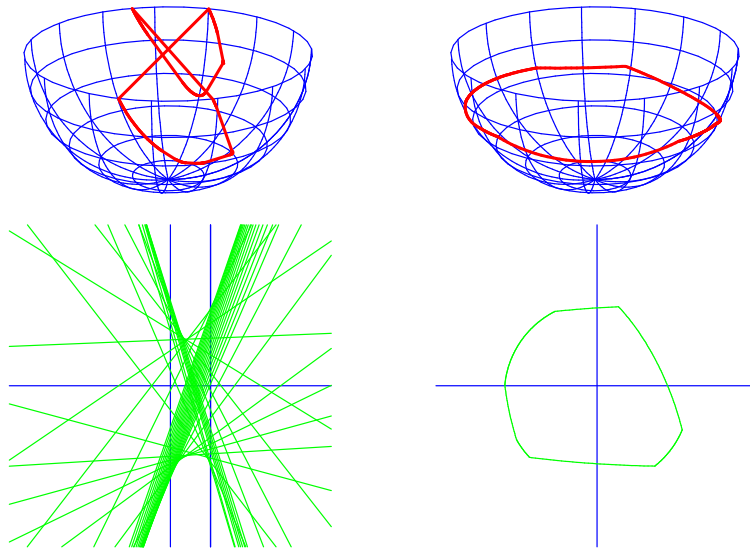


Figure 5.11: A bounded convex set bc always transforms to a gh (generalized hyperbola) – this is the generalization of the case shown in Fig. 5.4 .

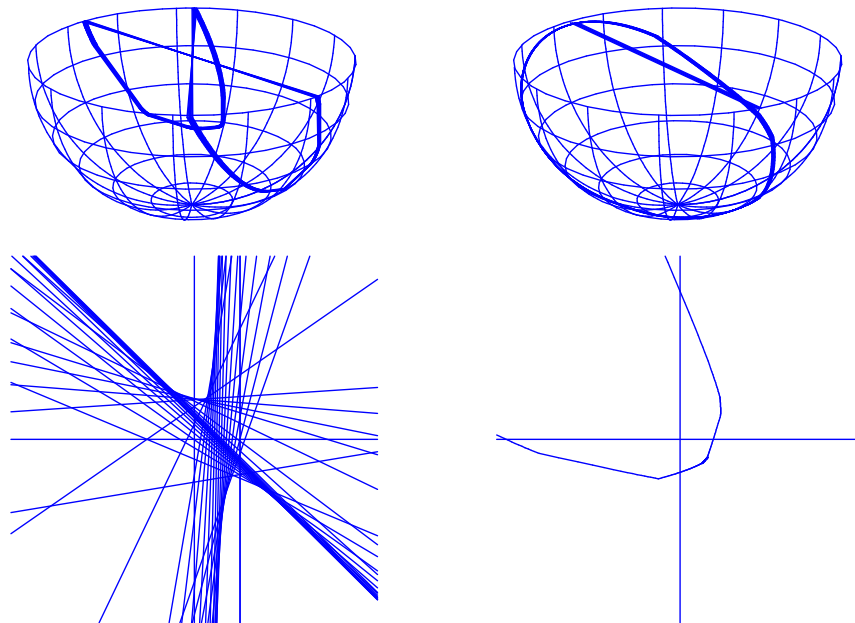


Figure 5.12: An unbounded convex set uc whose ideal points do not have slope 1 transforms to a gh (generalized hyperbola). This is the generalization of the case shown in Fig. 5.5.

Convex Sets and their Relatives

Consider a double-cone, as shown in Fig. 5.10, whose base is a bounded convex set rather than a circle. The three type of sections shown are generalizations of the conics and are

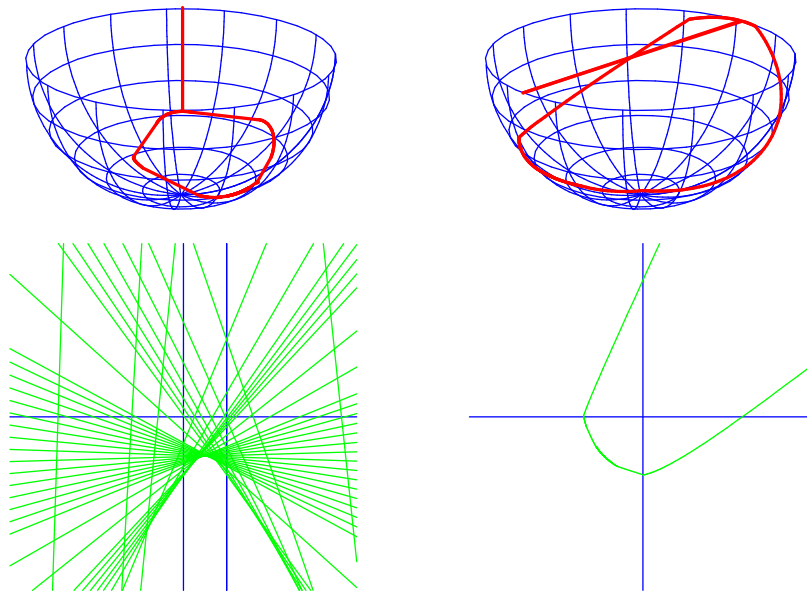


Figure 5.13: Unbounded convex set uc having ideal point with slope 1 transforms to a uc – self-dual case. This is the generalization of the case shown in Fig. 5.6.

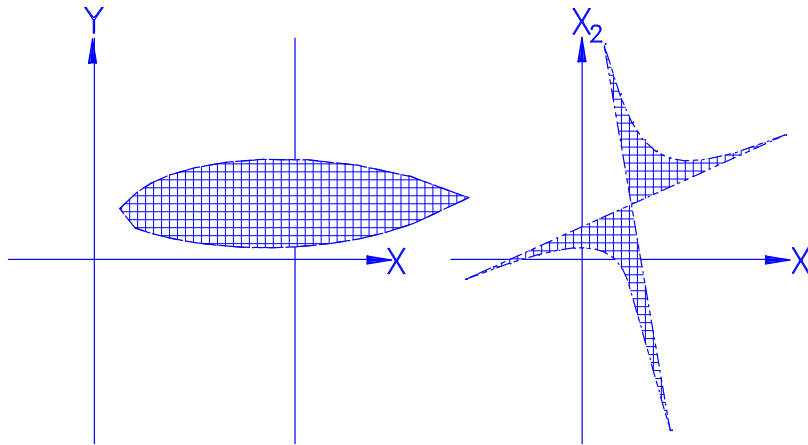


Figure 5.14: A gh whose supporting lines have slope $m \in [m_1, m_2]$ where the $m_1 < 1 < m_2$ are the asymptotes' slopes transforms to a bounded convex bc set. This is the generalization of the conic case shown in Fig. 5.7.

conveniently called *gconics*². They are either a :

bounded convex set is abbreviated by bc , or an

unbounded convex set is denoted by uc containing a non-empty set of ideal points whose slope m is in an interval $m \in [m_1, m_2]$, or a

²The corresponding regions have been previously referred to as *estars*, *pstars* and *hstars* [10], [13].

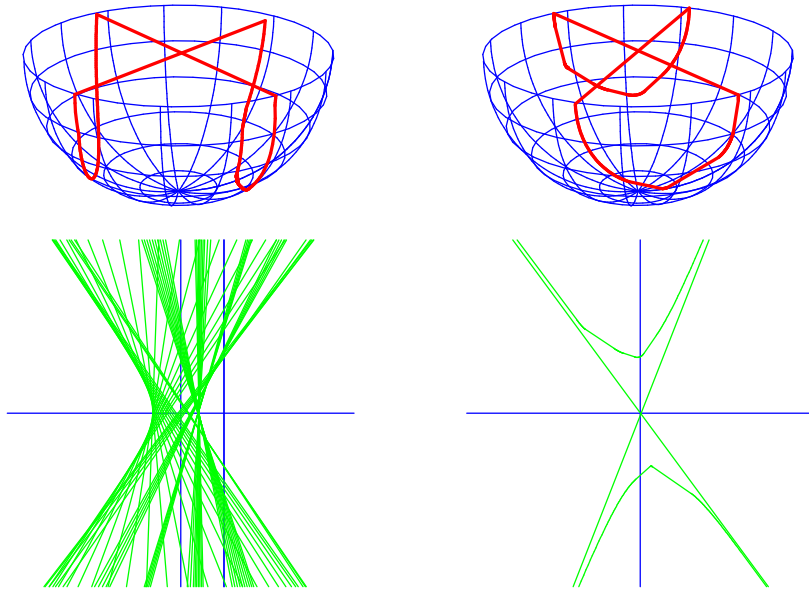


Figure 5.15: A gh with $1 \notin [m_1, m_2]$, where the m_i are the asymptotes' slopes, transforms to a gh – Self-dual case. This is the generalization of the case shown in Fig. 5.9.

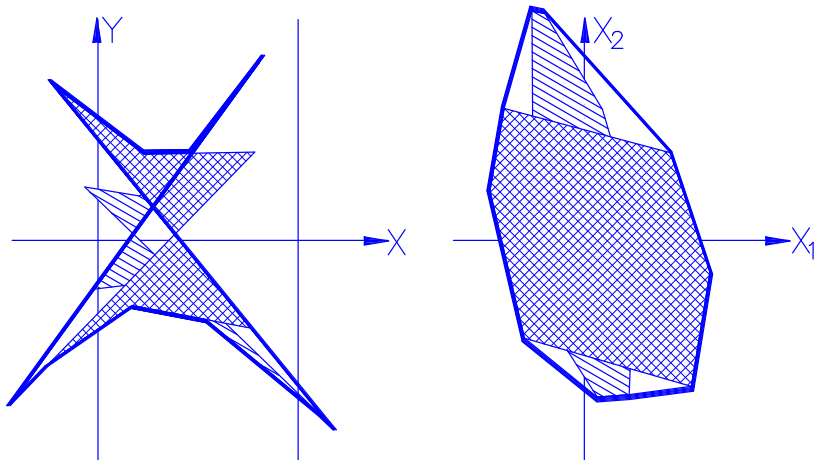


Figure 5.16: The Convex Union (also called “Convex Merge”) of bcs corresponds to the Outer Union of their images (ghs).

generalized hyperbola denoted by gh consisting of two full(not segments) lines ℓ_u, ℓ_ℓ , called asymptotes two infinite chains, convex-upward chain c_u above both asymptotes, and another convex-downward chain c_ℓ below both asymptotes.

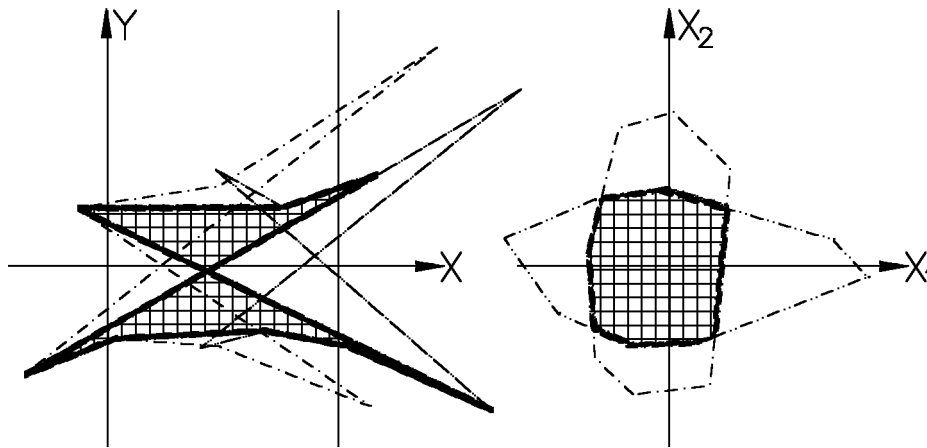


Figure 5.17: Inner intersection and intersections are dual.

Chapter 6

Approximate Planes & Flats

Motivation and a Topology for Proximity

In order to apply the results of the representation of flats their behavior in the presence of errors needs to be understood. While there are many sources of errors in the applications,



Figure 6.1: Pair of point clusters representing close planes. Note the hexagonal patterns.

from our viewpoint, it suffices to consider the accumulated errors in terms of the resulting variations $c_i \in [c_i^-, c_i^+]$ in the coefficients c_i of the linear equations. This generates a whole *family* \mathcal{F} of “close” flats. Even in R^3 the direct visualization of such a family of close planes is challenging. Let us examine the family of “close” planes

$$\{\pi : c_1x_1 + c_2x_2 + c_3x_3 = c_0, c_i \in [c_i^-, c_i^+], c_i^- < c_i^+\}.$$

Computing the two point representation in $\|\cdot\|$ -coords of some of these planes we see in Fig. 6.1 the corresponding pair of point clusters. The outline of two polygonal patterns can be discerned. Not only is the family of planes “visualizable” but also the variations in several directions.

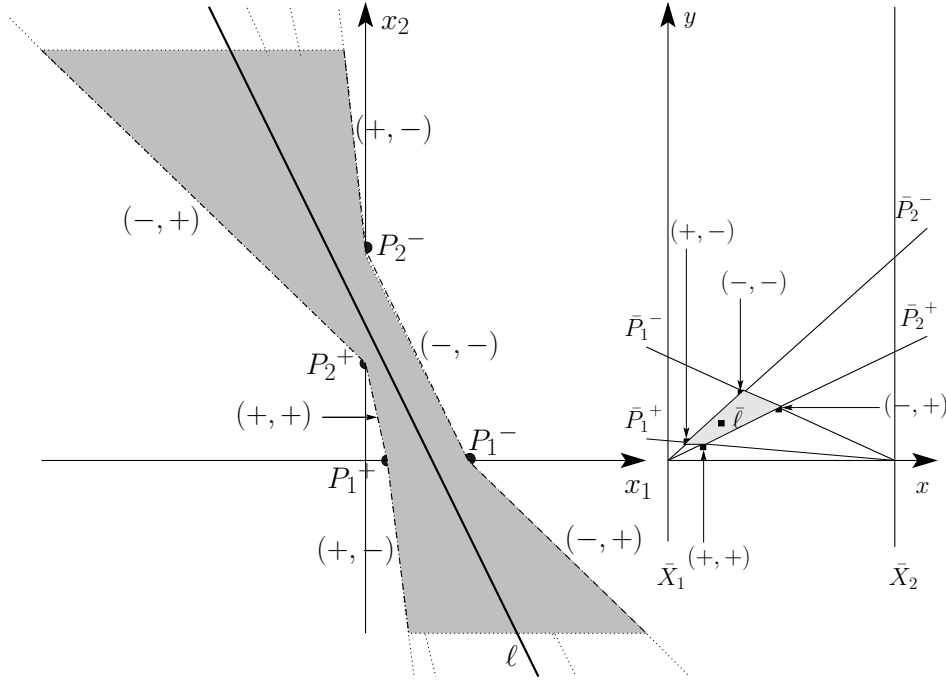


Figure 6.2: On the left is a region covered by lines “close” to ℓ and on the right are the points in $\|\text{-coords}$ representing the lines in the region. This is an instance of a *gh* (a “generalized hyperbola”) on the left $\rightarrow bc$ which here is a bounded convex quadrilateral.

Proximity of Lines and Line Neighborhoods

In \mathbb{R}^2 consider the collection of lines

$$\mathcal{F} = \{ \ell \mid \ell : c_1 x_1 + c_2 x_2 = 1, c_1, c_2 \in \mathbb{R} \}, .$$

and the neighborhood

$$NL = \{ \ell \mid \ell : c_1 x_1 + c_2 x_2 = 1, c_i \in [c_i^-, c_i^+] \quad i = 1, 2 \}. \quad (6.1)$$

The extreme lines obtained by the 4 different combinations are :

$$\begin{cases} (-, -) : c_1^- x_1 + c_2^- x_2 = 1 \\ (-, +) : c_1^- x_1 + c_2^+ x_2 = 1 \\ (+, -) : c_1^+ x_1 + c_2^- x_2 = 1 \\ (+, +) : c_1^+ x_1 + c_2^+ x_2 = 1 \end{cases} \quad (6.2)$$

An example is shown on the left part of Fig. 6.2 where the extreme lines in eq. (6.2) are constructed from the points:

$$P_1^+ = \left(\frac{1}{c_1^+}, 0 \right) \quad , \quad P_1^- = \left(\frac{1}{c_1^-}, 0 \right) \quad , \quad P_2^+ = \left(0, \frac{1}{c_2^+} \right) \quad , \quad P_2^- = \left(0, \frac{1}{c_2^-} \right) .$$

Checking the situation in $\|\text{-coords}$, on the right-part of Fig. 6.2, the lines in the unbounded region R_N are transformed into a simple *convex* quadrilateral \overline{NL} .

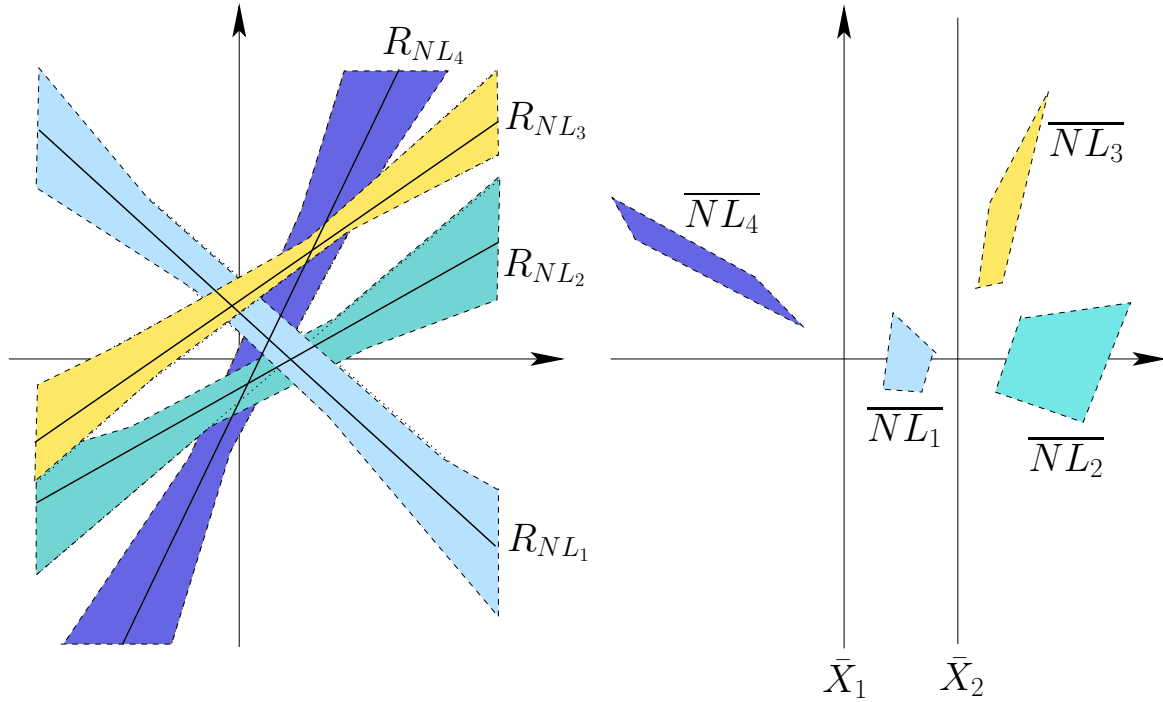


Figure 6.3: The regions R_i , $i = 1, 2, 3, 4$ covered by 4 families of lines in orthogonal and their images \overline{NL}_i in \parallel coordinates.

We enlarge the class of lines in NL replacing the 1 by c_0 and allowing it to vary within an interval

$$NL = \{ \ell \mid \ell : c_1 x_1 + c_2 x_2 = c_0, \quad c_i \in [c_i^-, c_i^+] \quad i = 0, 1, 2 \}. \quad (6.3)$$

Each such line ℓ is represented by the point

$$\bar{\ell} = \left(\frac{c_2}{c_1 + c_2}, \frac{c_0}{c_1 + c_2} \right) \quad (6.4)$$

The resulting \overline{NL} is now a *hexagon* with the left-most and right-most edges vertical. The vertices going counter-clockwise are $(-, +, -), (+, +, -), (+, -, -), (+, -, +), (-, -, +), (-, +, +)$. For clarity the three quadrilaterals corresponding to c_0^-, c_0^+ and $c_0 \in [c_0^-, c_0^+]$ are also shown separately in the upper portion of Fig. ?? with fewer details.

The generalization to \mathbb{R}^N is direct with a family of close lines being represented by $N - 1$ regions and comes out as a special case in what follows. For earlier treatments of line-neighborhoods and topologies for flats in \parallel -coords see [11] and [2]. The exposition here is adapted from [15].

Proximity of Hyperplanes

Formulation of the Problem in \mathbb{R}^N

In \mathbb{R}^3 for the plane

$$\pi : c_1x_1 + c_2x_2 + c_3x_3 = c_0, \tag{6.5}$$

$$\bar{\pi}_{1'23} = \left(\frac{c_2 + 2c_3 + 3c_1}{c_1 + c_2 + c_3}, \frac{c_0}{c_1 + c_2 + c_3} \right) = (1, 0) + \left(\frac{c_3 + 2c_1}{c_1 + c_2 + c_3}, \frac{c_0}{c_1 + c_2 + c_3} \right) \tag{6.6}$$

an observation showing that $\bar{\pi}_{1'} = \bar{\pi}_{1'23}$ can be obtained from

$$\bar{\pi}_{0'} = \bar{\pi}_{123} = \left(\frac{c_2 + 2c_3}{c_1 + c_2 + c_3}, \frac{c_0}{c_1 + c_2 + c_3} \right)$$

by a shift and the counter-clockwise cyclic permutation $c_1 \rightarrow c_3, c_3 \rightarrow c_2, c_2 \rightarrow c_1$. This combinatorial relation allows for a reduction in the number of indexed points that need to be considered. The analogous relations hold for \mathbb{R}^N .

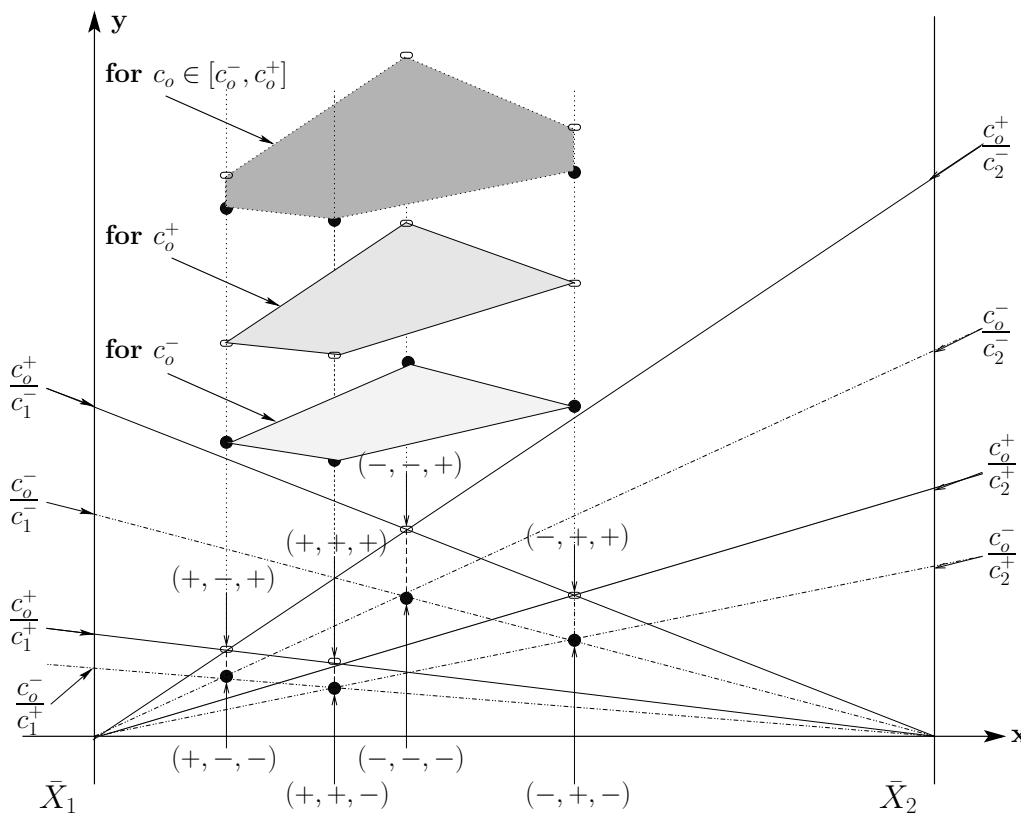


Figure 6.4: Construction of the neighborhood \overline{NL} for $NL = \{ \ell \mid \ell : c_1x_1 + c_2x_2 = c_0, c_i \in [c_i^-, c_i^+] \ i = 0, 1, 2 \}$. The “exploded” view also shows the quadrilaterals \overline{NL}_- for $c_0 = c_0^-$ and \overline{NL}_+ and $c_0 = c_0^+$ whose vertices are marked with black and blank oval vertices respectively. The complete \overline{NL} is a *hexagon* having two vertical edges, 3 vertices from \overline{NL}_- – the lowest ones, and three vertices from \overline{NL}_+ .

We proceed now with the study of the the class of all hyperplanes

$$\mathcal{F} = \{\pi \mid \pi : c_1x_1 + c_2x_2 + \dots + c_Nx_N = 1, c_i \in R \text{ for } i = 1, 2, \dots, N\},$$

Note that for convenience, the value of $c_0 = 1$ is used and is adjusted later to arbitrary values as for line neighborhoods. In the study of the $N - 1$ regions composing \overline{NH} , in view of the previous reduction, it suffices to investigate the region $\Omega = \overline{NH}_{0'}$ containing the points $\bar{\pi}_{0'}$. These are the function values of

$$f_N : \mathbb{R}^N \mapsto \mathbb{R}^2$$

in x, y coordinates,

$$f_N(\mathbf{c}) = (x(\mathbf{c}), y(\mathbf{c})) = \left(\frac{\sum_{j=1}^N (j-1)c_j}{S}, \frac{1}{S} \right), \quad (6.7)$$

reverting to homogeneous coordinates to accomodate ideal points. The subscript “0” is dropped when the context is clear. The c_j range in the N -dimensional “box”

$$\mathbf{B} = [c_1^-, c_1^+] \times \dots \times [c_N^-, c_N^+] \subset \mathbb{R}^N.$$

The stage is now set for the task ahead: to understand the properties of f_N , its action on B

$$\mathbf{B} \xrightarrow{f_N} \Omega = f_N(\mathbf{B}) \subset \mathbb{P}^2, \quad ,$$

and the structure of Ω representing the family of hyperplanes in \mathcal{N} .

The region in \mathbb{R}^N covered by “close” hyperplanes is a complex N -dimensional *gh* (“generalized hyperbola”) whose image in $\|\text{-coords}$ consists of $N - 1$ regions *in* \mathbb{R}^2 . As will be seen these are also *bc, uc, gh*. From these regions the properties of “close” hyperplanes can be ascertained and visualized without loss of information.

The Region Ω

Components and Structure of Ω

Lemma 6.0.1 $\Omega = \cap_{k=1}^N \Omega_k$. *Either*

- (a) Ω is a convex set strictly above or below the x -axis, or
- (b) Ω consists of two convex regions one above and the other below the x -axis.

In the second case, it will be seen, that there exists a combination of the c_j for which $S(\mathbf{c}) = \mathbf{0}$ resulting in Ω being a *gh*. For the construction of Ω we pick our cue from Fig. ?? and investigate the intersections $\bar{P}_m^k \cap \bar{P}_m^{k+1}$ and $\bar{P}_M^k \cap \bar{P}_M^{k+1}$ starting with the relations between the successive C_m^k and C_M^k , it turns out : that for

$$\left\{ \begin{array}{l} A_k = (c_1^+, c_2^+, \dots, c_{k-1}^+, c_k^-, c_{k+1}^-, \dots, c_N^-), \\ B_k = (c_1^-, c_2^-, \dots, c_{k-1}^-, c_k^+, c_{k+1}^+, \dots, c_N^+), \end{array} \right. \quad \text{with} \quad \left. \begin{array}{l} A_1 = (c_1^-, \dots, c_N^-) = B_N, \\ B_1 = (c_1^+, \dots, c_N^+) = A_N, \end{array} \right\} \quad (6.8)$$

$$\begin{cases} C_m^{(k-1)} = C_m^k + S(A_k), \\ C_M^{(k-1)} = C_M^k + S(B_k). \end{cases} \quad (6.9)$$

These $2N$ vertices are characterized by a *single* change of sign in the superscripts at the k th position. The successive line intersections $\bar{P}_m^k \cap \bar{P}_m^{(k-1)}$ are

$$C_m^k y + (k-1) = C_m^{(k-1)} y + (k-2) \quad \Rightarrow \quad y = \frac{1}{S(A_k)}, \quad (6.10)$$

and

$$\bar{P}_m^1 \cap \bar{P}_M^N = f(A_1) = f(B_N) \quad , \quad \bar{P}_m^N \cap \bar{P}_M^1 = f(B_1) = f(A_N). \quad (6.11)$$

If there is a combination of the coefficients \mathbf{c} such that $S(\mathbf{c}) = c_1 + c_2 + \dots + c_N = 0$, while these $c_k \in [c_k^-, c_k^+]$, then $y(A_k)$ and $y(A_{k+1})$ have different signs so that the above monotonicities become

Construction of Ω

We have been carefully skirting around the prospect of the sum $S(\mathbf{c}) = \sum_{j=1}^N c_j = 0$ for some $\mathbf{c} \in B$ and this is dealt with now. In the $\mathbf{c} \in \mathbb{R}^N$ the coefficient space $\pi_c : \sum_{j=1}^N c_j = 0$

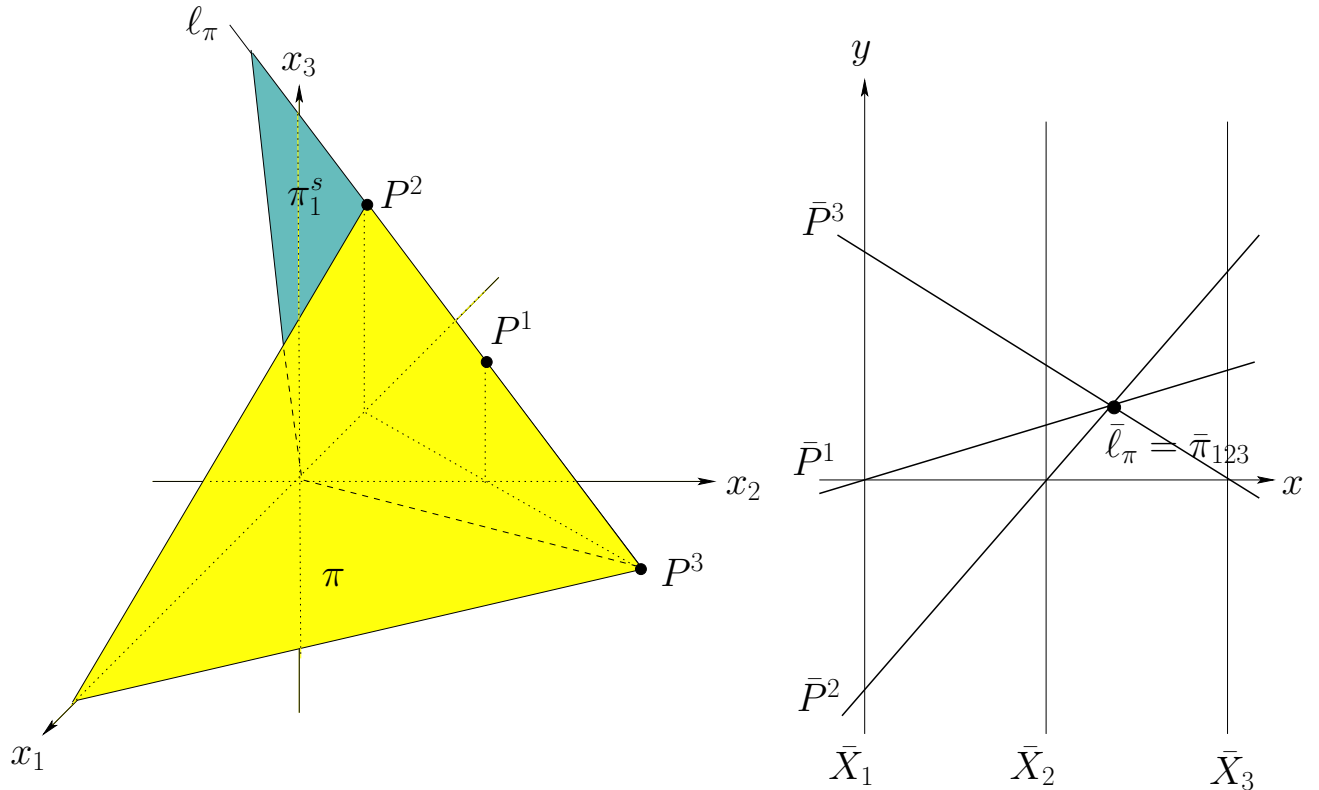


Figure 6.5: A plane π , its intersection $\ell_\pi = \bar{\pi}_{123}$ with the first super-plane π_1^s and the points $P^k = \ell_\pi \cap x_i x_j$ -plane for $k \neq i, j$.

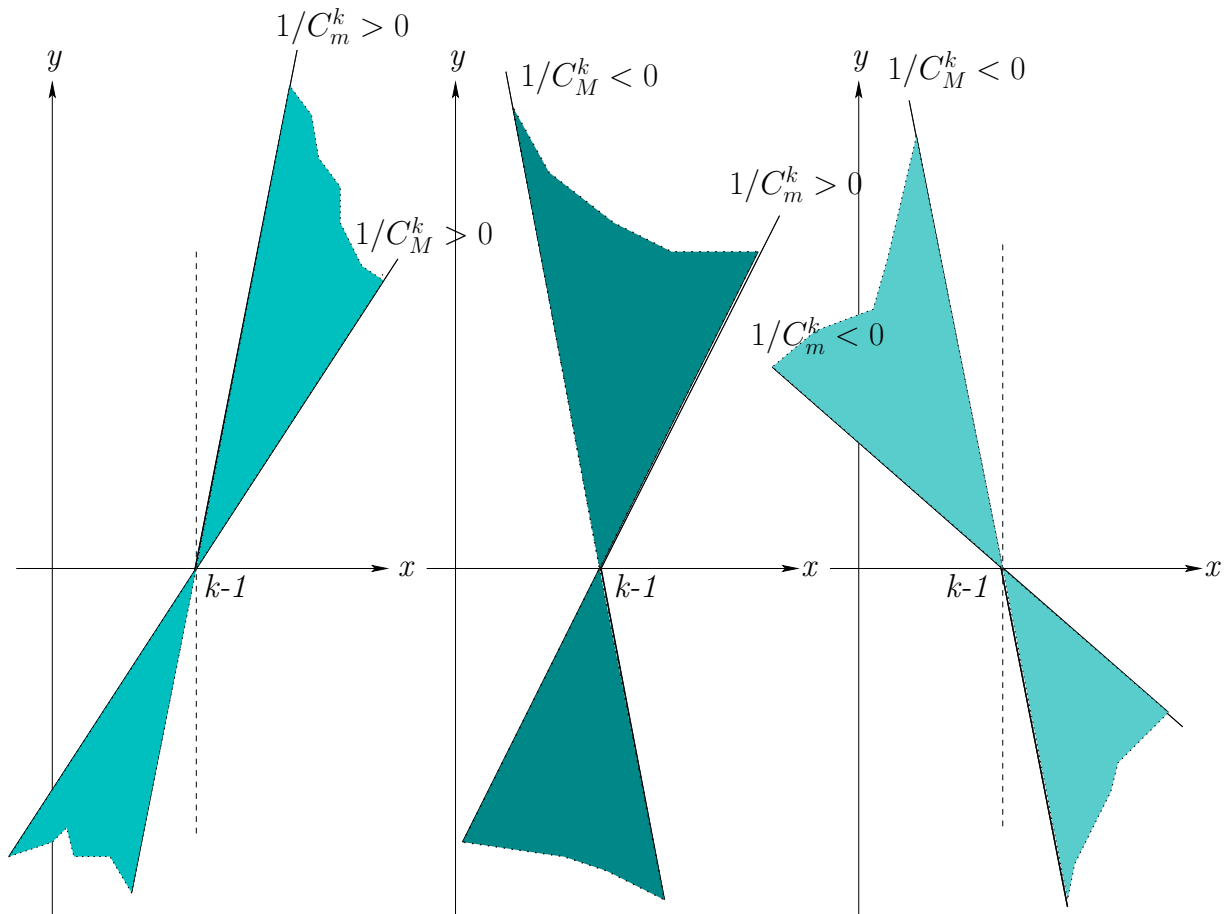


Figure 6.6: “Fan” regions Ω_k swept by the rotations of \bar{P}^k about the point $(k - 1, 0)$.

is a hyperplane and its relative position to the box B has important ramifications with respect to the corresponding Ω . So for the determination of Ω the procedure is to first check

Theorem 6.0.1 *The region Ω is $2N$ -agon above or below (but not intersecting) the x -axis, which is*

1. **bc** if $\pi_c \cap B = \emptyset$,
2. **uc** if $\pi_c \cap B = \{A_1\}$ or $\pi_c \cap B = \{B_1\}$,
3. **gh** if π_c intersects B at more than one edge, and has a vertical asymptote if in addition π_c contains a vertex of B .

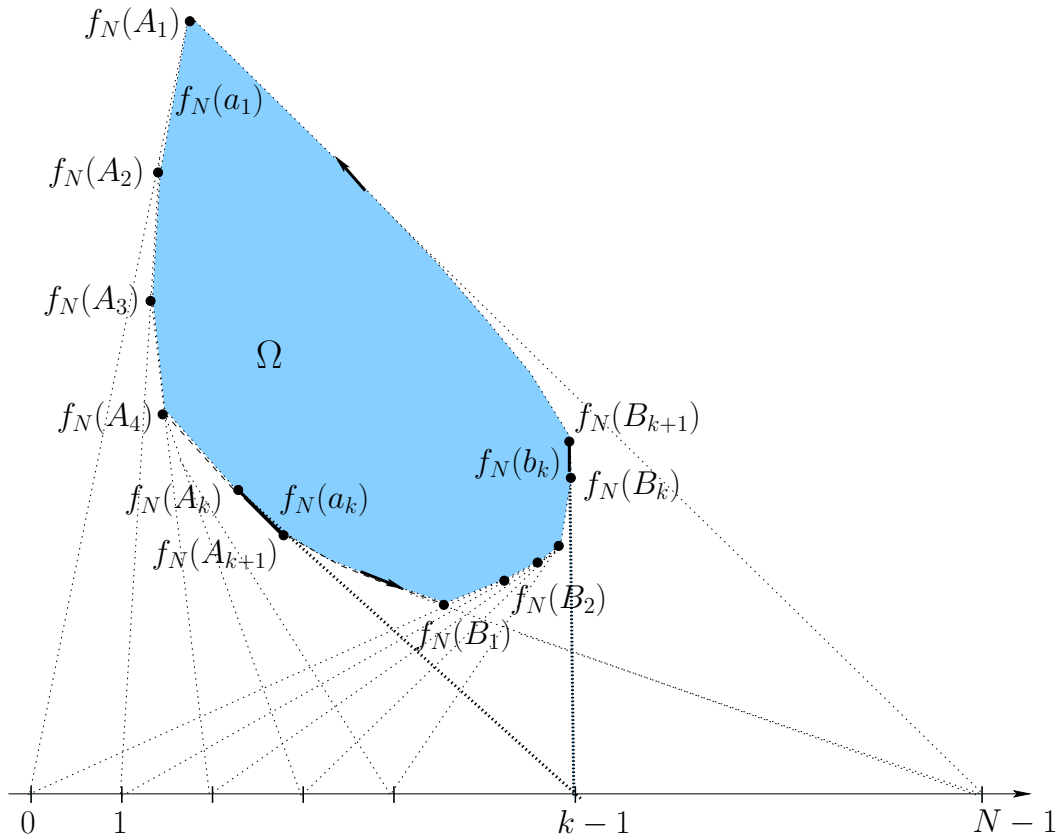


Figure 6.7: Construction of Ω . The k th region Ω_k contributes the vertices $f_N(A_k), f_N(B_k)$ to $\partial\Omega$, and together with the region Ω_{k+1} the vertices $f_N(A_{k+1}), f_N(B_{k+1})$ and edges $f_N(a_k), f_N(b_k)$ as highlighted.

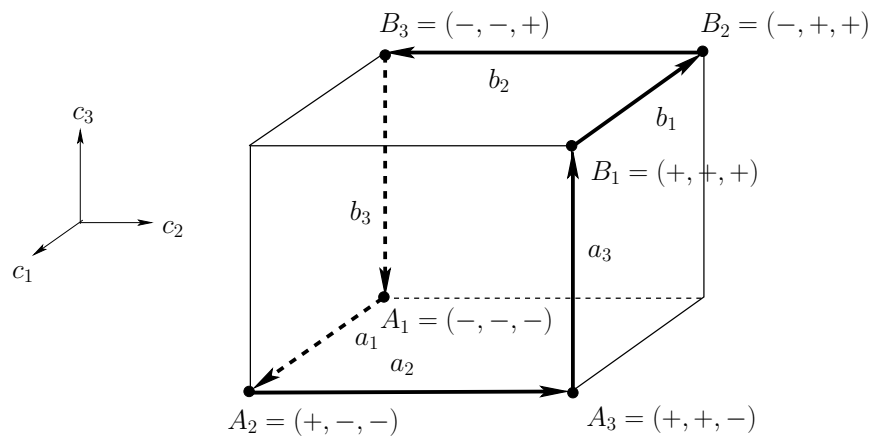


Figure 6.8: 3D-Box B in the space of coefficients showing the vertices and edges 3 each A_k, B_k, a_k, b_k along the path \mathcal{P} . The notation \pm indicates the sign of c_k^\pm at the k th component.

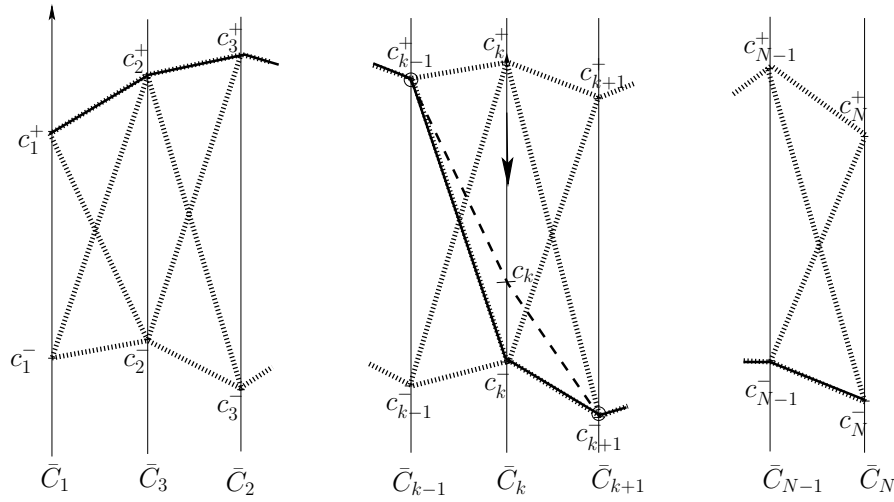


Figure 6.9: Image \bar{B} of domain B , which is an N -dimensional box in the coefficient space $c_1 \times c_2 \times \dots \times c_N$. The dotted lines are the polygonal lines representing the box's vertices. The solid line shows vertex \bar{A}_k and the dashed portion (together with the remaining solid line) shows one of the points on the edge \bar{a}_k the arrow on the \bar{C}_k axis is the direction of traversal from $c_k^+ \rightarrow c_k^-$. Each full traversal of $c_k \in [c_k^-, c_k^+]$ corresponds to an edge a_k , one of the N edges on the vertex A_k . The full path \mathcal{P} can be traced in this manner.

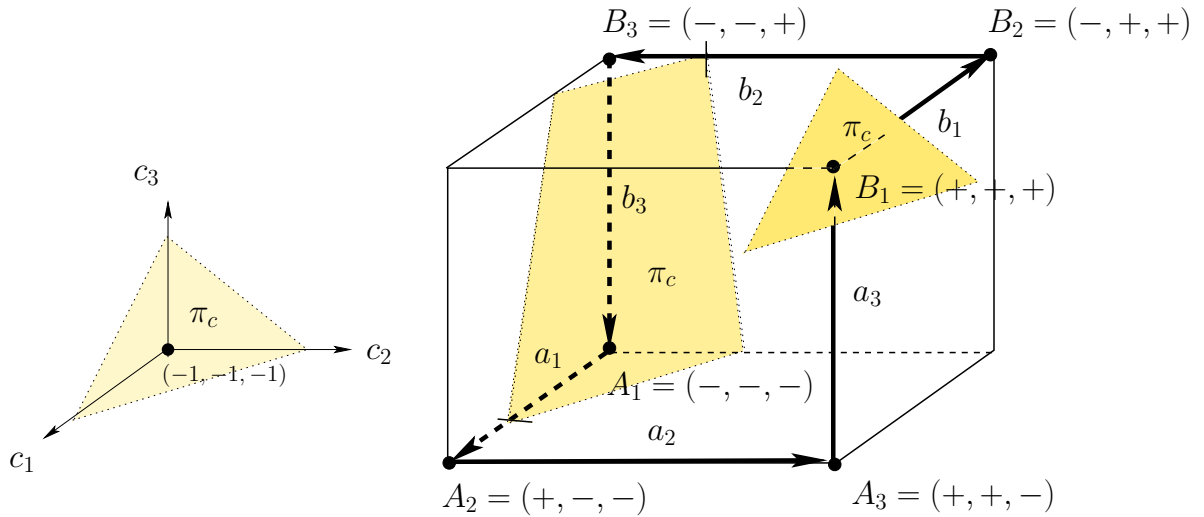


Figure 6.10: The B in the 3-D space of coefficients c_1, c_2, c_3 and its positions with respect to the plane $\pi_c : c_1 + c_2 + c_3 = 0$. Namely $\pi_c \cap B = \emptyset$, or if $\pi_c \cap B \neq \emptyset$ π_c is a supporting plane at either vertex A_1 or B_1 or π_c intersects two edges of the path \mathcal{P} .

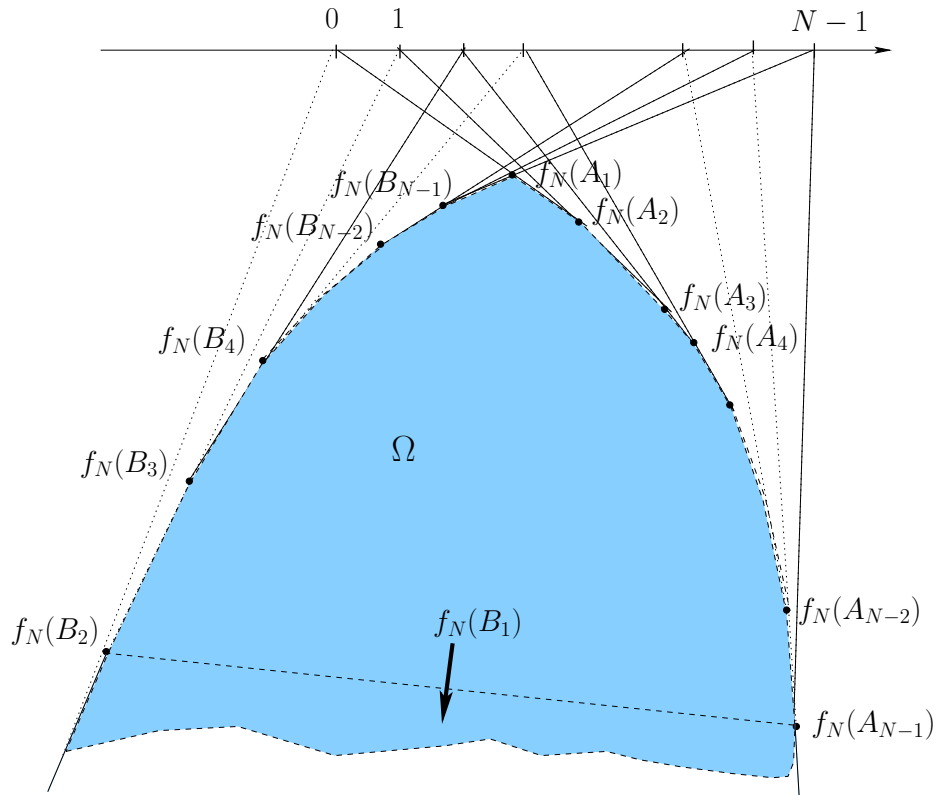


Figure 6.11: Ω can be a *uc*. Here $f_N(B_1)$ is an ideal point.

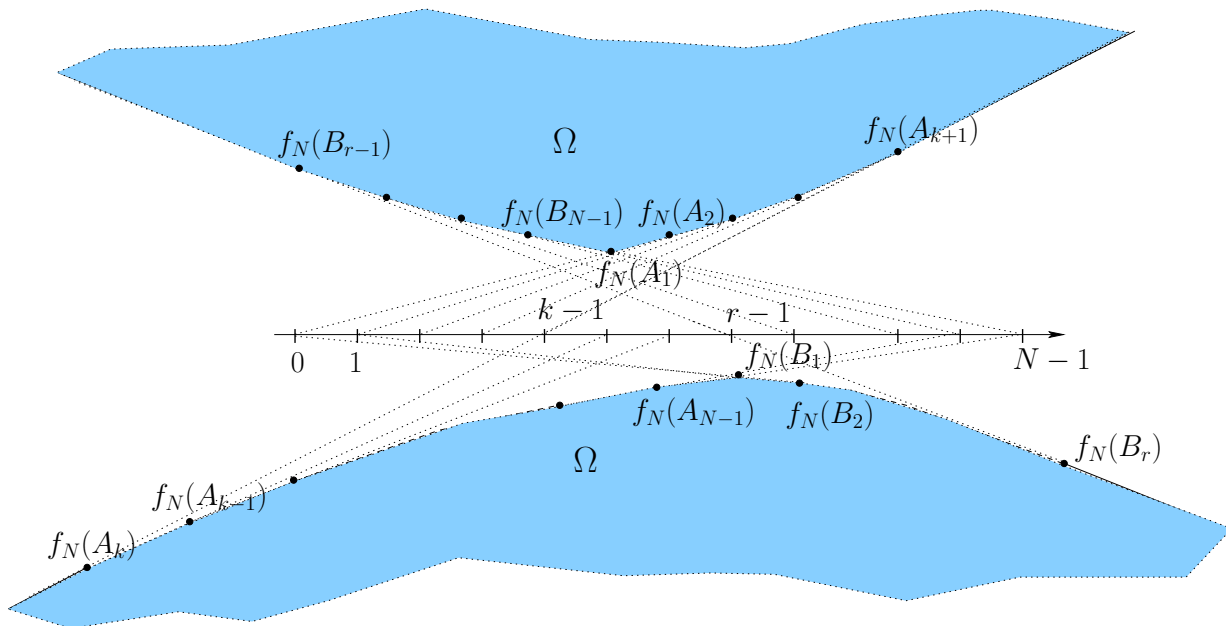


Figure 6.12: Ω can be a *gh*.

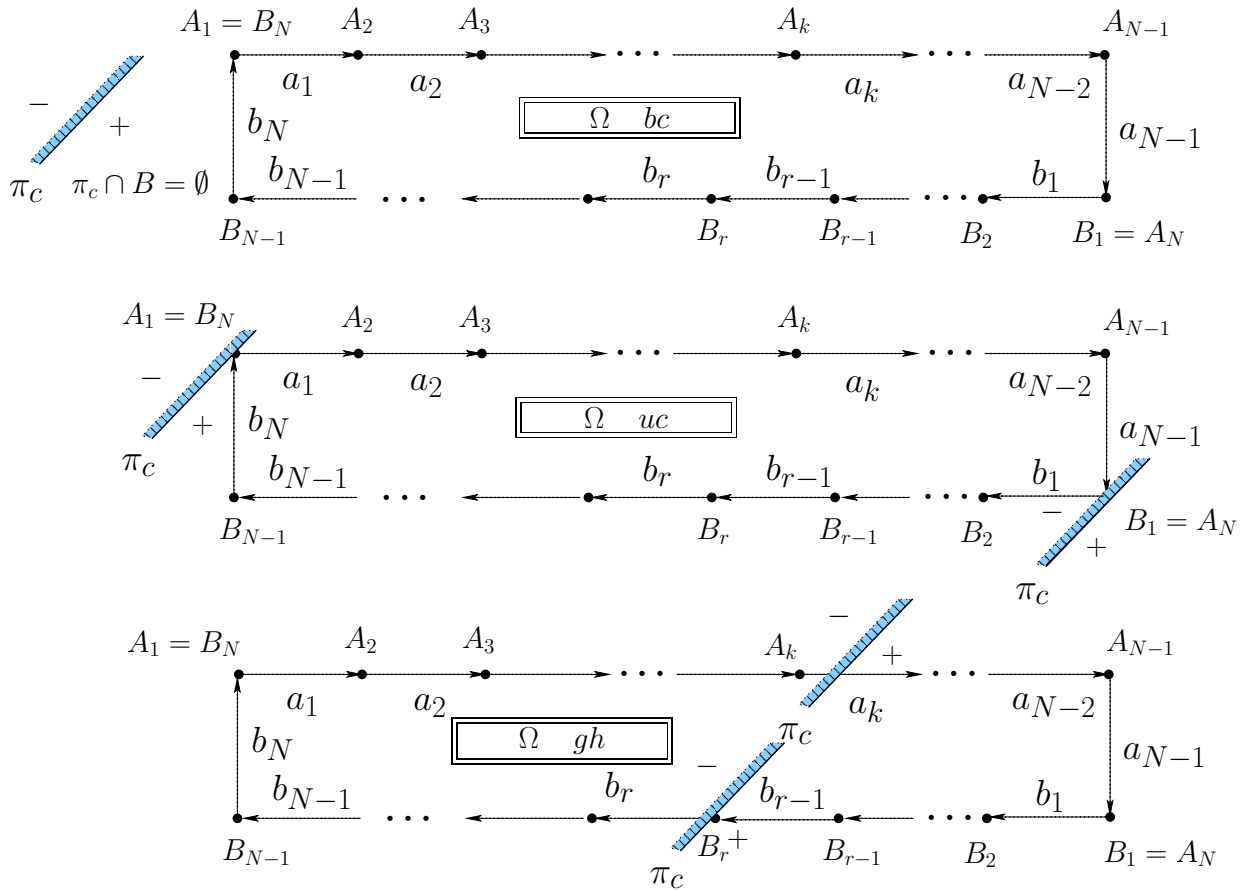


Figure 6.13: The intersection of the hyperplane π_c with the path $\mathcal{P} \subset B$ determines the type of the region Ω . When $\pi_c \cap B = \emptyset$ (top) Ω is a bc (bounded convex) $2N$ -agon as in Fig. 6.7, otherwise a uc (unbounded convex) when π_c is a supporting hyperplane to B at either vertex A_1 or B_1 (middle) Fig. 6.11, or as in the bottom part a gh (generalized hyperbola) Fig. 6.12 when π_c intersects more than one segment B . In addition, if π_c cuts through one of the vertices V then \bar{V} is an ideal point and is a vertical asymptote of Ω . (Exercise ??).

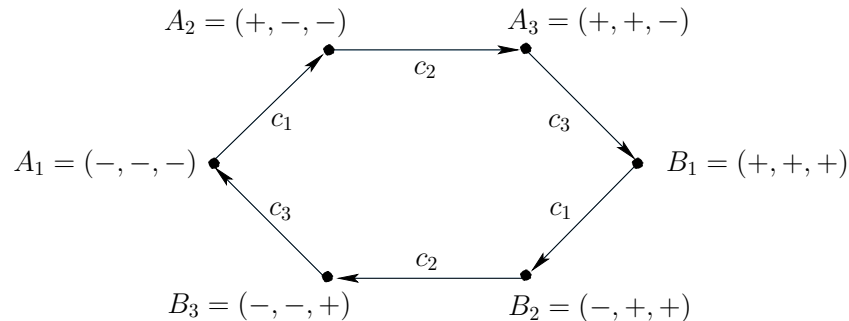


Figure 6.14: Pathway for the computation of $\partial\Omega$ for $N = 3$. The label c_i indicates the **only** coefficient varying along the edge. Starting from $A_1 = (-, -, -)$ the next vertex $A_2 = (+, -, -)$ is found by the variation of c_1 between its extreme values. In the same way all the remaining vertices are found.

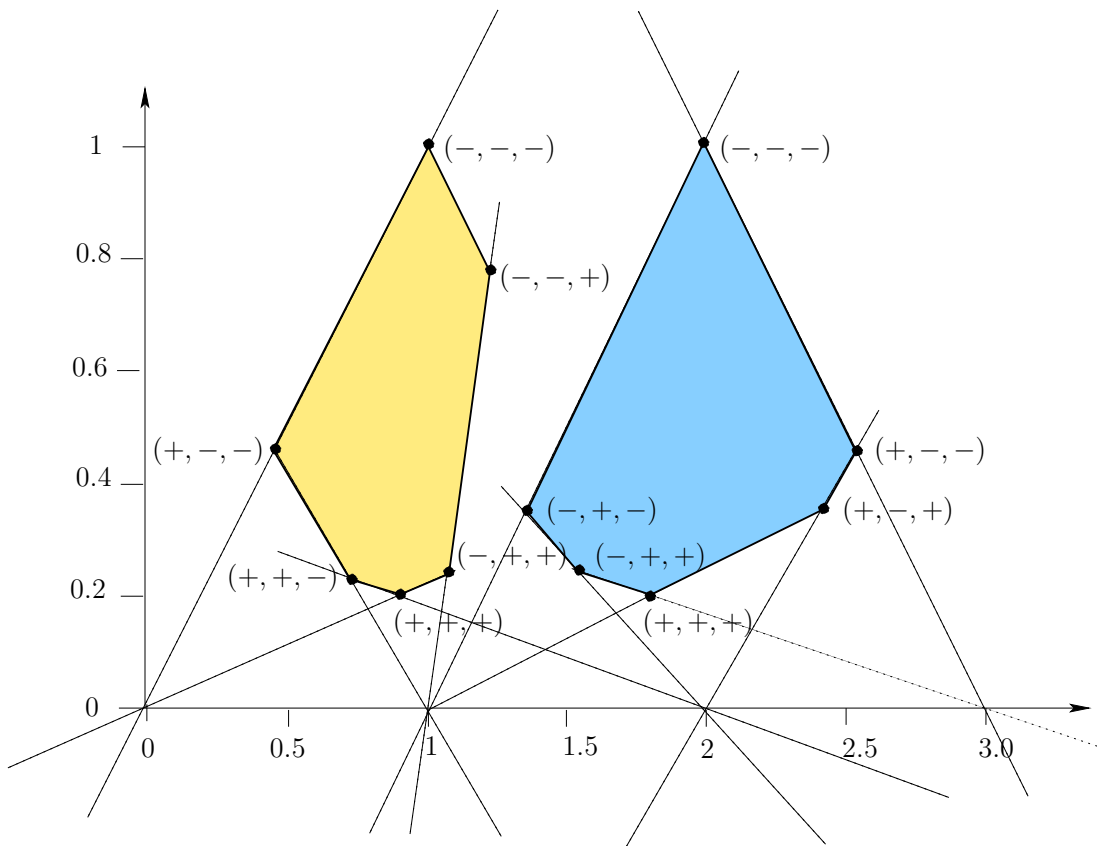


Figure 6.15: The hexagonal regions $\Omega = \overline{NH}_0'$ (on the left) and on the right \overline{NH}_1' for the family of planes with $c_1 \in [1/3, 1.5]$, $c_2 \in [1/3, 2.5]$, $c_3 \in [1/3, 1]$. Compare this picture with Fig. 6.1 at the beginning of the chapter.

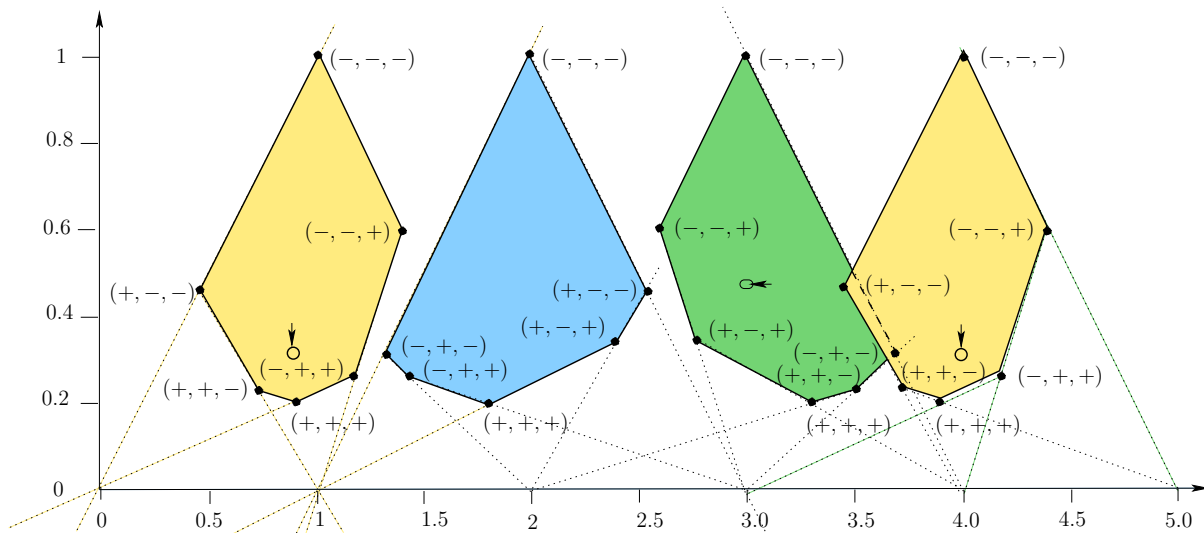


Figure 6.16: The four hexagonal regions for the family of planes with $c_1 \in [1/3, 1.5]$, $c_2 \in [1/3, 2.5]$, $c_3 \in [1/3, 1]$. Note that the last region $\overline{NH}_{3'}$ is identical to the first $\overline{NH}_{0'}$ translated 3 units to the right. Note the overlap in the last two regions which suggests that there may be planes π in this family with $c_3 = 0$ (when $\bar{\pi}_{2'} = \bar{\pi}_{3'}$) which is not possible from the c_k intervals' definition. However, there can not be points $\bar{\pi}_{2'} = \bar{\pi}_{3'} \in \overline{NH}_{2'} \cap \overline{NH}_{3'}$ with $\bar{\pi}_{0'} \in \overline{NH}_{0'}$ and $\bar{\pi}_{1'} \in \overline{NH}_{1'}$. For example, the two \circ with vertical arrows are the locations of $\bar{\pi}_{0'}$, $\bar{\pi}_{3'}$ in $\overline{NH}_{0'}$ and $\overline{NH}_{3'}$ for $(-, +, -)$ while the \square with horizontal arrow is the location of $(+, -, -)$ in $\overline{NH}_{2'}$.

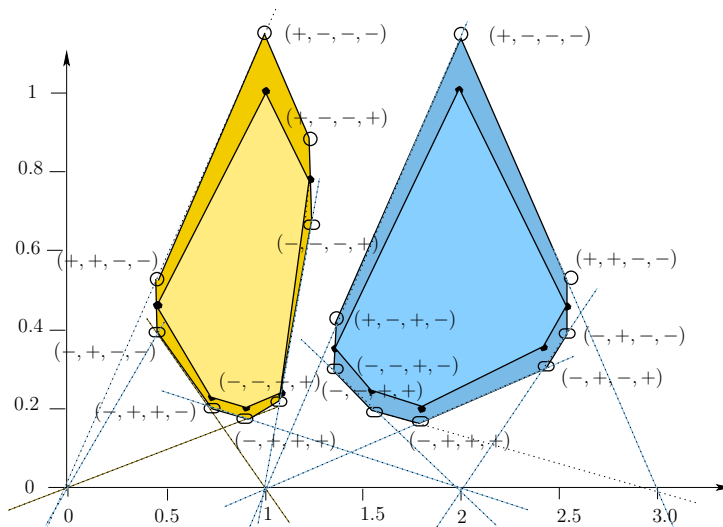


Figure 6.17: The hexagonal regions $\Omega = \overline{NH}_{0'}$ (on the left) and on the right $\overline{NH}_{1'}$ for the family of planes with $c_0 \in [.85, 1.15]$, $c_1 \in [1/3, 1.5]$, $c_2 \in [1/3, 2.5]$, $c_3 \in [1/3, 1]$. The superscript of c_0 is the first entry of the quadruples $(\pm, ., ., .)$ designating the vertices. Vertices with c_0^+ are marked by \circ and those for c_0^- with ellipses.

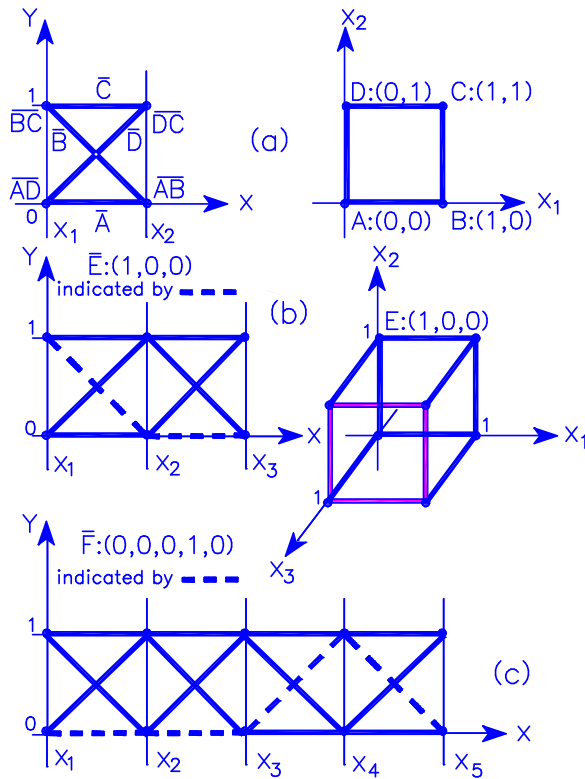


Figure 7.1: (a) Square (b) Cube in \mathbb{R}^3 (c) Hypercube in \mathbb{R}^5 – all edges have unit length

Chapter 7

Surfaces in \mathbb{R}^N

$$\pi : c_1x_1 + c_2x_2 + c_3x_3 = c_0 . \quad (7.1)$$

Denoting the coefficients by $\mathbf{c} = (c_1, c_2, c_3)$ and $\mathbf{u} = (1, 1, 1)$, the points representing the plane are given in the convenient inner-product (denoted by “.”) form :

$$\bar{\pi} = (\mathbf{c} \cdot \mathbf{d}_3^i, c_0, \mathbf{c} \cdot \mathbf{u}) = (\mathbf{c} \cdot \mathbf{d}_3^i, c_0, c_1 + c_2 + c_3) . \quad (7.2)$$

Specifically, the first coordinates of $\bar{\pi}$ for the index spacings due to the four standard axes triples used are :

$$\begin{cases} \mathbf{c} \cdot \mathbf{d}^0 = \mathbf{c} \cdot (0, 1, 2) = c_2 + 2c_3 \\ \mathbf{c} \cdot \mathbf{d}^1 = \mathbf{c} \cdot (3, 1, 2) = 3c_1 + c_2 + 2c_3 \\ \mathbf{c} \cdot \mathbf{d}^2 = \mathbf{c} \cdot (3, 4, 2) = 3c_1 + 4c_2 + 2c_3 \\ \mathbf{c} \cdot \mathbf{d}^3 = \mathbf{c} \cdot (3, 4, 5) = 3c_1 + 4c_2 + 5c_3 \end{cases} \quad (7.3)$$

The gradient vector of F, $\nabla F = \left(\frac{\partial F}{\partial x_1}, \frac{\partial F}{\partial x_2}, \frac{\partial F}{\partial x_3} \right) \Big|_P$, at the point P is normal to the surface σ at $P \Rightarrow$ the tangent plane π of σ at the point $P_0(t_0, s_0) = (x_1^0, x_2^0, x_3^0) = (\mathbf{x}^0)$ is given by

$$\pi(s, t) : \nabla F \cdot (\mathbf{x} - \mathbf{x}^0) = \sum_{i=1}^3 (x_i - x_i^0) \frac{\partial F}{\partial x_i}(x_1^0, x_2^0, x_3^0) = 0 .$$

The points representing $\pi(s, t)$, obtained from eq. (7.2) are :

$$\bar{\pi}_i(s, t) = (\nabla F \cdot \mathbf{d}^i, \nabla F \cdot (\mathbf{x}^0), \nabla F \cdot \mathbf{u}), \quad i = 0, 1. \quad (7.4)$$

Stated explicitly the point \mapsto pair-of-points mapping is

$$\mathbf{x} \in \sigma \mapsto \pi \mapsto (\bar{\pi}_{0'}, \bar{\pi}_{1'}) = (\bar{\pi}_{123}, \bar{\pi}_{1'23}) = ((x, y), (x', y)), \quad (7.5)$$

where by x' we denote the x -coordinate of $\bar{\pi}_{1'23}$ the y being the same for both points.

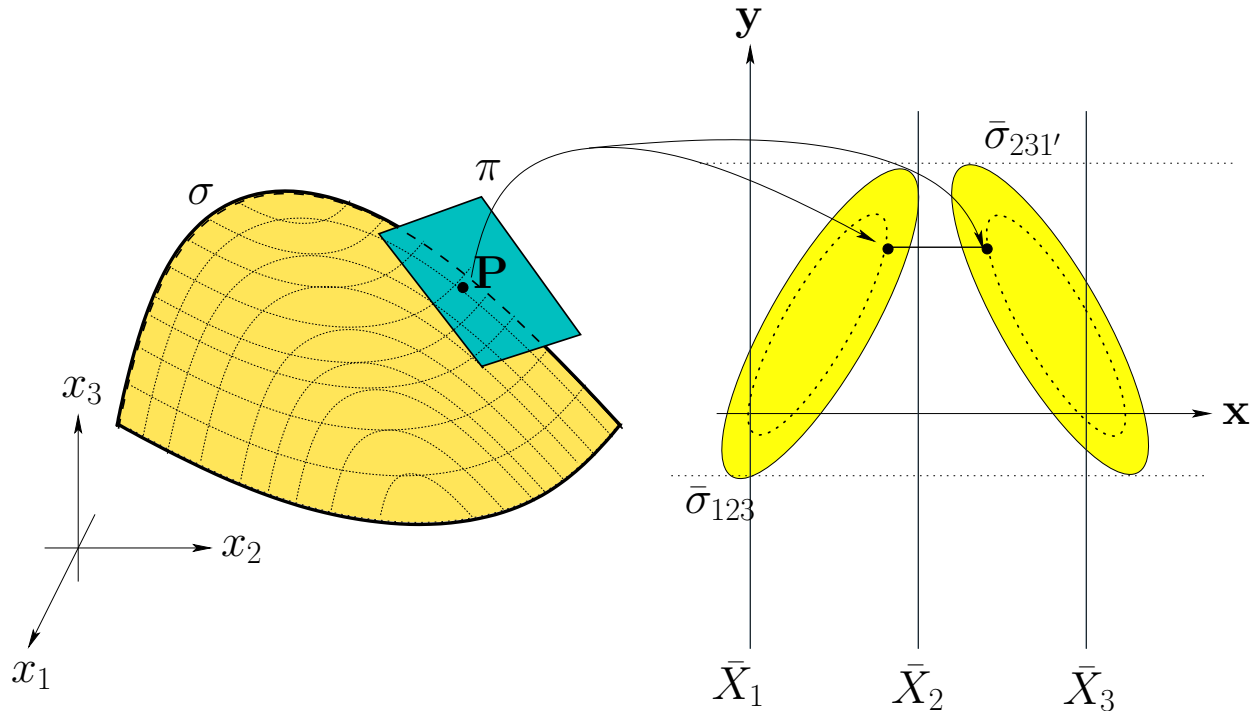


Figure 7.2: A surface $\sigma \in \mathcal{E}$ is represented by two planar regions $\bar{\sigma}_{123}, \bar{\sigma}_{231'}$ consisting of pairs of points representing its tangent planes.

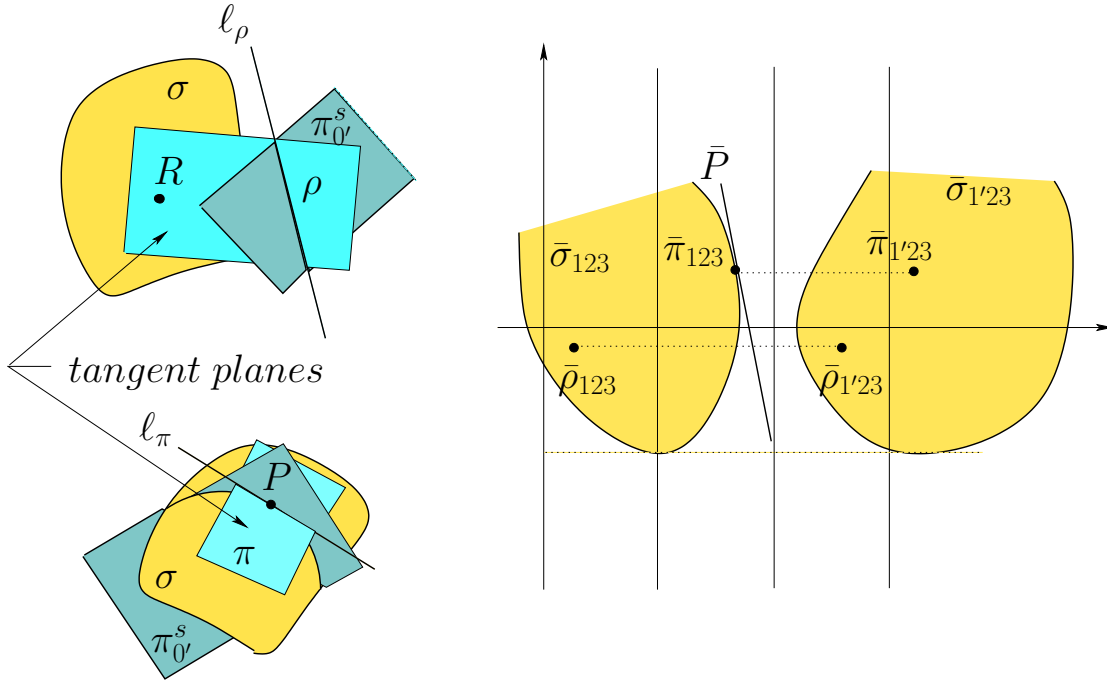


Figure 7.3: Formation of boundary contour

With the notation $F_i = \partial F / \partial x_i$

$$\begin{cases} x = \frac{F_2 + 2F_3}{F_1 + F_2 + F_3}, \\ y = \frac{x_1 F_1 + x_2 F_2 + x_3 F_3}{F_1 + F_2 + F_3}, \\ x' = \frac{3F_1 + F_2 + 2F_3}{F_1 + F_2 + F_3}. \end{cases} \quad (7.6)$$

These transformations are the direct extension of the 2-D point \leftrightarrow point curve transformations derived in Chapter ???. A word of caution, when the inter-axes distance $d \neq 1$, the right-hand-sides of x and x' above need to be multiplied by d and $2d$ respectively (see (5.5) in Chapter ??).

The generalization to the hyper-surfaces \mathcal{E} of \mathbb{R}^N is direct. The image of the tangent hyperplane at a point $P \in \sigma \in \mathcal{E}$ consists of $N - 1$ points determined from eq. (7.4) by using the appropriate axes spacing $\mathbf{d}_N^i, i = 0, \dots, N - 2$. The resulting transformation, the N-D extension of eq. (7.6) with N terms in the numerator and denominator, determines the point $N - 1$ -tuples mapping surface $\sigma \in \mathcal{E}$ into $\bar{\sigma}$ consisting of $(N - 1)$ planar regions

7.1 Boundary Contours

Lemma 7.1.1 (*Boundary of $\bar{\sigma}$ in \mathbb{R}^N*) For a $\sigma \subset \mathbb{R}^N$, $\partial \bar{\sigma}$ is composed of $N - 1$ curves which are the images of the intersections of σ with the first $N - 1$ superplanes.

An algebraic surface is one described by a polynomial equation providing an important special case of Lemma 7.1.1.

Corollary 7.1.1 (*Boundary of an algebraic surface*) The boundary $\bar{\sigma}$ of an algebraic surface σ of degree n is composed of $N - 1$ algebraic curves each of degree $n(n - 1)$ or less.

The corresponding known result in Algebraic Geometry is that the dual of a non-singular algebraic surface of degree n has degree $n(n - 1)^{(N-1)}$ [6], [17]. Here the boundary representations can be found with the aid of *Plücker's* results presented in Section ?? in Chapter ?. For F in eq. (7.6) a quadratic polynomial the corresponding surface is called *quadric* and in \mathbb{R}^3

$$\sigma : F(x_1, x_2, x_3) = (x_1, x_2, x_3, 1)\mathbf{A}(x_1, x_2, x_3, 1)^T, \quad (7.7)$$

\mathbf{A} being a symmetric 4×4 matrix for \mathbb{R}^3 and $(N + 1) \times (N + 1)$ for \mathbb{R}^N .

Corollary 7.1.2 (*Boundary of $\bar{\sigma}$ for σ a quadric*) A quadric surface $\sigma \subset \mathbb{R}^N$ is represented by $N - 1$ planar regions with conic boundaries.

This is the direct extension from conics in 2-D to quadrics in N-D and as for conics their type depends on their orientation as pointed out next.

Theorem 7.1.1 (*Representation of $\bar{\sigma}$ in \mathbb{R}^N*) A smooth hypersurface $\sigma \subset \mathbb{R}^N$ can be represented by $N - 1$ regions $\bar{\sigma}_{i,i+1} \subset \mathbb{P}^2$, $i = 1, \dots, N - 1$ with $\partial\bar{\sigma}_{i,i+1} = \bar{c}_{(i'-1),i'} = \overline{(\sigma \cap \pi_{i'}^{N_s})}_{(i'-1),i'}$.

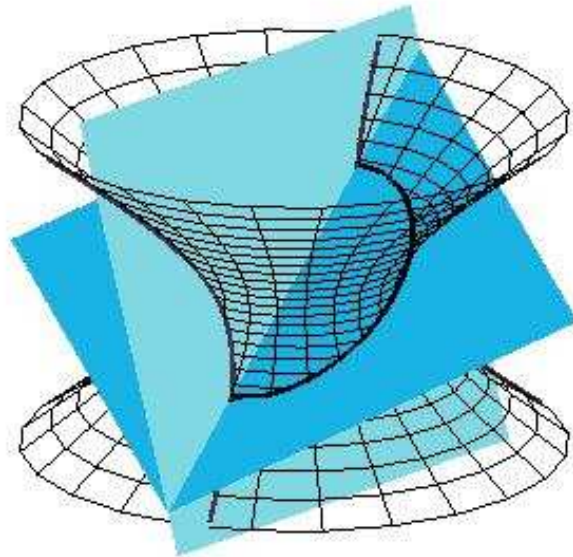


Figure 7.4: Intersection of a surface σ (here a hyperboloid of one sheet) with the two superplanes π_0^s , π_1^s . The points of the boundary $\partial\bar{\sigma}$ are the images of the tangent planes at the points of two curves $\sigma \cap \pi_0^s$ and $\sigma \cap \pi_1^s$.

To clarify the notation, π_i^{Ns} is the $i + 1$ *sp* (recall that the first one is also denoted by π_0^{Ns}). The image of the *space* curve $\pi_i^{Ns} \cap \sigma$ is the image of **only one** projection; we chose $(\pi_i^{Ns} \cap \sigma)_{(i-1),i'}$ corresponding to the adjacent axes $\bar{X}_{i'-1}, \bar{X}_{i'}$ for which $d = 1$ with the convention that for $i' = 1, \bar{X}_{(i'-1)} = \bar{X}_N$. A horizontal translation by $N + i - 1$ units to the left as shown in Fig. ?? is needed to obtain the correct x coordinate. For an object, a point P for example, the notation $\bar{P}_{i'}$ refers to the representation of P with respect to the N coordinates axes after the i th shift.

For \mathbb{R}^3 the preferred projections are $(\pi_1^s \cap \sigma)_{12}, (\pi_1^s \cap \sigma)_{1'3}$ and for $\mathbb{R}^4, (\pi_1^{4s} \cap \sigma)_{12}, (\pi_1^{4s} \cap \sigma)_{1'4}, (\pi_1^{4s} \cap \sigma)_{1'2'}$ and so on.

7.2 Developable Surfaces

The sphere can not be cut and then flattened undistorted. Motivated by map-making, surfaces were sought whose shape is “close” to spherical and can be unrolled into a plane without stretching or contracting. Euler first considered this problem, then starting in 1771 Monge made major contributions on the subject of *developable* surfaces. Monge pointed out potential applications especially to architecture leading perhaps to some of the modern contoured architectural marvels. Gauss and others followed with the development of the differential geometry of more genenal surfaces. Developable surfaces (“developables” for short), are the class $\mathcal{D} \subset \mathcal{E}$ which are the envelope of a one parameter family of planes, serve as an excellent starting point for our study of surface representation. Finding their image, matching and reconstruction algorithms is straight-forward and the results offer crucial guides on coping with the more general representation problems. The pioneering work, and the basis for the exposition here, on their representation and that of ruled surfaces is due to C.K.Hung [9], [12].

Theorem 7.2.1 (C.K.Hung – Developable Surfaces) – *Let a surface $\sigma \in \mathcal{D}$ with tangent planes given by eq. (??), and a neighborhood $U \subset I_t \subset \mathbb{R}$ where the two conditions :*

$$\frac{dx(t)}{dt} = \frac{\partial}{\partial t} \left(\frac{\mathbf{c}(t) \cdot \mathbf{d}^i}{\mathbf{c}(t) \cdot \mathbf{u}} \right) = 0, \quad \frac{dy(t)}{dt} = \frac{\partial}{\partial t} \left(\frac{c_0(t)}{\mathbf{c}(t) \cdot \mathbf{u}} \right) = 0, \quad (7.8)$$

are not simultaneously satisfied for $\forall t \in U$. Then the set of points $\{\bar{\pi}(t)_{i'} \mid t \in U\}$ representing the tangent planes eq. (??) are curves.

Theorem 7.2.2 *A developable with a well matched representation is (piecewise) reconstructable.*

7.2.1 Classes of Developables

Corollary 7.2.1 (C.K.Hung– Cylinders) *Elliptic cylinders in \mathbb{R}^3 are represented by a pair of hyperbolas.*

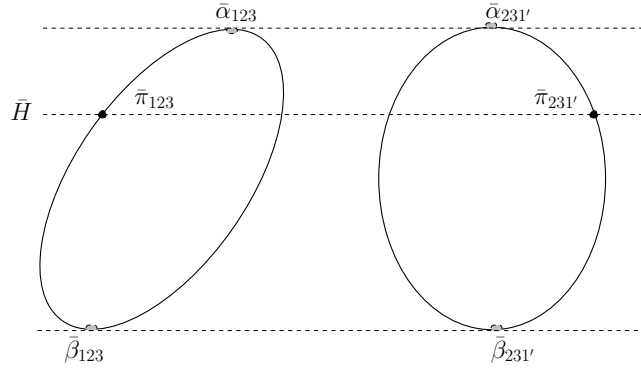


Figure 7.5: The pair of points $\bar{\pi}_{123}$, $\bar{\pi}_{231'}$ represents an unambiguous plane. The $\bar{\alpha}$ and $\bar{\beta}$ points are *a1* ambiguous in the first sense.

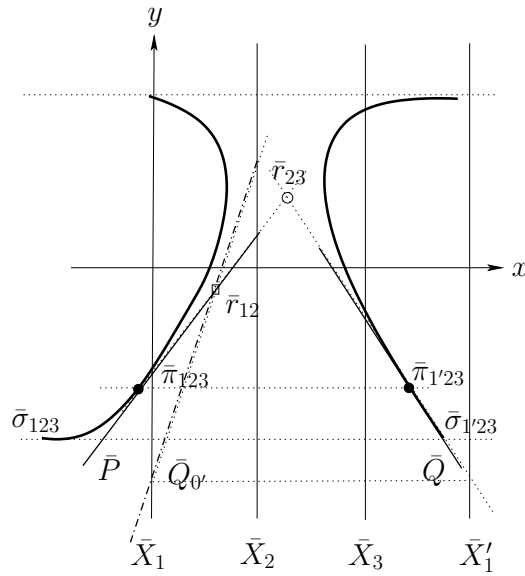


Figure 7.6: Reconstructing a developable. The ruling r is represented by $\bar{r}_{23} = \bar{P} \cap \bar{Q}$ shown by a \circ , and $\bar{r}_{12} = \bar{P} \cap \bar{Q}_0$ shown by a \square , where \bar{Q}_0 is the 1,2 part of the representation of Q with respect to the coordinate axes $\bar{X}_1, \bar{X}_2, \bar{X}_3$.

There are advantages in describing surfaces in vector notation which is due to the mathematical physicist W.J. Gibbs¹. A circular cylinder is given by :

$$\mathbf{x}(t, v) = \mathbf{b} + r(\hat{\mathbf{s}}_1 \cos t + \hat{\mathbf{s}}_2 \sin t) + v \hat{\mathbf{s}}, \quad (7.9)$$

where $\hat{\mathbf{s}}$ is the unit vector in the axis direction and two other unit vectors such that $\mathbf{s} = \hat{\mathbf{s}}_1 \times \hat{\mathbf{s}}_2$ which are implicitly given in terms of the basic unit vectors $\hat{\mathbf{e}}_i$, $i = 1, 2, 3$. The two parameters v, t are real numbers with $0 \leq t \leq 2\pi$. The constant vector \mathbf{b} and

¹He was an early advocate for *visualization* in science with his first two papers in 1873 : “Graphical Methods in the Thermodynamics of Fluids” and “A Method of Geometrical Representation of the Thermodynamics Properties of Substances by Means of Surfaces”.

the cylinder's axis of symmetry s share a point which is the center of a circle of radius r and a point on its circumference is given by the vector $\mathbf{p} = r(\hat{\mathbf{s}}_1 \cos t + \hat{\mathbf{s}}_2 \sin t)$. This vector is normal to the tangent plane

In Fig. 7.9 a general cylinder, with a ruling formed of cusps has two representing curves each with an inflection point, remind us of the *developable* \leftrightarrow *curve* duality. The representing curves seen in Fig. 7.10 indicate that a plane tangent to *two* rulings (i.e. bi-tangent) exists and is represented by crossing points one on each curve further illustrating the aforementioned duality. By the way this also points out that the crossing point and cusps in the representing curves in Figs. ?? and ?? correspond to bitangent planes and rulings which are the loci of inflection points in the developables.

Cones

A developable all of whose rulings intersect on a single *characteristic point*, eq. (??), is a *cone*.

Corollary 7.2.2 (*Cones – C.K.Hung*) *Circular Cones in \mathbb{R}^3 are represented by a pair of conic curves.*

Number of tangent planes parallel to \mathbf{u}	Represented by a pair of
0	ellipses
1	parabolas
2	hyperbolas

General developable surfaces can be described by

$$\mathbf{x}(s, v) = \mathbf{y}(s) + v\mathbf{g}(s), |\mathbf{g}(s)| = 1, a < s < b \quad (7.10)$$

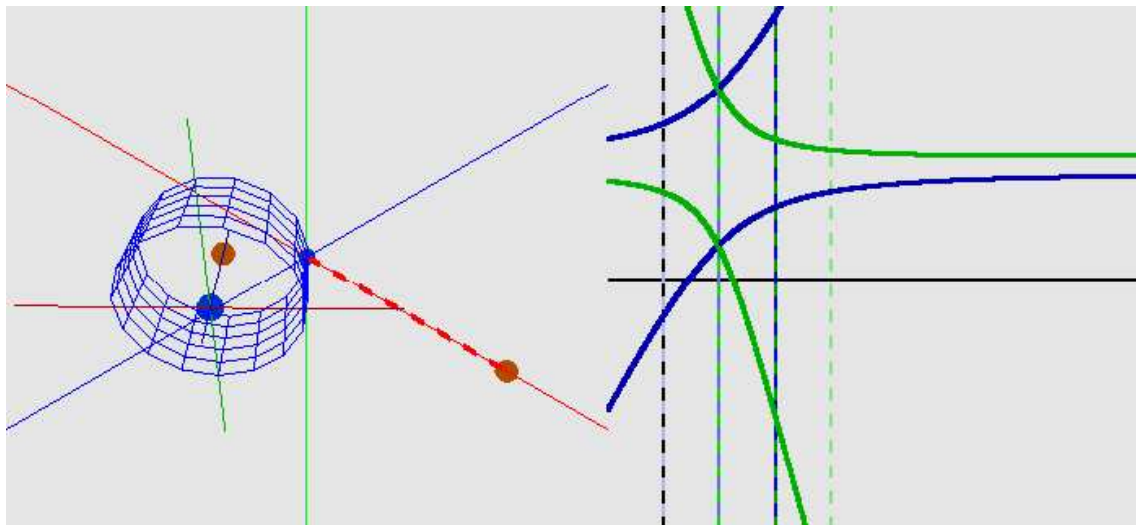


Figure 7.7: A pair of hyperbolas representing the cylinder with orientation (roughly $\alpha_1 = \alpha_2 = 1/\sqrt{2}$, $\alpha_3 = 0$) shown on the left. The \bullet are the “handles” for changing orientation in the software used and have no significance here.

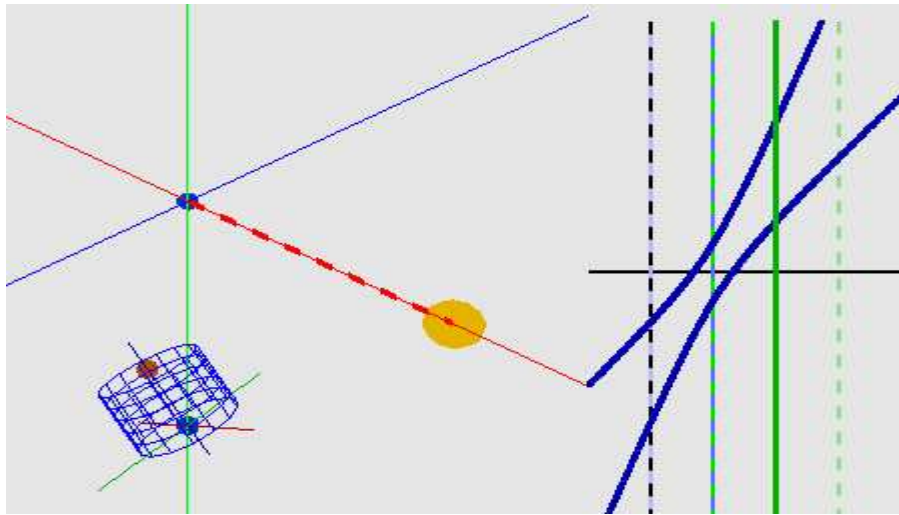


Figure 7.8: Two hyperbolas , one coincident with the \bar{X}_3 axis, representing the cylinder shown on the left.

a nice example being the developable helicoid

$$x_1 = a \cos s - av \sin s, \quad x_2 = a \sin s + av \cos s, \quad x_3 = b(s + v). \quad (7.11)$$

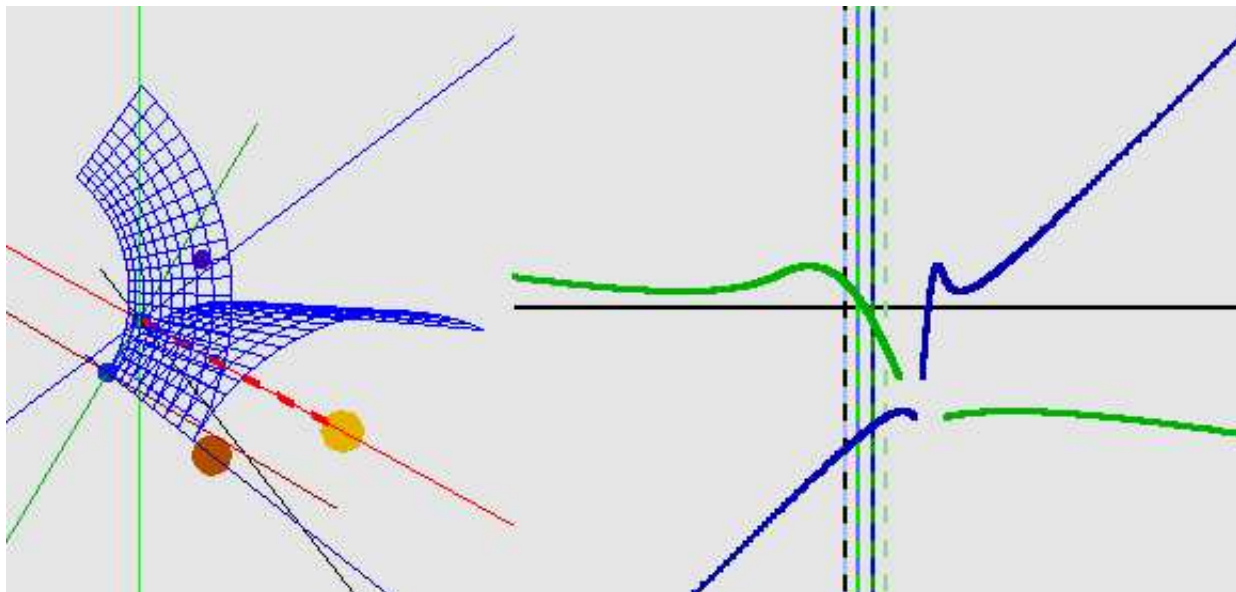


Figure 7.9: A general cylinder illustrating the *developable* \leftrightarrow *curve* duality with the ruling formed by cusps transforming to an *inflection* point in each of the representing curves.

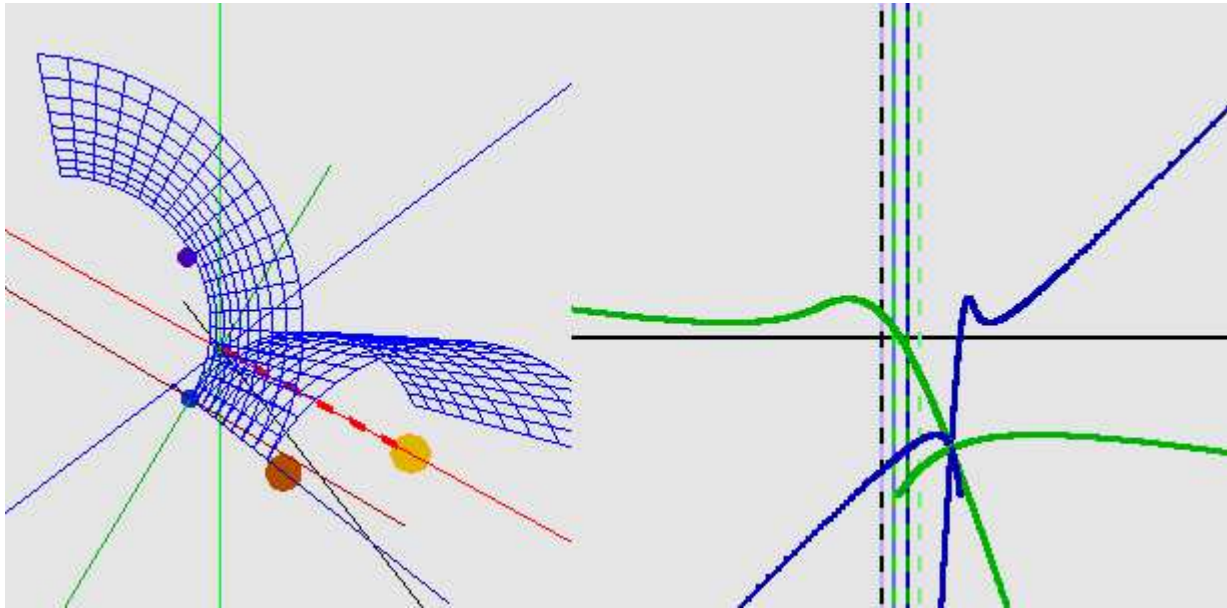


Figure 7.10: The two leaves of the surface in the previous figure are extended allowing for a *bitangent* plane, tangent to two rulings, represented by a *crossing point* together with the inflection points in each of the representing curves.

7.3 Ruled Surfaces

A famous ruled surface is the Moebius strip described by:

$$\begin{aligned}
 \mathbf{x} &= \mathbf{y}(\theta) + v\mathbf{g}(\theta), \quad -\frac{1}{2} < v < \frac{1}{2}, & (7.12) \\
 \mathbf{y}(\theta) &= (\cos \theta)\hat{\mathbf{e}}_1 + (\sin \theta)\hat{\mathbf{e}}_2, \\
 \mathbf{g}(\theta) &= (\sin \frac{1}{2}\theta \cos \theta)\hat{\mathbf{e}}_1 + (\sin \frac{1}{2}\theta \sin \theta)\hat{\mathbf{e}}_2 + (\cos \frac{1}{2}\theta)\hat{\mathbf{e}}_3.
 \end{aligned}$$

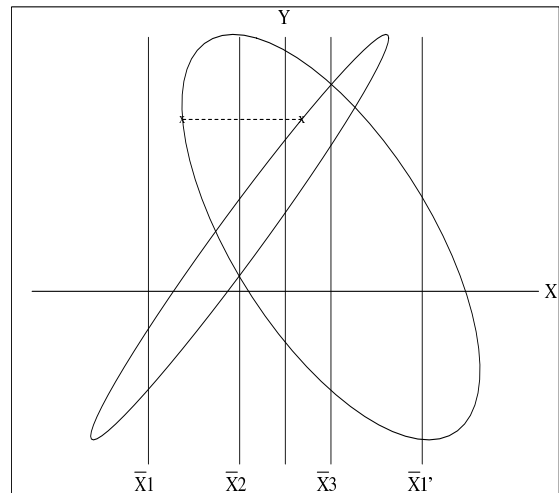
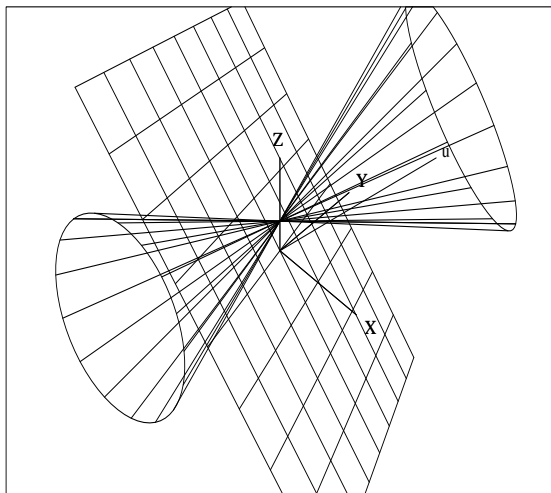


Figure 7.11: A circular cone without tangent planes parallel to the line u is represented by two ellipses. The two points, one on each ellipse, represent one of the tangent planes.

This is a *non-orientable* surface for the unit normal of a point changes its sense as the point traverses around the circle $y = \cos \theta \hat{e}_1 + \sin \theta \hat{e}_2$ ([14] p. 170). Below are some Figs. of a traversal on the Moebius strip corresponding to the circle, and its representation in $\|\text{-coords}$ for various orientations. MAJOR THANKS AND ACKNOWLEDGEMENTS TO CHAO-KUEI HUNG AND DAVID ADJIASHVILI FOR THESE FIGURES

7.4 Conclusions & Future Work

For the classes of smooth surfaces studied the representation is unique. That is, the surface σ can be reconstructed from its two representing planar regions. Recall from the hypercube example that the the generalization to hyper-surfaces \mathbb{R}^N is direct and immediate consisting of $N - 1$ linked regions. *ALL* surfaces can be immediately recognized from the regions representing them. As we pointed out developable surfaces can be non-trivial. This is also holds for ruled surfaces and quadrics which can be recognized by the conical regions representing them. For another, the prospect of transforming the description and design of surfaces into a planar problem *without loss of information* is exciting. Perhaps more so in treating the *approximation* of surfaces one can equivalently treat the approximation of the corresponding planar regions. Earlier [15] it was shown that families of proximate planes in \mathbb{R}^3 are represented by 2 convex hexagons whose shape and size completely characterize the specific collection of planes. Conversely, this is also a characterization of “nearly” planar surfaces. Recall the easy representation of *general* developable surfaces by curves rather than regions. We surmise that in $\|\text{-coords}$ thin curved strips represent families of “nearly”) developable surfaces. Similar observations can be made about “nearly” quadric surfaces. These remarks together revisiting the intuitive picture of the hypercube Fig. 7 should shows the power and potential of this

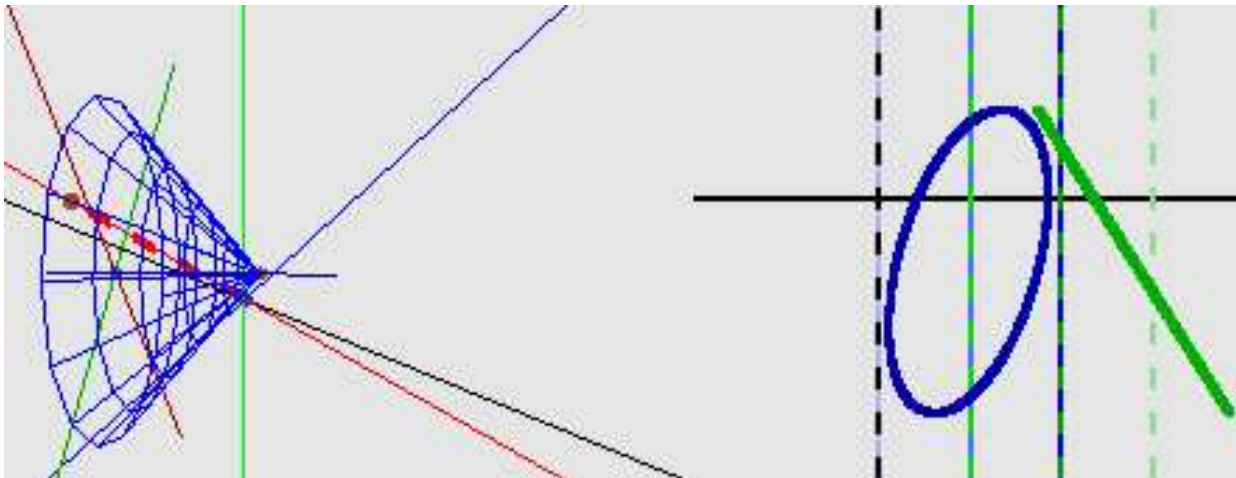


Figure 7.12: Another cone without tangent planes parallel to u is represented by two ellipses one collapsing to a line segment.

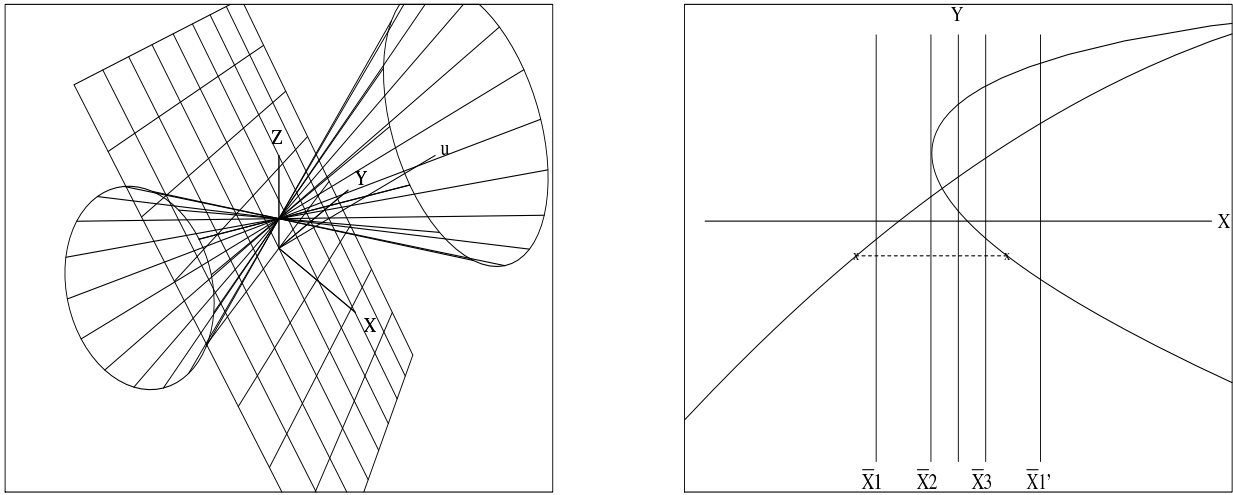


Figure 7.13: A circular cone with one tangent plane parallel to the line u is represented by two parabolas. The two points, one on each parabola, represent one of the tangent planes.

representation.

We propose next to develop these ideas and bring them to a stage where they can be conveniently used. This should include an efficient algorithm for the construction of interior points for these surfaces. This will substantially increase the variety and scope of the Models (MS) that can be constructed for Process Control and Decision Support

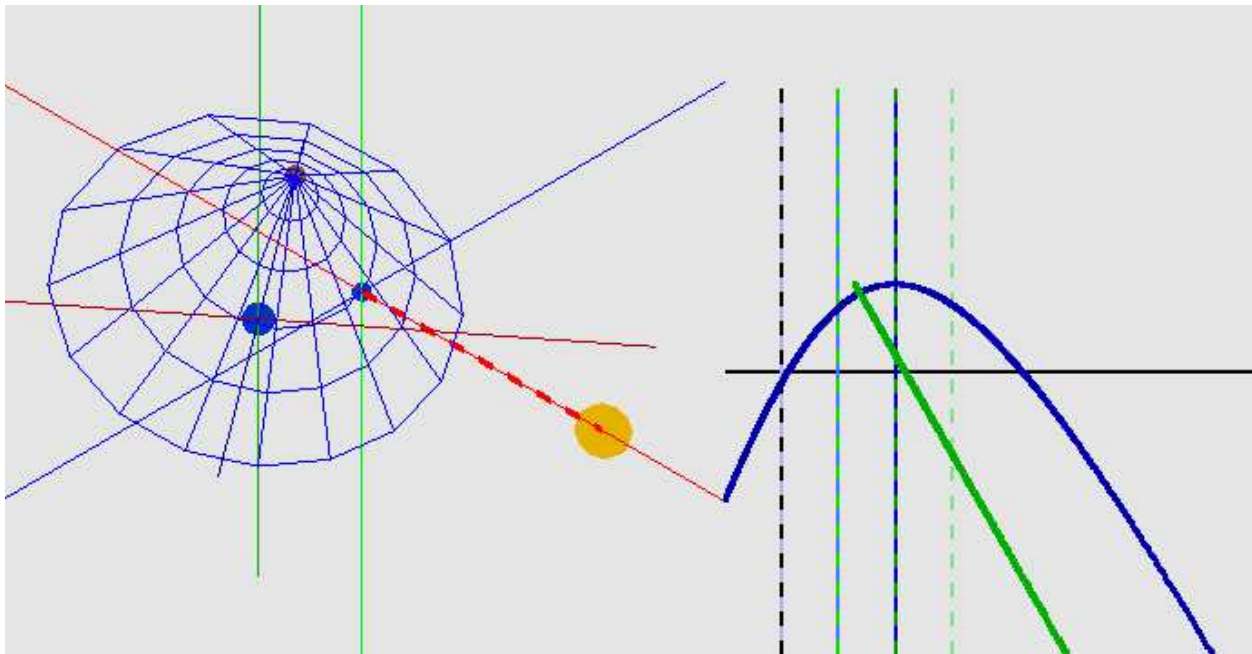


Figure 7.14: A circular cone with one tangent plane parallel to the line u is represented by two parabolas one collapsing to a half-line.

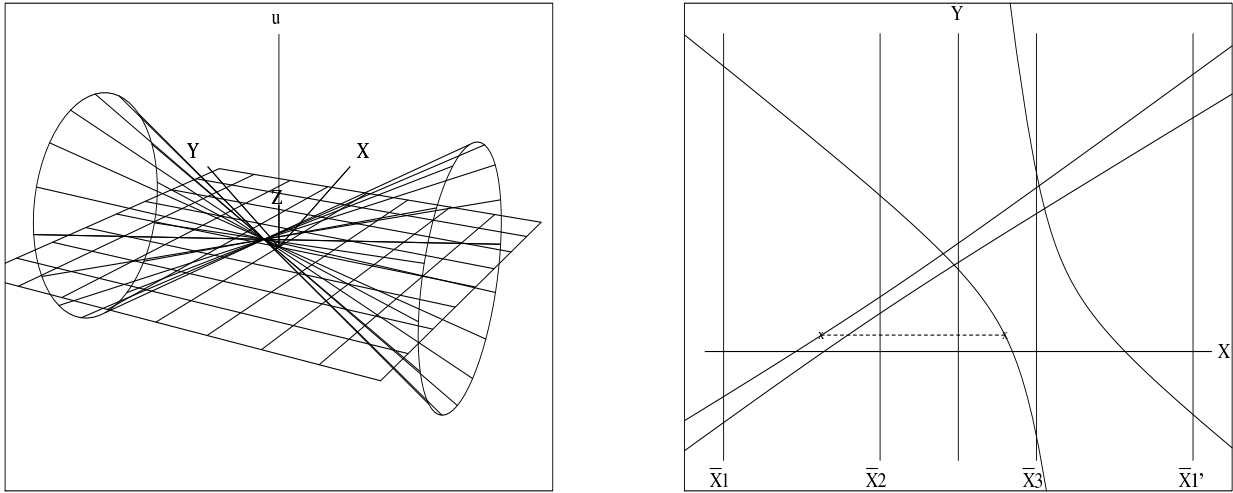


Figure 7.15: A circular cone with two tangent planes parallel to the line u is represented by two hyperbolas. The two points, one on each hyperbola, represent one of the tangent planes.

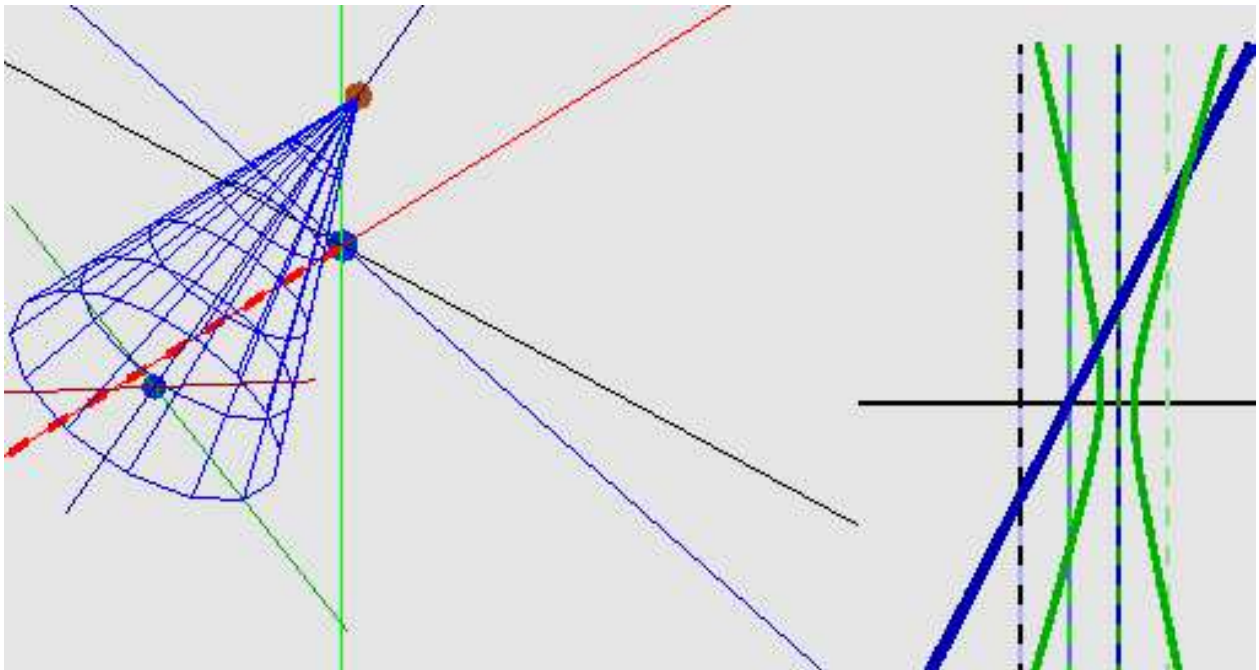


Figure 7.16: Circular cone with two tangent planes parallel to the line u is represented by two hyperbolas one of them collapsing to a line.

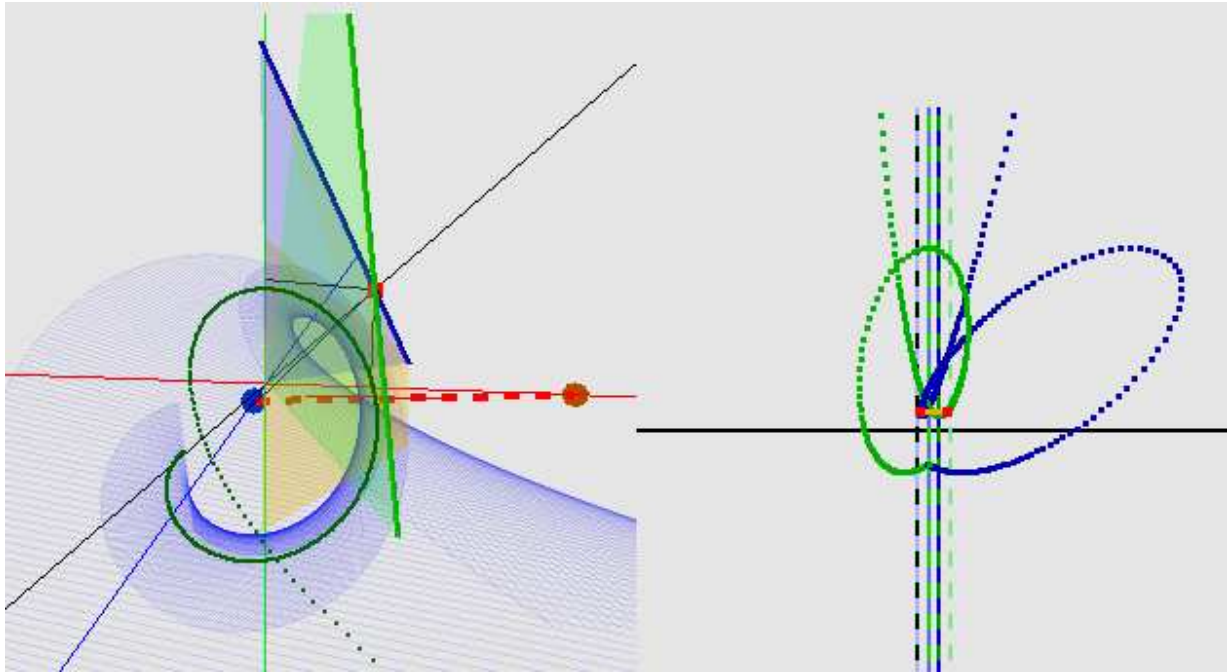


Figure 7.17: Developable Helicoid and its representation for the orientation shown. The two points on right represent the tangent plane on the right.

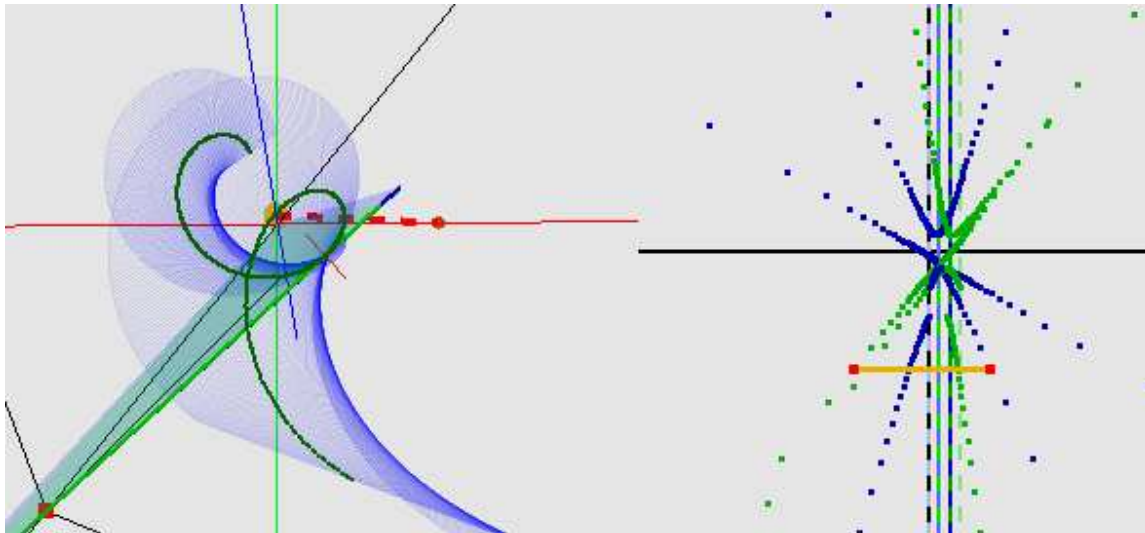


Figure 7.18: Developable Helicoid and its representation for the orientation shown. The two points on right represent the tangent plane on the right.

and which was the point of departure for this work. As an illustration an example based on ellipsoids is shown in Fig. 7.25 modeling a process process with 20 parameters. A feasible state of the process is any interior point such as that shown by the polygonal line. As a result of the constraints applied one-by-one on the parameters the available ranges of remaining parameters decrease and are shown by the intermediate curves between the

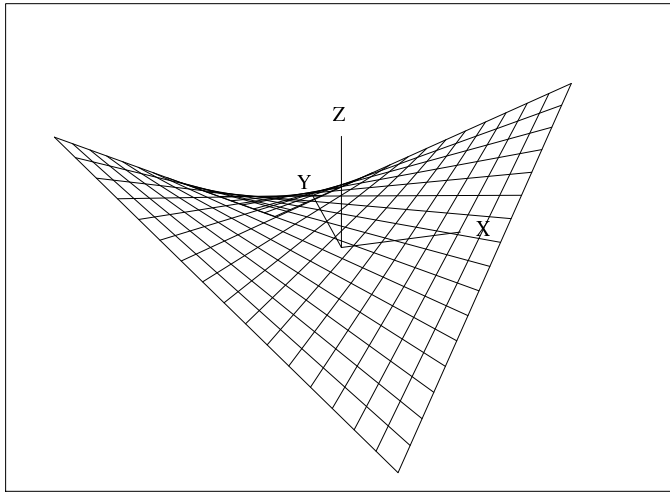


Figure 7.19: The saddle – a doubly-ruled surface.

axes. The very restricted ranges for X_{13}, X_{14}, X_{15} show that these are the “critical parameters” for this state; where the point is “bumping” the boundary. We would like to be able to such constructions and interpretations with models of much more complex processes using the class of surfaces studied here.

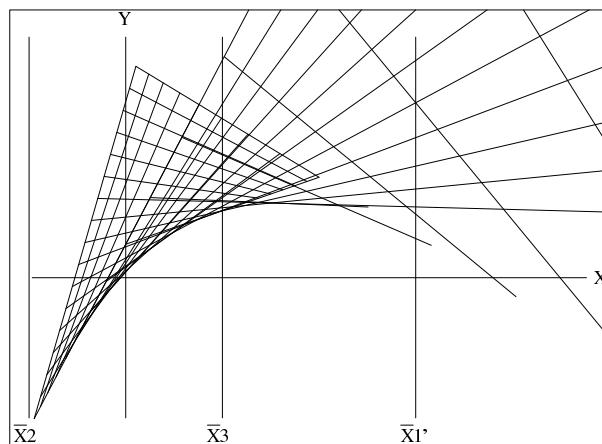


Figure 7.20: One of the two regions representing the saddle. Note the conic curve (parabola) boundary.

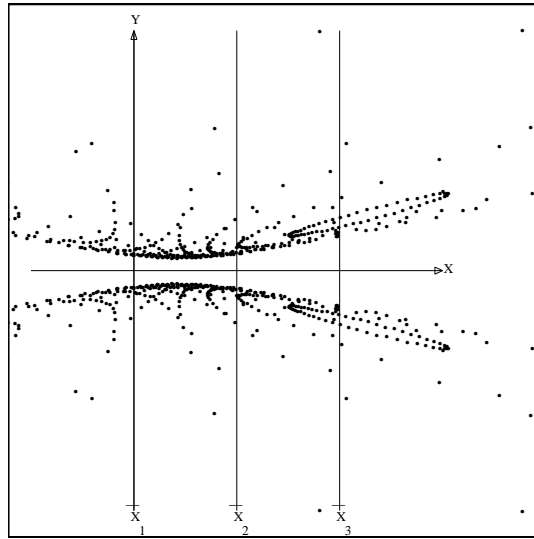


Figure 7.21: One of the two hyperbolic regions representing a sphere in \mathbb{R}^3 .

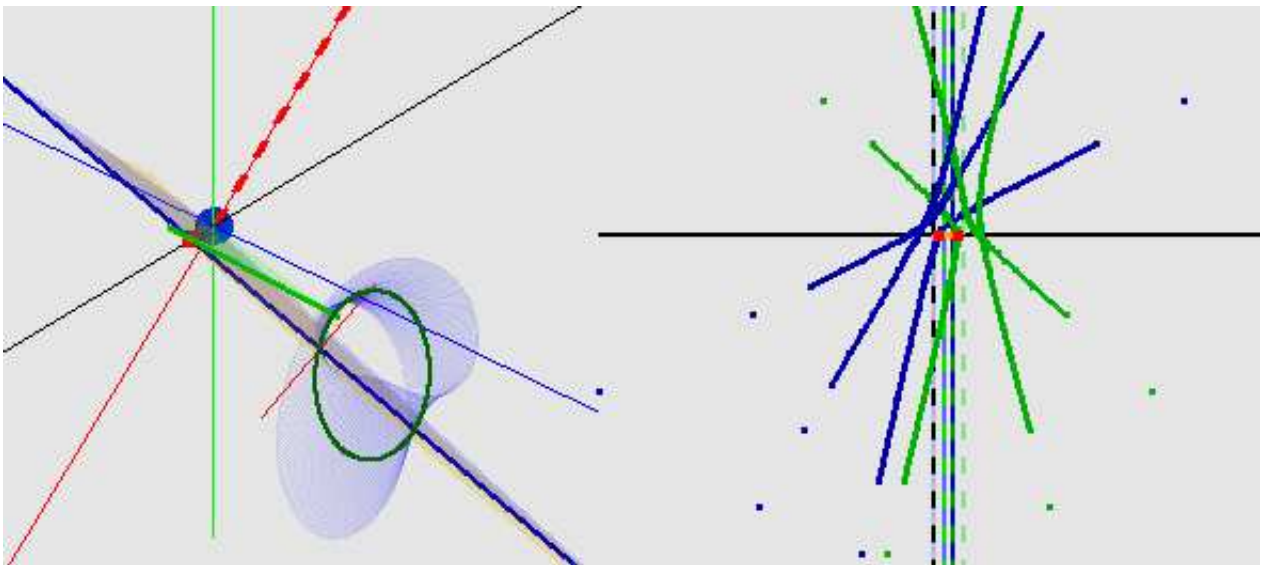


Figure 7.22: One traversal around a Moebius strip. Note the persistent intersection between two pairs of curves. Is that characteristic of non-orientability?

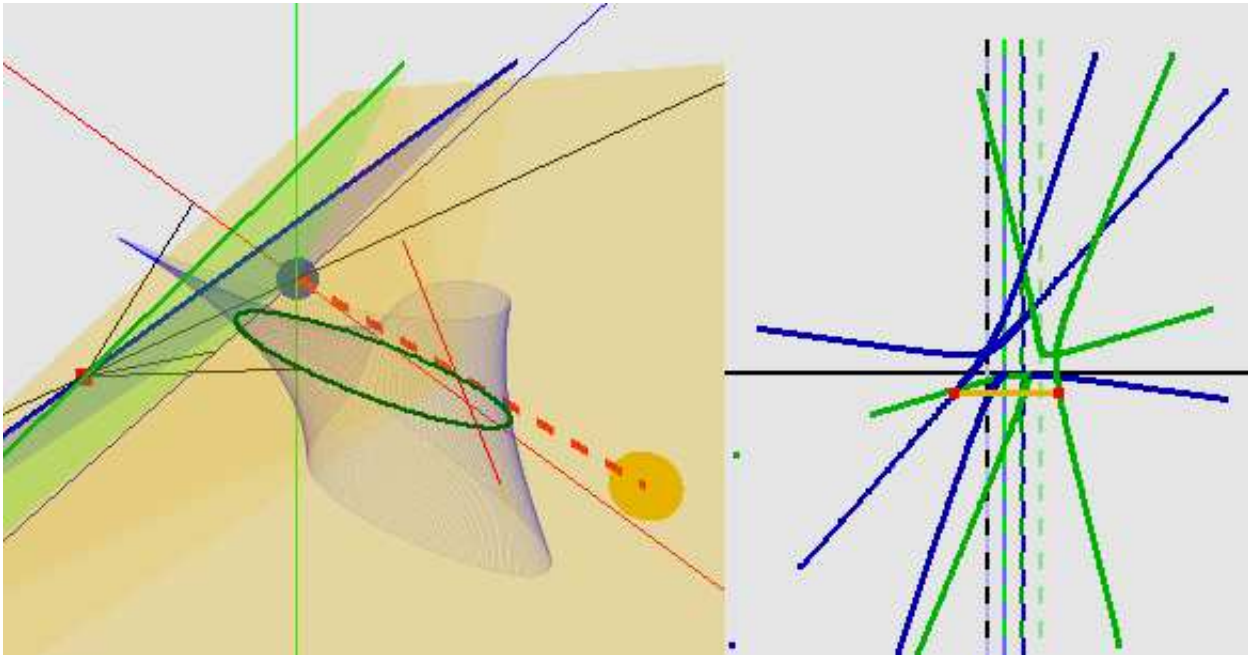


Figure 7.23: One traversal around a Moebius strip. Note the persistent intersection between two pairs of curves. Is that characteristic of non-orientability?

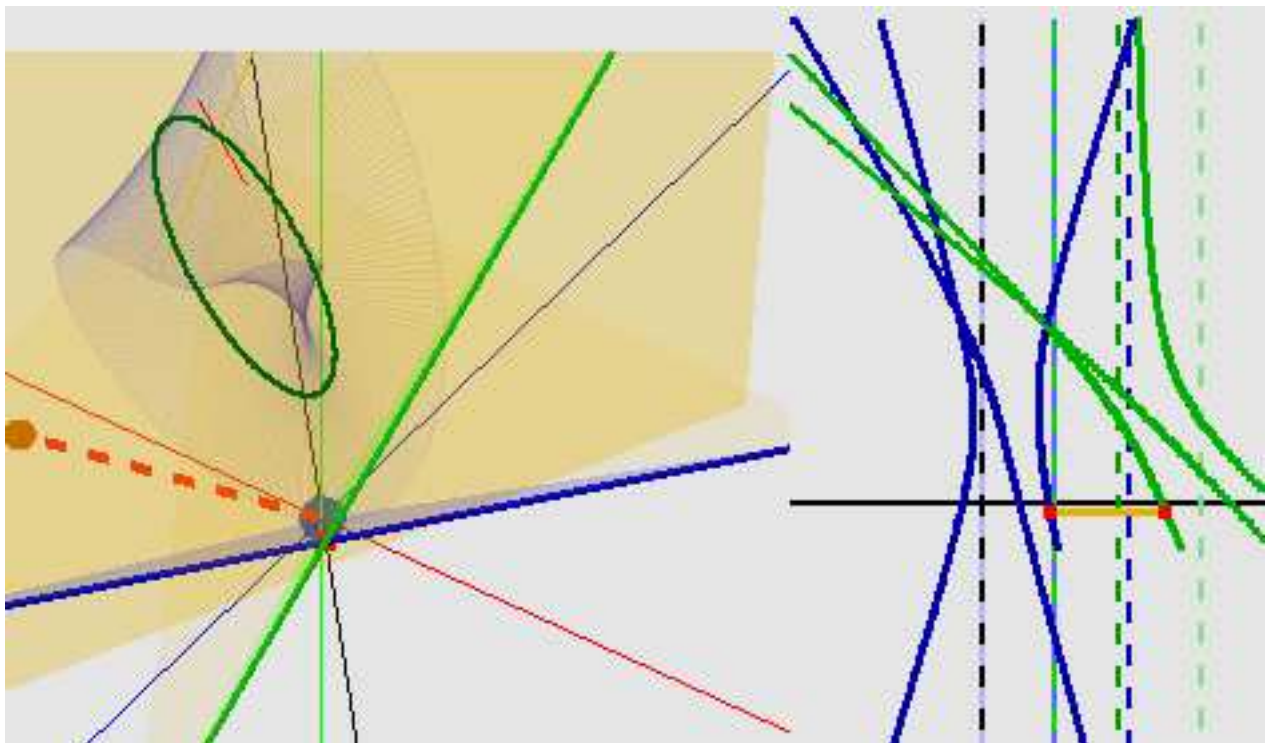


Figure 7.24: One traversal around a Moebius strip. Note the persistent intersection between two pairs of curves. Is that characteristic of non-orientability?



Figure 7.25: Interior point construction in a convex 20-dimensional ellipsoid. This can be the model of a process depending on 20 parameters. An interior point is constructed and represented by the polygonal line shown with the values of the 20 parameters being a feasible state of the system.

Bibliography

- [1] A.F. Beardon. *The Geometry of Discrete Groups*. Springer-Verlag, New York, 1983.
- [2] A. Chatterjee. *Visualizing Multidimensional Polytopes and Topologies for Tolerances*. Ph.D. Thesis, Dept. Comp. Sci., Univ. of S. Calif., 1995.
- [3] D. Cox, J. Little, and D. O’Shea. *Ideals, Varieties, and Algorithms*. 2nd edition, Springer-Verlag, New York, 1997.
- [4] B. Dimsdale. *Conic Transformations – IBM LASC Tech. Rep. G320-2713*. IBM LA Scientific Center, 1981.
- [5] B. Dimsdale. *Conic Transformations and Projectivities – IBM LASC Tech. Rep. G320-2753*. IBM LA Scientific Center, 1984.
- [6] L. Ernstrom. A plucker formula for the singular projective varieties. *Commut. Algebra.*, 5-9:2897–2901, 1997.
- [7] J. Harris. *Algebraic Geometry*. Springer-Verlag, New York, 1992.
- [8] W. Hodge and D. Pedoe. *Methods of Algebraic Geometry, Vol. II*. Cambridge Univ. Press, Cambridge, 1952.
- [9] C.K. Hung and A. Inselberg. *Parallel Coordinate Representation of Smooth Hypersurfaces*. Univ. of S. Calif. Tech. Report # USC - CS - 92 -531, Los Angeles, 1992.
- [10] A. Inselberg. The plane with parallel coordinates. *Visual Computer*, 1:69–97, 1985.
- [11] A. Inselberg and B. Dimsdale. Multidimensional lines ii: Proximity and applications. *SIAM J. of Applied Math.*, 54-2:578–596, 1994.
- [12] A. Inselberg and C.K. Hung. *A New Representation of Hypersurfaces in Terms of their Tangent Hyperplanes*. In *Tutorial on Multidimensional Visualization – ACM SIGGRAPH*, 1995.
- [13] A. Inselberg, M. Reif, and T. Chomut. Convexity algorithms in parallel coordinates. *J. ACM*, 34:765–801, 1987.
- [14] M. M. Lipschutz. *Differential Geometry*. Shaum’s Outlines on Math., McGraw-Hill, New York, 1969.

- [15] T. Matskewich, A. Inselberg, and M. Bercovier. *Approximated Planes in Parallel Coordinates*. Proc. of Geometric Model. Conf., St. Malo, Vanderbilt Univ. Press, 257-266, 2000.
- [16] R. J. Walker. *Algebraic Curves*. Springer-Verlag, New York, 1978.
- [17] V. O. Ya. Some integral calculus based on euler characteristic, lect. notes. *Amer. Math. Monthly*, 1346:127–138, 1988.